Non-invasive ambient pressure estimation using non-linear ultrasound contrast agents

Andersen, Klaus Scheldrup; Jensen, Jørgen Arendt

Publication date:
2009

Document Version
Publisher's PDF, also known as Version of record

Non-invasive ambient pressure estimation using non-linear ultrasound contrast agents

Klaus Scheldrup Andersen

May, 2009

Center for Fast Ultrasound Imaging
Department of Electrical Engineering
Technical University of Denmark

SUBMITTED IN PARTIAL FULFILLMENT OF THE
REQUIREMENTS FOR THE DEGREE OF
DOCTOR OF PHILOSOPHY
AT
THE TECHNICAL UNIVERSITY OF DENMARK
May 2009

Signature of Author

Contents

Preface

More than six years have gone since I first entered the world of Center for Fast Ultrasound Imaging (CFU) at the Department of Electrical Engineering at the Technical University of Denmark. What first started out as small and concrete projects as an engineering aspirant, three years later turned into another three years with a high degree of responsibility and self-discipline. From the beginning of this PhD project, I suddenly had to define and lead my own projects. What was scarier at that time was that I had to start everything related to the field of ultrasound contrast agents up by myself. The former solid rocks like my supervisor Jørgen Arendt Jensen and the rest of my colleagues did not have much experience in this area.

When presenting my project to people with knowledge of contrast agents, I have often been met with curiosity but also skepticism and I still remember the quotes *"quiet impossible"* and *"svært vanskelig"* said by people with personal experience within the topic. After three years of research, I cannot fully disagree with these opinions! Still, I am very excited I have had the opportunity to work within the interesting field of microbubbles and investigate something with a big potential but not yet has been solved.

Although most effort has been on designing and setting up equipment for the measurements, and the number of experiments carried out is limited, it is my hope that the findings described in this thesis can contribute to the continuous search for a robust and sensitive approach for measuring the local blood pressure non-invasively.

Klaus Scheldrup Andersen
May, 2009

Acknowledgments

First of all, I would like to express my respect to and thank my supervisor Prof. Jørgen Arendt Jensen. His great knowledge within ultrasound and signal processing in general is admirable, and his high demands and perfectionism has always kept me going and striving for results and well documented reports, papers, and presentations. Just as important, he has been a good support in the personal struggles, which I have encountered within the recent years and I am thankful for that.

Another special thank you goes to engineering assistants Kjeld Martinsen and later on Jens Chr. Jensen. Without them, the experiments would never have been a reality. I am deeply grateful to their suggestions and solutions and their interest in the outcome of my measurements.

I would also like to thank MD Kristina Rue Nielsen for pulling the strings at the University Hospital of Copenhagen (Rigshospitalet), providing contrast agent and saline, and most of all becoming a close friend.

I thank Dr. Svetoslav Nikolov for always taking the time to help and being a provider of a solution to any given problem. Also, Elna Sørensen deserves a big thank you for always being very helpful and kind to me, disregarding the subject. I have truly appreciated the help and the conversations we have had over the years! Henrik Laursen should be acknowledged for keeping the network running and solving the numerous IT-related problems I have encountered.

I thank Gert Seerup from BK Medical A/S for being my sparring partner regarding contrast agents in Denmark and being helpful in every manner. I also thank Prof. Nico de Jong for giving me the opportunity to visit his lab. Likewise, I would like to thank Rik Voss who took care of me during the stay and has shown interest to my work ever since.

Another big thank you goes to my good friend and former colleague Dr. Fredrik Gran for his constant support, guidance, and great knowledge. Niels Oddershede and Jacob Kortbek are another two friends and former colleagues I have enjoyed spending my time with.

Furthermore, I thank all the PhD students and definitely also the rest of the staff in building 349 for being a part of my life for the last three years.

My mom and stepfather (whom I have always considered to be my real dad) deserve an infinite gratitude for their constant and genuine support. Also, my uncle deserves a special thank you for challenging me in my childhood and inspiring me to become an engineer.

Last but not least, I would like to show my deepest gratitude to my beloved girlfriend, Rikke, for supporting me and setting my mind at ease in so many ways, especially during the last turbulent period. Finally, I thank my friends and family in general for always believing in me

and my ability to succeed.

Abstract

Many attempts to find a non-invasive procedure to measure the blood pressure locally in the body have been made. This dissertation focuses on the approaches which utilize highly compressible ultrasound contrast agents as ambient pressure sensors. The literature within the topic has been reviewed. From this, the appropriate pressure dependent acoustic properties of the microbubbles can be summarized to be the resonance frequency, the disappearance time, and the subharmonic response.

During this thesis, the ambient pressure sensitivity of the subharmonic response has been investigated through simulations and initial experimental measurements.

By simulations, a parameter study has investigated what mechanisms of the driving pulse are important to optimize the ambient pressure sensitivity when utilizing the subharmonic component. Investigating two different types of microbubbles clearly showed that two factors are important when striving for an optimum sensitivity. First, the amount of subharmonic energy reduction, when increasing the ambient pressure, is very sensitive to the acoustic excitation pressure. Second, the study also indicated that the amount of reduction in subharmonic energy is increased as the length of the excitation pulse is extended.

To carry out measurements in the laboratory, an experimental setup has been established. As the focus has been on preparations for future *in vivo* measurements, the setup was designed to match a clinical situation. Under the current measurement conditions, this setup showed that the subharmonic component by itself cannot be used as an ambient sensitivity measure. Instead, a new technique looking at the ratio of the subharmonic energy to the energy of the fundamental component was used. Doing so, an ambient pressure dependent behavior of the microbubbles was observed, indicating this to be a more robust measure. When increasing the ambient pressure, the relation decreases linearly. Likewise, decreasing the ambient pressure makes the relation increase linearly. Although the approach seems to reduce factors like time dependency, a high standard deviation was still observed. This could be caused by several reasons and more measurements are needed to investigate it further.

CHAPTER

ONE

Introduction

The blood pressure is a vital sign of the state of health of the human body. Physically, it is an expression of how much force is applied per unit area $[\mathrm{N/m^2}]$ on the vessel walls enclosing the blood. During a heart cycle, the blood pressure in the arteries will change depending on if the heart contracts or relaxes. The maximum blood pressure is denoted the systolic pressure and occurs near the end of the cardiac cycle when the ventricles are contracting. When the ventricles are filled with blood and the heard is relaxed, the lowest pressure, called the diastolic pressure, occurs. Ordinarily, when confronted by the words *blood pressure*, one would think of the systolic and diastolic pressure measured at the same height as the heart, as this is a common procedure at the doctor's office. Non-invasive approaches for measuring the traditional systolic and diastolic blood pressure have existed since the end of the 19th century. Today, it is carried out with a sphygmomanometer, which comprises an inflatable cuff, a manometer, and equipment for detecting the blood flow. However, the sphygmomanometer will only give an estimate of the overall blood pressure at the level of the heart but the blood pressure depends on where in the body it is measured. Furthermore, knowledge of the blood pressure locally in the body can help doctors to diagnose diseases in vessels and other organs that are related to the blood pressure. Thus, today local blood pressure measurements are used daily to diagnose severe heart, lung, and kidney diseases. For this, two different approaches are used in the hospital. One procedure is to use an A-cannula which is also used to measure the gases in the blood at the same time. This is most often used in intensive care units for continuous monitoring. Another procedure is to insert a catheter with a pressure sensor and guide it to the area of interest through the vessels. Both approaches are invasive, meaning the skin must be penetrated. The A-cannula often causes an infection because of the metallic contact, which irritates the skin. And especially the presence of a thin plastic tube inside the body must be considered inconvenient to the patient and also connected to a certain risk. Besides, as the sensors are located inside the vessel of interest, both approaches introduce changes to the blood flow and thereby the blood pressure. Furthermore, it is not possible to monitor all areas inside the body using neither of these approaches. Therefore, finding a non-invasive and reliable procedure to measure the human blood pressure locally in the body is of high interest.

This thesis concerns approaches to estimate ambient pressure changes utilizing contrast agents for diagnostic ultrasound. An ultrasound contrast agent is essentially a liquid consisting of millions of micrometer-sized bubbles, which are injected intravenously into the circulatory system. To make the microbubbles effective scatterers to the ultrasound, they consist of air or another gas. This makes them highly compressible and their immediate size is, thereby, very sensitive to the surrounding pressure. Consequently, any change in bubble size will also change the acoustic characteristics of the bubble. If a relation between the ambient pressure and the response of a contrast agent when insonified by ultrasound can be found, a completely

new method for pressure measurements can be developed. This could lead to a non-invasive approach to estimate the blood pressure at selected places in the human body. Not only would it be more convenient to the patient. Potentially, it would be possible to image real-time spatial pressure differences using conventional ultrasound imaging techniques, like it is done with color flow mapping today. As will be clear from Chapter 3, the following three properties have shown to be useful to detect the ambient pressure sensitivity of the microbubbles.

Resonance frequency A microbubble can be considered as a harmonic oscillator, which, like any other mechanical system, will have a natural eigen frequency where it will both scatter and absorb the ultrasound with high efficiency. As the resonance frequency is a function of the bubble size, it will change when the ambient pressure causes the bubble to shrink or expand.

Disappearance time Because of diffusion processes, a microbubble will dissolve and, with time, disappear when injected into a liquid like blood or water. The time before the bubble is dissolved, or not detectable using ultrasound anymore, is primarily influenced by gas diffusion and surface tension, which changes according to the size of the bubble.

Subharmonic response When exciting a contrast agent microbubble in a specific way, it will generate a non-linear response at half the frequency of the excitation frequency. Recently, experiments have shown that the generation of the subharmonic frequency component is also influenced by the ambient pressure, and the subharmonic response will reduce if the surrounding pressure is increased.

1.1 Perspective of PhD project

The main purpose of this project has been to design and establish an experimental measurement setup to investigate the possibilities of combining the physical interaction between ultrasound and contrast agents for detecting ambient pressure changes. Traditionally, these kind of experiments have been focusing on the proof of concept by creating near-optimum measurement conditions. But, as future *in vivo* studies have been in focus from the beginning of this project, the emphasis has been to find an approach which can be used in a clinical situation. The measurements carried out in this thesis have investigated the sensitivity of the subharmonic response as described above.

Despite the growing number of experiments within hydrostatic pressure measurements, no real parameter study, investigating the response of microbubbles in respect to ambient pressure changes, has been performed. Therefore, additionally to the measurements, a simulation study has also been carried out. The purpose of this parameter study was to optimize the sensitivity of pressure measurements through bubble response simulations investigating the complex mechanisms for subharmonic generation.

As the research area was completely new at the department at the beginning of this project, a review of the existing literature on the subject has also been carried out. The purpose was to gather all publications to investigate the approaches which has been suggested up to now.

1.2 Organization of thesis

The thesis is devided into six chapters and four appendices. Following the Introduction, another two introductory chapters are presented. These present a general introduction to ultrasound contrast agents and a literature survey of the research considering ambient pressure dependent behavior of contrast agents, respectively. The next two chapters presents the work carried out in connection to the PhD project.

Chapter Two: Ultrasound contrast agents Appetizing chapter introducing ultrasound contrast agents in general.

Chapter Three: Ambient pressure estimation A historical review of the research concerning ambient pressure estimation utilizing the acoustic behavior of bubbles when subjected to diagnostic ultrasound.

Chapter Four: Theoretical parameter study Presents a theoretical parameter study, which has been carried out on the side along with the laboratory measurements. Except from the introduction and future perspectives, this is an extraction of the submitted journal paper in Appendix D.2.

Chapter Five: Experimental measurements Concerns the measurements carried out in this thesis. It starts with a description of the designed measurement setup and ends with a presentation of the measurement procedures and the achieved results.

Chapter Six: Conclusion Summarizes the findings presented in this dissertation.

Appendix A: Measurement of impulse responses Presents an investigation of four different transducers, which have been considered for the experiments.

Appendix B: Pressure controller library Contains a table, which briefly describes the available routines for a software library that has been developed to control an ambient pressure regulation unit from a PC.

Appendix C: Trial protocol for measurements Describes the procedure and necessary equipment to carry out an experiment involving contrast agent and ambient pressure management.

Appendix D: Papers Reprint of the four papers, which have been produced during this PhD project. Three of these are conference papers whereas one has been submitted to the *Journal of the Acoustical Society of America* and is currently under review. The first two papers concern the simulation study while the last two is based on the measurements described in Chapter 5. The results are, however, not presented in the same way and Chapter 5, thus, gives a more thorough and appropriate presentation of the laboratory experiments carried out within the last year.

CHAPTER

TWO

Ultrasound contrast agents

This Chapter is intended as a general introduction to ultrasound contrast agents (UCAs). The idea of UCAs has existed for 40 years and the field has already been intensively studied and several books (e.g. [1, 2, 3, 4]) and even more dissertations have been published on the subject. As entire theses have been used to understand and model contrast agents, this Chapter will only give a general overview and describe some of the physical properties. For a thorough description of the physics and acoustics of a contrast agent, the reader is encouraged to consult the textbook by Hoff [2]. Also the books by Brennen [5] and Leighton [6], describing cavitation and dynamics of bubbles in general, should be considered.

2.1 General introduction

An UCA consists of small particles, that are injected into the circulatory system by a painless venous injection either by bolus or infusion. When the idea of UCAs was first suggested, the purpose was, solely, to increase the scatter from blood, which is typically 30 to 60 dB weaker than reflections from solid tissue [2]. This is in the low range of the dynamic image scale of current systems and, therefore, blood appears to be nearly black in an ordinary ultrasound image. Basically, a contrast agent consists of millions of bubbles in an inactive medium like saline. Since these bubbles are injected into the blood, they must be small enough to pass the capillaries in the lungs, which has a mean diameter of 5 μm [7, 8]. In diagnostic ultrasound with frequencies between 1 and 10 MHz, the acoustic wavelength varies between 1.5 mm and 150 μm, which is much bigger than the bubble diameter. A way to make the bubbles effective scatterers anyway, is to let them consist of a highly compressible medium such as air or another type of gas [2]. Due to the compressibility, they will undergo volumetric oscillations according to the ultrasound pressure field and, thereby, scatter much more energy than solid particles of the same size. When an UCA is injected into a peripheral vein, it increases the echoes from blood vessels about 25 dB [1]. This effect lasts for several minutes and, thus, the microbubbles recirculate in the blood numerous times before the gas complete dissolves. The microbubbles are in general well tolerated in the body but like any other drug, adverse reactions may occur. This is, however, very rare and seldom relevant in clinical studies. According to the European Public Assessment Report (EPAR) from the European Medicines Agency (EMEA), the most common side effects of the UCA SonoVue (Bracco, Milano, Italy) are headache (2.3 %), injection site reactions like burning (1.7 %), and injection site pain (1.4 %) [9].

Today's use of UCAs has redefined the role of diagnostic ultrasound imaging in several ways. First of all, as the contrast agent increases the echo from blood, an increase in signal-to-noise ratio (SNR) is obtained. This, of course, improves all existing techniques like flow imaging and

B-mode imaging. In traditional flow imaging, the increased SNR has improved the velocity estimates. But it has also made it possible to detect smaller vessels and vessels further away from the transducer. In B-mode imaging, the increased echoes from the blood has made it easier to distinguish between blood and tissue. This has, specifically, improved the success rate of wall motion studies when delineating the endocardial border [3]. Another existing technique, which has also been improved is Second Harmonic Imaging but this is primarily because of the non-linear properties the microbubbles possess. As the understanding of the fundamental properties and behavior of microbubbles has increased, new and better contrast agents have been, and still are being, developed. Another result of the better understanding is that UCAs are now used in many other ways than solely increasing the scatter from blood as they were initially designed for. One very interesting application is Perfusion Imaging, which makes it possible to map how the blood propagates to muscles and other organs. In this way, the amount of blood flow to, for instance, the myocardium can be seen in real-time. This technique has also leaded to improved visualization of especially small tumor vessels. UCAs have also contributed to new imaging modalities like Power Doppler Imaging, Super Harmonic Imaging [10], Subharmonic Imaging [11, 12], and Radial Modulation Imaging also know as SURF Imaging [13, 14]. Some of these are already implemented on commercial ultrasound systems, while others are in the pipeline. But even more applications are being investigated by research groups all over the world. One of these small branches is ambient pressure estimation, which this dissertation concerns.

2.1.1 Evolution of contrast agents

The idea of ultrasound contrast agents was first founded in 1968 by Gramiak and Shah [15] who carried out some ultrasound experiments while injecting saline into the aorta using a catheter. During this, they discovered some very strong echoes from places they were not used to. Around the same time, it was reported that almost all fluids generate a similar effect after injection [16, 17]. The conclusion to these findings was that the high reflections were caused by free air bubbles, which where generated because of cavitation at the tip of the catheter during the injection [16, 18]. From this moment it became clear that bubbles could be useful in ultrasound imaging when investigating scattering from blood. However, the free gas bubbles were very instable and it took about 10 years before Carroll et al. 1980 [19] succeeded in encapsulating gas bubbles of nitrogen in gelatin. From their experiments, the great potential was proved right but as the particles were around 80 μm in diameter, they were too large to be injected into the circulatory system. Four years later, Feinstein et al.1984 [20] produced some stable microbubbles of air encapsulated by an albumin shell, which could pass the pulmonary capillaries and stand the circulatory system. This, in fact, leaded to the commercially available contrast agent, Albunex (Mallinckrodt Medical Inc., St. Loius, MO), which was approved in 1992 [21]. The first agent that was approved was Echovist (Schering AG, Berlin, Germany) in 1991, which consists of galactose micro-particles containing air. However, this agent could only be used for examination of the right heart and venous system as it was not stable enough to survive the pulmonary passage after injection. Since then, several agents have passed through the necessary clinical trials and are now approved in Europe, North America, and more recently Japan. UCAs are often categorized into three generations. The first generation consisted of microbubbles of air, which in some cases were encapsulated in a shell. Although some of these agents (e.g. Levovist by Schering AG, Berlin, Germany) were actually capable of passing through the heart and pulmonary capillaries, they did not last longer than a few minutes after injection [22, 23]. The development of the second generation of UCAs was initiated around 1990 and these are differentiated from the first generation by having an improved stability and

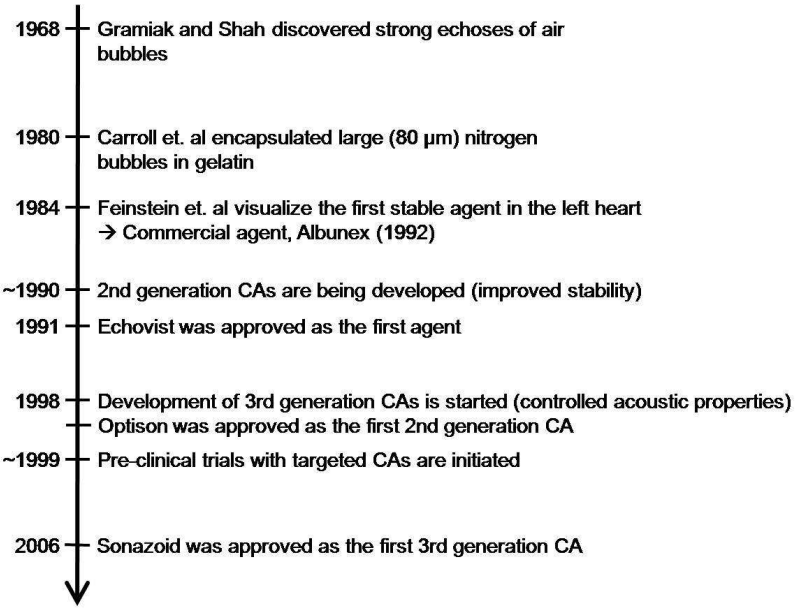

Figure 2.1: Time line summarizing the development of ultrasound contrast agents.

longer persistence. First of all, they are all surrounded by a shell, which in some cases is only tens of nanometres in thickness. Beside stabilizing the microbubbles by separating the gas-to-liquid interface, which slows the dissolution time [24], the shell also makes it possible to produce more similar bubbles and, thereby, reducing the size distribution. Another difference between the first and second generation agents is that the gas core no longer consists of air but a different gas with a low solubility to decrease the diffusion process, which is the rate of time it takes for the gas to dissolve into the blood. The third generation has the same stability as the second generation but is distinguished from it by having a narrow size distribution and more controlled acoustic properties. For instance, it is likely to believe that an agent with improved subharmonic generation will be presented in the near future. An example of a third generation agent is Sonazoid (Nycomed-Amersham, Oslo, Norway), which were approved for the first time in the world in Japan 2006. It consists of perflourocarbon particles in a thin surfactant membrane with a well defined size distribution having a mean diameter of approximately 3 μm [2, 25]. Finally, within the last decade a completely new area of interest has arisen at a great rate. The idea of target-specific microbubbles is to coat the bubbles with a ligand or glue, which is designed to bind to specific cells and structures in the body [26, 27]. This will make some of the bubbles stick to the desired cells, thereby, allowing imaging of these molecular targets. Besides Molecular Imaging, another potential application of the modification of the shell is to use the microbubbles to transport drugs through the circulatory system to a specific location in the body. The ligand will make the bubbles stick to the desired tissue long enough to burst them and release the drugs inside. The perspective that such a technique can replace existing chemotherapy, thereby, reducing the amount of drugs to a minimum and only attacking the sick cells, has intensified the research on microbubbles in general and development of contrast agents for molecular imaging and target drug delivery in particular. The evolution just described is briefly summarized in Fig. 2.1.

2.1.2 Commercially available contrast agents

The information on available agents is not straight forward to access. However, Table 2.1 intends to list the contrast agents, which have been approved for clinical examination in either USA, Canada, Europe, or Japan. The first three contrast agents are all part of the first generation and it has been announced that the production of Echovist and Levovist will be stopped. For a

Agent	Manufacturer	Approved	Gas core	Shell
Echovist	Schering AG	1991	Air	None
Albunex	Molecular Biosystems Inc.	1993	Air	Albumin
Levovist	Schering AG	1995	Air	Palmitic acid
Optison	GE Healthcare	1998	Octafluoropropane	Albumin
SonoVue	Bracco Diagnostics, Inc.	2001	Sulphurhexaflouride	Phospolipid
Definity	Lantheus Medical Imaging	2001	Octafluoropropane	Phospolipid
Imagent	IMCOR Pharmaceutical Co.	2002	Perfluorohexane	Phospolipid
Sonazoid	Nycomed-Amersham	2006	Perfluorobutane	Surfactant

Table 2.1: List of currently approved contrast agents.

description on size distribution, application use, and recommended doses of the agents listed in Table 2.1 and also some agents used for research purposes only, the reader should consult the home page of the respective manufacturer or possibly also [4, 28, 21].

2.2 Physical properties

2.2.1 Linear behavior

As mentioned in Section 2.1, a microbubble is much smaller than the wavelength used for diagnostic ultrasound. Therefore, a bubble placed in an ultrasound field will undergo the oscillatory motion of the field. As illustrated in Fig. 2.2, a positive pressure of the ultrasound wave will make the bubble compress, while a negative pressure will make it expand. This means that the bubble will experience a periodic change in radius according to the ultrasound pressure field. Like vibrations in any oscillating system, the radial oscillations have a natural (resonant) frequency at which it will both scatter and absorb the ultrasound with high efficiency. The most simple example of such an oscillating system is a mass on a spring as depicted in Fig. 2.3. Such a system needs two things for a mechanical oscillation to occur, that is a restoring force (elasticity) and inertia. When the system is displaced from equilibrium, the elasticity will provide a restoring force to get the system back to equilibrium. However, because of the inertia the system will overshoot. This constant play between the elasticity and inertia property will make the system oscillate with a natural frequency defined as [2]

$$\omega_0^2 = \frac{k}{m}, \tag{2.1}$$

where k is the elasticity and m is the inertia. In this simple bubble analogy, the restoring force can be compared to the gas. Correspondingly, the inertia can be considered as the mass of the surrounding liquid, which is set into motion when the bubble oscillates. Assuming the bubble

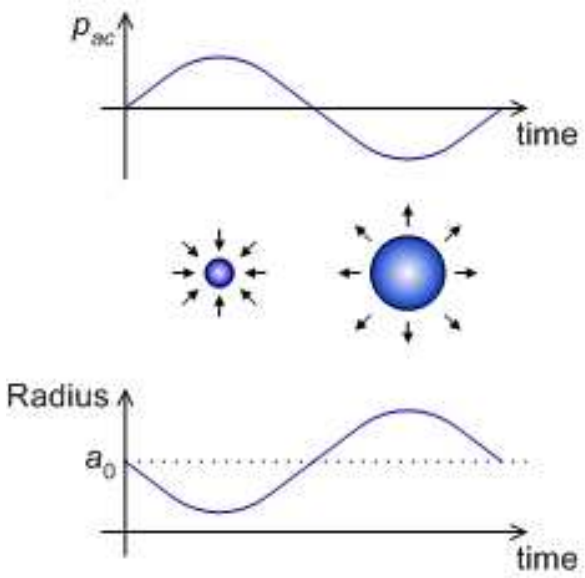

Figure 2.2: Example of bubble size behavior when driven by a low acoustic pressure field. The upper graph shows the acoustic pressure while the bottom part illustrates the bubble radius with a_0 being the equilibrium size at rest.

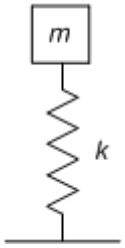

Figure 2.3: Mechanical system consisting of a mass, m, on a spring with spring constant k. This is the most simple example of a system causing a mechanical oscillation due to elasticity and inertia.

to be a linear oscillator, the resonance frequency of a free bubble can be shown to be [29]

$$f_r = \frac{1}{2\pi a}\sqrt{\frac{3\kappa p_e}{\rho}}, \tag{2.2}$$

where a is the bubble radius, κ is the polytropic exponent of the gas, p_e is the equilibrium pressure inside the bubble, and ρ is the density of the surrounding liquid. This derivation has a lot of assumptions like linear behavior, adiabatic (no heat transfer) conditions, and no surface tension. Still, (2.2) gives a simple analogy to bubble behavior and as can be seen, the resonance frequency is inversely proportional to the bubble radius. A more appropriate model, which also incorporates the shell of current microbubbles, is derived in [2].

2.2.2 Non-linear behavior

When a microbubble is excited using a low acoustic pressure, the bubble oscillates at the same frequency as the excitation frequency. Increasing the acoustic pressure, however, the oscillatory

motion of the bubble will change since the expansion phase and contraction phase of the bubble are not equal. In this case, the gas can be compared to a non-linear spring. As the bubble is compressed by the pressure field, it becomes more stiff and resists further reduction in size [4]. Conversely, in the rarefaction phase of the ultrasound pulse, the bubble becomes less stiff and, therefore, enlarges much more. The consequence of this non-linear motion is harmonics in the sound scattered from the bubble. The harmonics are defined according to the fundamental frequency, f_0, as

- Higher harmonics: $2f_0, 3f_0, 4f_0, \ldots$
  - Superharmonics: $\sum (2f_0, 3f_0, 4f_0, \ldots)$
- Subharmonics: $\frac{1}{2}f_0, \frac{1}{3}f_0, \ldots$
- Ultraharmonics: $\frac{3}{2}f_0, \frac{5}{2}f_0, \ldots$

The first higher harmonic component is also known as the second harmonic and often the first subharmonic is simply referred to as the subharmonic component. These terms are also used throughout this dissertation.

Because of this behavior, a microbubble is said to have three different vibration regimes according to the excitation pressure. At acoustic pressures below approximately 60 and 100 kPa, small linear oscillations are seen. When increasing the driving pressure, non-linear vibrations and, thereby, harmonic backscattering is observed. By increasing the acoustic pressure above 1 MPa, the oscillations become so large that the bubble bursts. This produces a transient backscatter behavior and a broad range of frequencies is seen in the spectrum. In practice, there are no sharp transitions between these regimes because of different bubble sizes in the UCA population. Also, these transitions highly depend on the acoustic properties of the specific agent as well as the excitation pulse frequency and shape. Thus, a bubble is most easily destroyed when excited at its resonance frequency [30]. Likewise, the subharmonic component is generated at lower acoustic pressures when the bubble is driven at twice the resonance frequency [31].

2.2.3 Bubble dynamics model

Modeling the acoustics of bubbles in a fluid is a still ongoing investigation, which was initiated by Lord Rayleigh [32] in 1917 who studied damages to ship propellers due to bubble cavitation. In 1933, Minnaert [29] explained the characteristic resonance frequency of free bubbles given in (2.2) when he did a theoretical and experimental study of bubbles' emission of sound. Since then, several modifications to the existing models and new theoretical models on how to predict the behavior of an oscillating UCA microbubble have been presented. Most models are based on modifications of the Rayleigh-Plesset [33] equation and are capable of handling shell encapsulating bubbles. This includes the models used by de Jong and Hoff 1993 [34] and Church 1995 [35]. Other models are based on the modified Herring equation to describe the radial motion (e.g. Morgan et al. 2000 [36]). Within the last decade, optical techniques have been introduced to study the microbubbles using high-speed camera systems capable of producing image sequences at several millions of frames per second. A well known example of such a system is the Brandaris 128 with a frame rate of 50 millions fps [37]. Although this approach is solely based on measurements in the laboratory, and usually only investigates a single or perhaps a few microbubbles at a time, it is still a valuable tool for understanding and

model the behavior of the bubbles. Using this technique, Marmottant et al. 2005 [38] have developed a model, which recently has seemed to obtain wide acceptance. This model is based on the Rayleigh-Plesset equation and incorporates a new non-linear behavior to describe large amplitude oscillations.

2.2.4 Ambient pressure dependent properties

As mentioned in the Introduction, three acoustic properties have been suggested as a measure for detecting changes in the pressure surrounding the microbubbles. This Subsection very briefly summarizes the theoretical derivations that can be used to predict the findings described in the literature survey in Chapter 3.

The shift in resonance frequency, caused by a change in the ambient pressure, has been derived theoretically to [39]

$$\frac{\Delta f}{f_r} = \frac{5}{6}\frac{\Delta P}{P_0}, \tag{2.3}$$

where Δf is the change in frequency, ΔP is the change in pressure, and P_0 is the initial ambient pressure. Equation (2.3), thereby, indicates that the shift in resonance frequency is linearly related to the relative pressure change.

The second acoustic property is the disappearance time. This refers to the time it takes before a bubble dissolves because of diffusion processes, which cause the gas inside the bubble to travel to the surrounding liquid. An expression of the disappearance time when applying an ambient overpressure has been derived to [40]

$$\frac{da}{dt} = \frac{D\, d_T}{a}\, \frac{\frac{C_i}{C_0} - 1 - \frac{2\sigma}{ap_a} - \frac{p_{ov}}{p_a}}{1 + \frac{4\sigma}{3a}p_a} \left[1 + \frac{a}{\sqrt{\pi Dt}}\right], \tag{2.4}$$

where t denotes time, D is a diffusion constant, d_T is a constant based on the temperature and the given medium, C_i/C_0 is the ratio of dissolved gas concentration to saturation concentration, σ denotes the surface tension, and p_a and p_{ov} is the ambient pressure and the applied overpressure, respectively. The actual mechanism responsible for the bubble disappearance is the surface tension, which generates an overpressure inside the bubble. However, from (2.4) it can be seen that the time before the bubble disappears is actually also related to the local pressure.

The final acoustic property that has shown to be sensitive to the surrounding pressure is the generation of the subharmonic component. Although the simulation study to be presented in Chapter 4 support the experimental findings, which will be described in Chapter 3, no theoretical explanation for this property has yet been presented. However, it is likely to believe that damping and, perhaps, microbubble stifness are the main mechanisms for this property as they control how the bubble oscillates [41].

CHAPTER

THREE

Ambient pressure estimation

This Chapter presents a historical overview of the research concerning ambient pressure estimation utilizing the acoustic behavior of bubbles when subjected to diagnostic ultrasound. However, the Chapter begins with an introduction to an existing non-invasive approach, which does not make use of contrast agents. The review is, primarily, structured chronologically according to time. But for easy discussion and presentation, achievements and findings by the same research group have in most cases been gathered. It should be noted that more publications on the subject do exist but have still been excluded due to either time considerations, as they have not been read carefully, or a sort of misfit in respect to the main thread of this review. Furthermore, it is possible that other publications exist but are unknown to the author of this thesis.

Comment on measuring unit

The literature normally denotes blood pressure in millimeter of mercury, mmHg. However, the SI-unit of pressure is Pascal and, therefore, this will be used throughout this thesis. As the literature to be presented is a mix of the two measuring units, conversion has in some cases been carried out. In this case, the original value will be listed in brackets after the denotion in Pascal. The relation between millimeter of mercury and Pascal is $1\,\text{ATM} = 760\,\text{mmHg} = 101.325\,\text{kPa}$ and gives the following conversion factors:

$$1\ \text{mmHg} = 133.322\ \text{Pa} \quad \Longleftrightarrow \quad 1\ \text{kPa} = 7.5\ \text{mmHg}.$$

To give a general idea of the relation, a similar graph as presented by Hoff [2] is shown in Fig. 3.1.

3.1 History and present

As mentioned in the Introduction, the blood pressure can already be measured non-invasively using a cuff. But this will only give an estimate of the overall systolic and diastolic pressure around the heart. And as invasive approaches are both inconvenient to the patient and also accompanied with risk of infection and other injuries, many attempts to find a reliable non-invasive method have been made over the years.

One non-invasive approach to measure the blood pressure locally, which already exists, was suggested by Evans et al. 1989 [42] and the idea is to measure the pressure gradient across the valves of the heart. For this, existing methods for blood flow estimation (Doppler ultrasound)

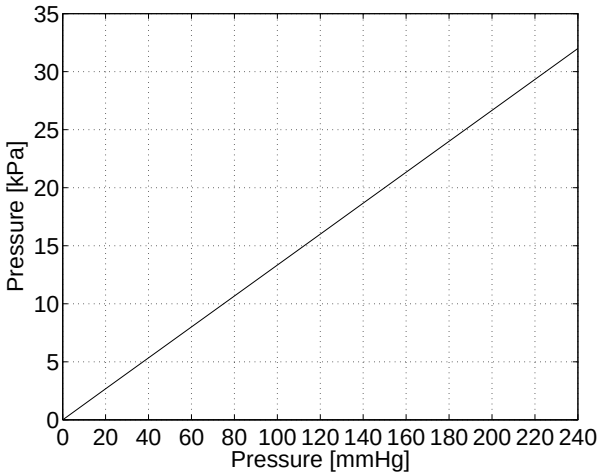

Figure 3.1: Relation between the traditional measuring unit of blood pressure, mmHg, and the standard SI-unit for pressure, Pascal.

is combined with a modification of the Bernoulli equation [42, 43]. The method was, however, concluded not to provide reliable or reproducible blood pressure values by Straus et al. 1993 [44] and by Baumgartner et al. 1993 [45] who compared the approach with measurements using a pressure catheter. The same conclusion was made by Reddy et al. 2003 [46] who investigated the approach for a tail-cuff method, which is used to measure the systolic, diastolic, and mean blood pressure in mice.

Another type of approach, which is still being investigated, is to combine contrast agent microbubbles and diagnostic ultrasound. Fairbank and Scully 1977 [47] was the first to suggest that ultrasound reflectivity of tiny air bubbles injected into the circulatory system could be used to detect pressure differences in the four chambers of the heart. Combining the equation of motion for a mass on a spring system and the resonance frequency of a free bubble, originally derived by Minneart [29] and later reviewed by Devin [48], they predicted the resonance frequency of the bubbles to be nearly proportional to the surrounding pressure as the resonance frequency is related to the bubble size, which will shrink if the surrounding pressure is increased. To investigate this experimentally, they produced free air bubbles with a diameter between 20 and 40 μm by vibrating a micropipette in the water. For the ultrasound acquisition, they used a separate broadband transmitter and receiver. Although a frequency shift in the scattered spectrum was observed in some cases, the results were concluded inconclusive either because of non-uniform bubbles causing a broadening of the resonance spectrum or because of too large bubbles having a resonance frequency below the range of the receiving transducer. Hök 1981 [49] followed the concept by Fairbank and Scully utilizing the interaction between ultrasound and air bubbles. To solve the problem concerning the wide spread in bubble volume, he suggested to use modulation of the pressure surrounding the bubbles by means of a high amplitude low frequency tone burst emitted from a secondary transducer. Furthermore, for the presented experiments, the echo amplitude from a single bubble was used instead of the resonance frequency technique. Although the results under *"ideal experimental conditions"* indicated that hydrostatic pressure could be obtained non-invasively, it was concluded that the rapid dissolution time necessitated considerably research and development before the approach could be tested clinically [49]. Another approach was presented by Newhouse and Shankar [50, 51] in 1986. They showed theoretically and experimentally that accurate bubble size measurements are possible using a double frequency technique for determination of the sum and

difference frequencies. With this approach they demonstrated that ambient pressure changes from 2.7 to 13.3 kPa (20 to 100 mmHg) could be estimated. However, once again, the rapid dissolution time of the free air bubbles prevented any practical implementation at that time.

Common for all experiments carried out until the late Eighties is the poor stability of the free or encapsulated air bubbles available at that time. Since the introduction of the more stable second generation ultrasound contrast agents, new attempts to take advantage of the ambient pressure dependent acoustic properties have been initiated. In 1989, Tamura et al. [52, 53] used encapsulated microbubbles to experimentally detect ambient pressure changes by exploiting the shift in resonance frequency. For this, they introduced a twin-frequency technique to remove attenuation effects and, thereby, improving the sensitivity. Doing so, it was possible to detect changes in the ambient pressure of 6.7 kPa (50 mmHg) and it was concluded that contrast agents have the potential to determine the blood pressure, but the detecting system as well as the microbubbles, still, needed to be improved.

As the use of the new type of microbubbles spread, different groups started to report changes in reflectivity from the bubbles after injection into the circulatory system due to the local blood pressure [54, 55, 40] and several groups established ambient pressure regulating equipment to investigate this phenomenon [56, 57, 58, 59]. All investigated the contrast agent Albunex (Molecular Biosystems Inc., San Diego, CA, USA) and, unanimously, found that an irreversible effect of microbubble disappearance takes place when hydrostatic over pressure is applied. Vuille et al. 1994 [57] found that the Albunex microbubbles disappeared within 3 minutes of injection into water. Increasing the surrounding pressure made the bubbles disappear even faster. The change in intensity was finally explained by de Jong et al. 1993 [40] and de Jong and ten Cate 1996 [60] who investigated this in laboratory experiments as well as *in vivo*. Like [57], they found that the microbubble shrinks faster if the surrounding pressure is increased and as the scattering cross-section is a function of the bubble size, this causes a decrease in the echo response [39].

In 1993, Schlief and Poland [61] applied for a patent describing an ultrasonic manometry process, which, based on scattered signals from microbubbles could, potentially, be used to measure blood pressures. For this, they suggested, as the majority of the techniques up to then, to measure the shift in resonance frequency in an ensemble of microbubbles. However, a poor sensitivity prevented small pressure changes to be measured [62] and no new results have been presented since.

Hoff and Sontum 1998 [63, 2] presented an approach to characterize an ultrasound contrast agent based on correlating the measured size distribution and acoustic attenuation spectra measured using two seperate transducers to cover a broad frequency range from 1.5 to 8.0 MHz [64, 65]. Along with these measurements, they also measured the attenuation spectra before, during, and after applying a hydrostatic pressure of 16 kPa (120 mmHg) for 30 seconds to investigate the bubble resistance to the surrounding pressure. When performing the measurement on the contrast agent NC100100 (Nycomed AS, Oslo, Norway), which is similar to Sonazoid and contains microbubbles with a perflourocarbon gas core encapsulated in a surfactant membrane, three interesting observations were made. First, a shift of 0.8 MHz toward higher frequencies was seen in the attenuation spectra. At the same time, a decrease of 10 dB in the amount of attenuation was also observed when increasing the pressure. Furthermore, both these effects were seen to be reversible as the attenuation spectra was the same after releasing the ambient pressure as before it was applied. Beside these effects, one more thing could, possibly, be concluded from the results presented in [63] as the amount of acoustic attenuation seems to

be dependent on the excitation frequency. Finally, it is stated that the above effects are dependent on the type of microbubbles. Thus, it is noted that air-filled particles encapsulated in a polymeric shell seems to be insensitive to the applied overpressure while a third type of microbubbles disappeared when the ambient pressure was increased [63]. This conclusion makes future studies with the third generation contrast agents very interesting.

Initial experiments by Bouakaz et al. 1999 [62] supported the findings by Hoff and Sontum [63], indicating an increase in resonance frequency when a static over pressure is applied. However, when measuring the frequency shift of Quantison (Quadrant, Nottingham, UK), which consists of air bubbles encapsulated in human albumin, it was concluded to be too small to provide a measure which is sensitive enough for measuring small ambient pressure changes. Instead, they suggested an approach for measuring the disappearance time of free bubbles [62, 66]. These were generated at the region of interest by rupturing the microbubbles using a low-frequency high acoustic amplitude pulse, as demonstrated by Frinking et al. 1999 [67]. The decay in echo response was then determined with a second transducer positioned perpendicular to the first using a sequence of excitation pulses with low acoustic pressure. Using this approach, they showed that the scattered energy of the free bubbles decreases exponentially as a function of time. Furthermore, measuring the disappearance time at four different hydrostatic overpressures between 0 and 26.7 kPa (200 mmHg), they found that it decreases as the ambient pressure is increased. These findings were compared to theoretical predictions, using the differential equation (2.4) describing the bubble size as a function of time, and concluded to be in close agreement. Despite successful *in vitro* experiments and suggestions for further sensitivity improvements [66], no *in vivo* results or further investigations using this approach have been presented yet. Part of the explanation might be found in Tickner et al. 2001 [68] who claim that the approach will be inaccurate in the presence of noise. To circumvent this, Tickner et al. suggested to use the same high intensity excitation pulse for generating the free bubbles and for monitoring the decay in energy response of a sample population. Like Bouakaz et al. [62], they also found the decay to be exponential and getting shorter with increasing ambient pressure. Moreover, they demonstrated that the sensitivity increases when the initial bubble size is decreased or a higher acoustic pressure is used [68]. However, both of these solutions will put a further limitation to the maximum ambient pressure possible to detect. For a sample of biSphere (Point Biomedical Corporation, San Carlos, CA) encapsulated microbubbles of air with a diameter of 4 μm, the accuracy of this method was found to be approximately 10.3 kPa (77 mmHg) when testing in the pressure range from 0 to 20 kPa (150 mmHg).

Around the same time, Shi et al. 1999 [69] investigated the response of a custom designed (*in vitro* batch) suspension of the galactose-based contrast agent Levovist (Schering AG, Berlin, Germany) at five different hydrostatic pressures in the range from 0 to 24.8 kPa. For this, they used a setup with two single element transducers positioned at an angle of approximately 60 degrees to each other and separated from the liquid containing the contrast agent by a thin plastic window. After injecting the contrast agent, the ambient pressure was adjusted and the ultrasound data was acquired at exactly the same time after injection at each pressure level. This procedure, thereby, significantly reduces factors like time dependency and dissolution. From the measurements, they found that the response of the first and second harmonic component is almost insensitive to changes in the pressure surrounding the microbubbles. The amplitude of the subharmonic component, however, was shown to decrease linearly (in logarithmic scale) by 9.9 dB when the surrounding pressure was increased from 0 to 24.8 kPa. Based on these findings, they proposed the concept of subharmonic aided pressure estimation (SHAPE), which potentially, can estimate internal pressure variations by transmitting at one frequency but re-

ceiving at half that frequency using filtering techniques. The idea of utilizing the subharmonic signal amplitude to estimate pressures was, furthermore, claimed in a U.S. patent in 1999 [70]. In 2005 Forsberg et al. [71] performed an *in vivo* experiment on two mongrel dogs for proof of concept of this approach. For this, the same transducer setup, positioning two transducers at an angle of 60 degrees to each other, was used. However, as real-time imaging was not possible during the measurement, the transducers were placed blindly. Furthermore, to establish direct contact between the transducers and the aorta, an incision to the vessel was performed. This setup made it *extremely difficult to obtain consistent data* but a reduction of 9 dB in subharmonic amplitude was still observed as the blood pressure increased from 2.7 to 8.0 kPa (20 to 60 mmHg) [71]. As this is the same amount of reduction as for the laboratory experiment in [69], but measured over a significant lower pressure interval (5.3 kPa), other factors must also affect the result. Since then, the same group has investigated different contrast agents in test measurements in the laboratory, all using the same measurement setup with two transducers positioned at confocally right angles to each other as presented in [69]. In total, the following six contrast agents has been investigated: Levovist, Definity (Lantheus Medical Imaging, N Billerica, MA), Optison (GE Healthcare, Princeton, NJ), Sonazoid (GE Healthcare, Oslo, Norway), QFX (Nanfang Hospital, Guangzhou, China), and ZFX (Zhifuxian, Xinqiao Hospital, the Third Military Medical University, Chongqing, China). The results are briefly summarized by Leodore et al. 2007 [72, 73] and again in Forsberg et al. 2008 [74], which also includes the results using the two agents from China. The results for all experiments are extremely similar, almost suggesting that the is no difference between the contrast agents. When increasing the ambient pressure from 0 to 24.8 kPa, the amplitude of the fundamental and second harmonic component reduces by 2.4 and 1.8 dB, respectively for all the agents [74]. The amplitude reduction of the subharmonic component varies slightly more between agents and is seen to decrease by 9.9 dB for Levovist to 13.3 dB for Sonazoid [74]. As a last note in [74], it is mentioned that a mode for subharmonic imaging has been implemented on a Logic 9 ultrasound scanner system. This was used to test SHAPE in real-time on a tissue mimicking phantom connected to a peristaltic flow pump, which is used to mimic the blood pressure. Unfortunately, the documentation describing the implementation and measurement procedure is very poor and the results few. But mimicking the blood pressure of the femoral artery with ambient pressure seems to produce extremely good results with a sensitivity of approximately 0.5 kPa (4 mmHg). Please note that this is based on this author's personal observations as no comment or discussion regarding the results is given in [74]!

Adam et al. 2005 [75, 76] has performed a thorough study investigating the behavior of Optison microbubbles under different ambient pressure conditions. Beside investigating the acoustic scattering and attenuation under constant elevated pressures, they also studied the dynamic changes. This was carried out using cyclic ambient pressure to mimic left ventricular pressure changes in the pressure range 0 to 20 kPa. The investigation was carried out using a single element transducer as transmitter/receiver and a hydrophone for the corresponding attenuation investigation. In the study, they found that the amplitude of the subharmonic response is highly correlated to the cyclic ambient pressure but the correlation takes between 50 and 100 seconds to build up. As the amplitude of the response is also affected by the amount of the maximum ambient pressure, they conclude that *in vivo* blood pressure may be estimated from the amplitude of the subharmonic response. The correlation, however, only exists for a limited amount of time (135 seconds) when the ambient pressure is increased further to variate between 0 and 25 kPa, possibly because of rapid bubble destruction under these pressure conditions [75].

Despite the many experiments and attempts to describe the pressure dependent behavior, no real

parameter study has been performed until 2008. At this time, Andersen and Jensen [77, 78] (Chapter 4) investigated the fundamental and subharmonic response as a function of driving pulse and ambient over pressure through simulations. The main purpose was to optimize the subharmonic sensitivity to the ambient pressure and two very clear tendencies were found. First, the linear reduction of the subharmonic component, or the pressure sensitivity, is dependent on the acoustic driving pressure and peaks when in the upper end of the growth stage, which occurs when the acoustic driving pressure causes the subharmonic to increase rapidly from background noise level to be clearly visible in the spectrum. Second, the investigation also showed a clear relation between ambient pressure sensitivity and the length of the driving pulse. Thus, the sensitivity was found to increase as the pulse length is increased.

The majority of the experiments just described have been carried out under near-optimum measurement conditions to demonstrate the proof of concept using the respective approaches. In 2008, Andersen and Jensen [79, 80] (Chapter 5) presented an experimental design which resembles a realistic clinical setup using a single transducer for acquiring the scattered ultrasound data. The setup was tuned to investigate the subharmonic ambient pressure sensitivity based on the findings by Shi and colleagues [69, 71] and Adam et al. [75]. Using this setup, it was not possible to detect the sensitivity of the subharmonic amplitude as demonstrated in [69]. However, using the relation of the subharmonic energy to the energy of the fundamental component, a clear ambient pressure dependent behavior was observed indicating this to be a more robust measure for clinical use. Despite a relatively high standard deviation, a resolution of ± 3.66 kPa was achieved in one of the measurements. However, this was obtained using an excitation pressure of 500 kPa and indications of bubble destruction were seen.

CHAPTER

FOUR

Theoretical parameter study

Although the human blood pressure varies between 0 and approximately 25 kPa (1 kPa = 7.5 mmHg), it should still be possible to distinguish pressure differences as low as 1-3 kPa to measure the blood pressure in the small veins and arteries. Therefore, the sensitivity is a crucial factor when evaluating new approaches for non-invasive local blood pressure measurements. The theory as well as experimental measurements show that the microbubble response is very dependent on how the bubble is being excited. Furthermore, as initial theoretical experiments indicated that the ambient pressure sensitivity changes according to the driving pulse, a parameter study was initiated. For this, an existing simulation model has been used to examine the response at different ambient pressure settings using numerous excitation variations. When tuning the the driving pulse, factors like shape, length, and acoustic pressure were varied to investigate the importance. The following sections is an extraction from the journal paper [78] in Appendix D.2, which is initially based on the conference paper [77] in Appendix D.1.

4.1 Method

The investigation has been performed using the Matlab (The Math Works Inc., Natick, Mass., USA) environment. To carry out the simulations, the free simulation program Bubblesim by Hoff [2] is used. Bubblesim is a toolbox that calculates the oscillation and scattered echo for a specified contrast agent microbubble and excitation pulse. It numerically solves a second order ordinary differential equation (ODE) that has been combined from a set of equations, each equation modeling different parts (bubble, shell, and surrounding liquid) of the system that makes up a contrast agent microbubble. In Bubblesim, the following four different models are implemented: The Rayleigh-Plesset [33] (R-P) model, the Trilling [81] model, the Keller-Miksis [82] model, and a modified version of the R-P model, which is an intermediate model of the R-P on one side and the Trilling and Keller-Miksis models on the other. The largest disadvantage of the R-P model is that it does not include radiation damping, which is energy loss caused by radiation of sound. This is accounted for in the Trilling and the Keller-Miksis models, which both include a finite but constant speed of sound in the liquid. However, both the Trilling and Keller-Miksis model has a risk of becoming numerical unstable when the bubble wall velocity becomes comparable to the speed of sound (acoustic Mach numbers, $M = \dot{R}/c$, around unity). This happens for high oscillation amplitudes and causes the models to have an unphysical negative inertia. Instead, Hilgenfeldt et al. [83] have used a modified version of the R-P model that includes the radiation damping term from the Trilling and Keller-Miksis models. This version is implemented in Bubblesim and the model selected for the parameter investigation. It was chosen because of its numerical stability, which is important when doing

many simulations spanning a wide range of variable changes. The modified R-P model is [2]

$$\rho R\ddot{R} + \frac{3}{2}\rho\left(\dot{R}\right)^2 - p_L + p_{ov} + p_{ac}(t) - \frac{R}{c}\cdot\dot{p_L} = 0, \tag{4.1}$$

where ρ is the surrounding liquid density, R is the bubble radius, $\dot{R} = \frac{dR}{dt}$ denotes derivation w.r.t. time t, p_L is the pressure at the bubble surface, p_{ov} is the static background overpressure, p_{ac} is the driving acoustic pressure, and c is the speed of sound. The first term describes the pressure as function of the bubble wall acceleration, whereas the second term describes the pressure as a function of the bubble wall velocity. $p_\infty = p_{ov} + p_{ac}$ is the background pressure describing the pressure in the liquid far from the bubble surface. p_L includes contributions from the gas, the viscosity, and the effects of the shell encapsulating the bubble. Finally, the last term including $\dot{p_L} = \frac{dp_L}{dt}$ is the one accounting for the radiation damping. Any numerical solver can be used to solve the ODE in (4.1). Examples are the Runge-Kutta algorithm of order 4 and 5 (`ODE45`) and the multistep ODE solver of variable order from 1 to 5 (`ODE15s`), which are both available in Matlab as a standard. In this study, the solver of variable order has been selected as it should be more reliable and stable for solving situations where the differential equation becomes stiff [2]. This occurs for example when the bubble radius changes slowly during the expansion phase but goes through very fast changes in radius and velocity under compression. The choices on simulation model and numerical solver, as well as other general setup parameters, for the simulations in this study are summarized in Table 4.1.

Parameter	Designation
ODE solver	`ODE15s`
Simulation model	`Modified Rayleigh-Plesset`
Thermal damping	`Isothermal`
Liquid	`Water`

Table 4.1: List of simulation parameters regarding the general setup of Bubblesim.

In its standard form, Bubblesim has a flexible graphical user interface, which makes it easy to perform single simulations for minor investigations. In this study, a batch mode has been created for two reasons: It gives a bit more control and, more importantly, it makes it possible to perform multiple simulations automatically, which is essential in a parameter study like this. Furthermore, one modification has been made to Bubblesim. In its original form, it is not possible to change the ambient overpressure parameter denoted p_{ov} in (4.1). Since this is crucial, when investigating microbubbles' sensitivity to ambient pressure changes, this feature has been enabled by small modifications to the source code.

While the bubble size distribution can be determined with a multisizer, it is somewhat more difficult to specify the parameters related to the surrounding shell of today's UCA microbubbles. One way to do this is to perform a combination of experiments and model fitting as described by de Jong and associates [84, 34, 2]. This will, however, only give an estimate of proper designations and usually an interval for some of the parameters is given. The procedure has been used by Yu et al. [85] and Hoff [2] to estimate suitable parameters for the commercial contrast agents Levovist (Schering AG, Berlin, Germany) and Sonazoid (GE Healthcare, Oslo, Norway), respectively. These values used in the investigation were fixed for all simulations and are listed in Table 4.2. Before a simulation can be carried out, a driving pulse must be selected. Since the emphasis of this study was to optimize the subharmonic sensitivity to ambient pressure changes as a function of the excitation pulse, a large number of different driving pulses

Contrast agent	Bubble Radius [μm]	Shell Thickness [nm]	Shear Modulus [MPa]	Shear Viscosity [Pa s]
Levovist	3.0	6.0	80	1.3
Sonazoid	3.2	4.0	52	0.99

Table 4.2: List of the parameters from Yu et al. [85] and Hoff [2] used to describe the two different types of bubbles for the simulations in Bubblesim.

were examined. The driving pulse was generated based on four different characteristics being the center frequency, f_c, the number of pulse cycles, N_c, the maximum acoustic pressure, p_{ac}, and the shape of the pulse. The possible designations used for the investigation are listed in the upper part of Table 4.3. The center frequency was selected based on a preliminary study optimizing the energy of the subharmonic component to the fundamental as shown for Sonazoid in Fig. 4.1. As can be seen from Table 4.3, 30 different settings for the acoustic pressure is used.

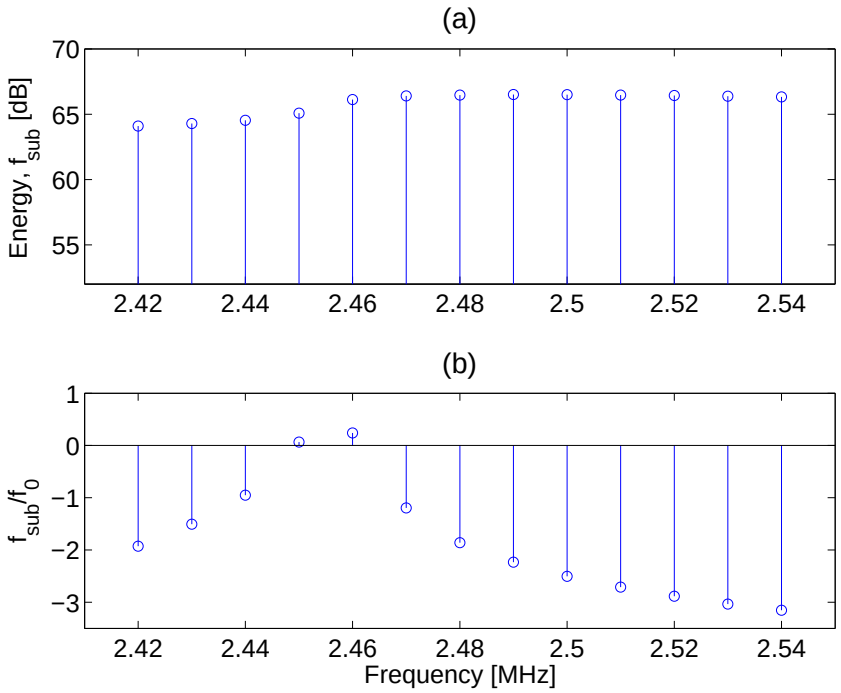

Figure 4.1: (a) shows the energy of the subharmonic component as a function of emitted frequency, while (b) shows the relation of the subharmonic to the fundamental component.

This was decided to ensure determination of the growth stage of the subharmonic component with a reasonable precision. Although an acoustic pressure of 950 kPa will probably destroy the microbubbles in real measurements, the high values were selected to cover the entire range of subharmonic growth and saturation. The bottom row of Table 4.3 lists the designations of the ambient overpressures which were used in the simulations. As can be seen, the range covers the interval between 0 and 25 kPa in steps of 5 kPa. In this way, the most common human blood pressure values are covered. Combining all the parameters in Table 4.3 gives a total of 3600 different simulations for each contrast agent.

When Bubblesim has completed a simulation, the simulated scattered pressure is returned and the Fourier transformation is applied. Next, a search for the fundamental (f_0), the first subhar-

Parameter	Designation	Unit
f_c	2.06 2.46	[MHz]
N_c	1 2 5 10 20 32 48 64 128 256	[cycles]
p_{ac}	100 150 200 250 275 300 325 350 375 400 425 450 475 500 550 575 600 650 675 700 725 750 775 800 825 850 875 900 925 950	[kPa]
Pulse shape	'rectangular' 'hanning'	
p_{ov}	0 5 10 15 20 25	[kPa]

Table 4.3: List of parameters used in combination with the contrast agents listed in Table 4.2. Combining all settings gives 3600 simulations in total for each agent.

monic ($\frac{1}{2}f_0$), and the second harmonic ($2f_0$) component is performed and the energy of each component is calculated. The center frequencies of the harmonic bands were selected as multiples of the emitted center frequency, f_c. It should, however, be noted that initial simulations show that the frequency of the subharmonic component shifts slightly as the acoustic driving pressure is increased. The energy has been chosen over the peak amplitude since this is a more robust measure. The bandwidth to calculate the energy within was selected as the -10 dB bandwidth of the excitation pulse.

4.2 Results and discussion

This section presents the results obtained through the simulation study. First, the fundamental, subharmonic, and second harmonic dependence on acoustic pressure will be presented. This is a natural step for two reasons: First of all, generation of the subharmonic component must be ensured before looking into the ambient pressure dependency. Another reason is to see at which acoustic pressures the growth stage of the subharmonic occurs for the two types of microbubbles. Along with this investigation, the scattered responses and spectra have been examined to ensure useful responses and proper selection of the bandwidth intervals to calculate the energy of the respective frequency components within. Since these results are rather trivial and takes up a lot of space, only a few selected examples are presented in this section. In the last part of this section, the influence of ambient overpressure will be examined.

4.2.1 Dependence on acoustic pressure

Fig. 4.2 shows the energy of the subharmonic, fundamental, and second harmonic component of Sonazoid as a function of acoustic pressure when a rectangular driving pulse for a different number of cycles is used. Each curve has been normalized by 88 dB, which corresponds to the maximum energy observed among all simulations for both agents. Examining the subharmonic component, three characteristic stages are clearly observed. In the occurrence stage for acoustic pressures below 300 kPa, the subharmonic is weak compared to the other components. For acoustic pressures in the interval between 300 kPa and 425 kPa, the subharmonic increases rapidly and this part can be characterized as the growth stage. When increasing the acoustic pressure further, the growth eases off and can be compared to the saturation stage observed in measurements. Finally, when the acoustic pressure exceeds 875 kPa the energy decreases again. At these levels, the corresponding spectra look more noisy and should be discarded. The

pattern is the same for pulses of other lengths than displayed here, although the subharmonic component cannot be distinguished from the fundamental for driving pulses smaller than 5 cycles. The chaotic behavior at high acoustic pressure levels predicted in the simulations is actually in good correspondence with experimental results of free bubbles achieved by Lauterborn and Cramer [86]. Looking at the fundamental, it increases almost linearly as expected. However, a slight drop is seen in the pressure interval corresponding to the growth stage of the subharmonic.

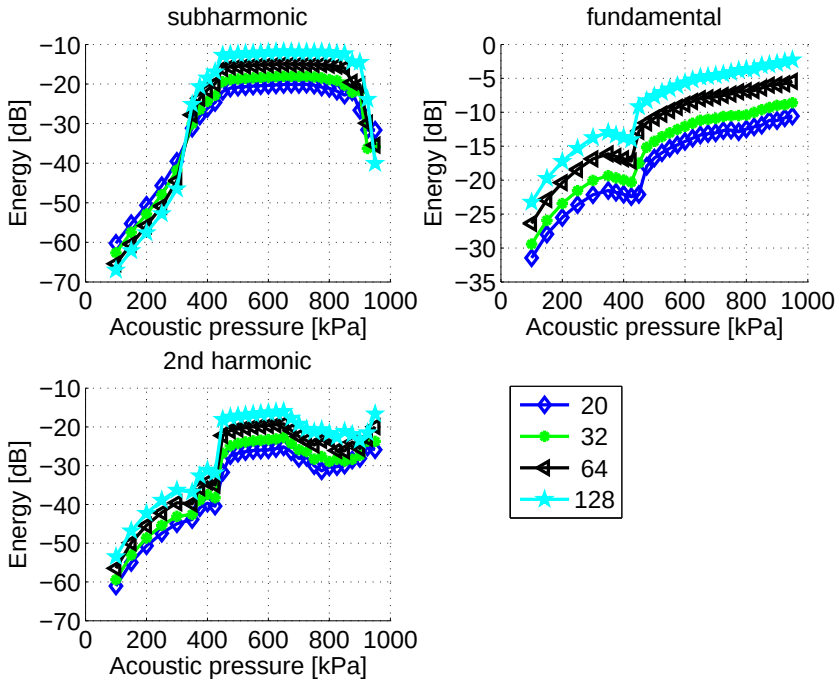

Figure 4.2: Energy as a function of acoustic pressure for Sonazoid. The driving pulse is a rectangular shaped sinusoid. Upper left graph shows the subharmonic behavior, upper right shows the first harmonic, and lower left presents the behavior of the second harmonic component. Each curve represent a different number of cycles in the driving pulse as displayed in the legend to the lower right in the figure.

When the shape of the driving pulse is changed by applying a Hanning window, especially the subharmonic and second harmonic change behavior as can be seen in Fig. 4.3. Regarding the subharmonic component, the three stages pattern is the same as observed for the rectangular driving pulse, although the interval of the growth period seems to have increased. This makes sense since less energy is transmitted using a Hanning shaped driving pulse compared to a rectangular signal of the same acoustic strength. Another interesting observation is that the acoustic pressure interval of the growth stage now is more dependent on the length of the driving pulse. The same pulse length dependent behavior is also seen for the second harmonic component. The fundamental, on the other hand, does not seem to be affected much although the small drop in energy observed for the rectangular driving pulse is hardly visible anymore.

The results for the simulations of Levovist as a function of acoustic pressure using a rectangular driving pulse is shown in Fig. 4.4 (a). Once again, the three stages behavior of the subharmonic component is observed. However, now the growth stage first occurs in the interval from 600 to 900 kPa. Although the increase in energy is the same, the interval is much higher than experimental results achieved by Shi et al. [69], who observed it to be between 300 and 600 kPa

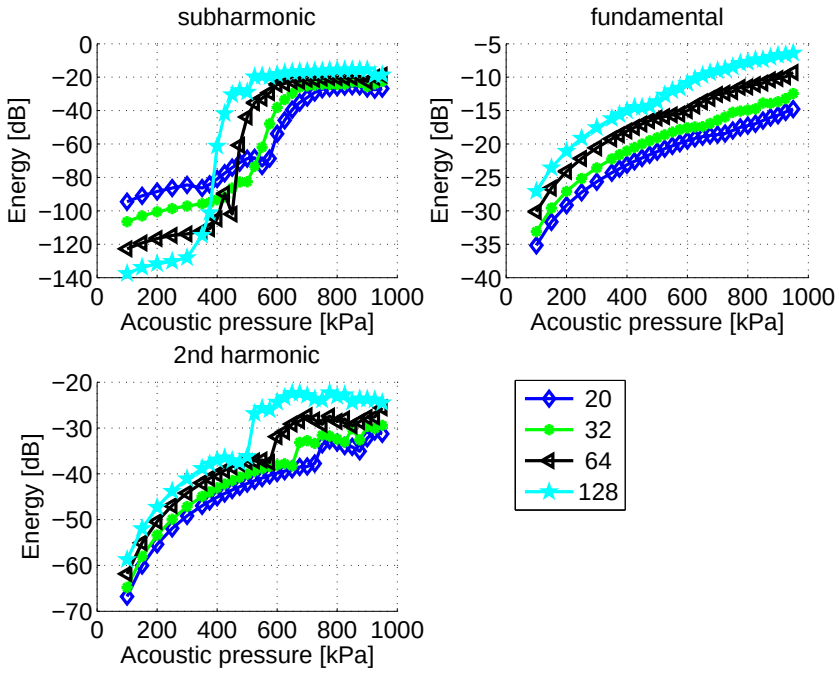

Figure 4.3: Energy as a function of acoustic pressure for Sonazoid. The driving pulse is a Hanning shaped sinusoid. Upper left graph shows the subharmonic behavior, upper right shows the first harmonic, and lower left presents the behavior of the second harmonic component. Each curve represent a different number of cycles in the driving pulse as displayed in the legend to the lower right in the figure.

for Levovist using a 64 cycles rectangular driving pulse with a center frequency of 2 MHz. The fundamental and second harmonic more closely resembles the obtained measurement results, except the simulated saturation is not as pronounced in the measurements. The simulations of Levovist using a Hanning shaped excitation pulse indicates it is very hard to generate the subharmonic component for this type of driving pulse, see Fig. 4.4 (b). In fact, the subharmonic component is hardly visible in any of the spectra, not even a the very high driving pressures. Regarding the fundamental and second harmonic component, they are similar to what was observed using the rectangular driving pulse.

Except, possibly, for the last setup, common for all the simulations is that the subharmonic component has a threshold and is present only above a certain acoustic pressure. This observation was also reported by Prosperetti [41] who examined this experimentally on free bubbles and, as mentioned, by Shi et al. [69]. One difference between the simulations and the measurements is, however, that the simulated threshold seems to be higher than the measured. A reason for this can be the selection of the shell parameters for Levovist as the simulated threshold of Sonazoid is comparable to the measured threshold of Levovist. In contrast to the threshold behavior of the subharmonic, the higher harmonics seems to be present to various degrees for all driving pressures.

Finally, one interesting observation regarding the scattered pressure, when using the Hanning shaped driving pulse for excitation of Sonazoid, should be noted. When the driving pressure is increased to a level where the subharmonic is generated, the scattered response suddenly changes characteristics halfway in the pulse as shown in Fig. 4.5 (a). In the first half, the traditional harmonic distortion is clearly observed but no subharmonics. Halfway in the signal,

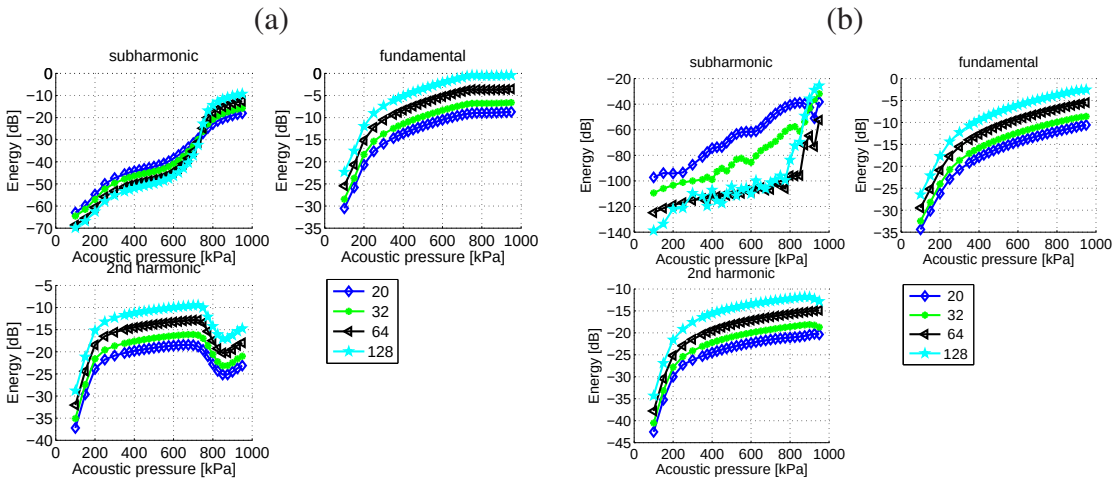

Figure 4.4: Energy as a function of acoustic pressure for Levovist. The driving pulse is a rectangular shaped (a) and Hanning shaped (b) sinusoid, respectively. Upper left graph shows the subharmonic behavior, upper right shows the first harmonic, and lower left presents the behavior of the second harmonic component. Each curve represent a different number of cycles in the driving pulse as displayed in the legend to the lower right in the figure.

the characteristic oscillation at twice the driving period is seen and continues for the rest of the scattered response. As can be seen from the corresponding spectrum in Fig. 4.5 (b), this is what gives rise to the sub- and ultraharmonics.

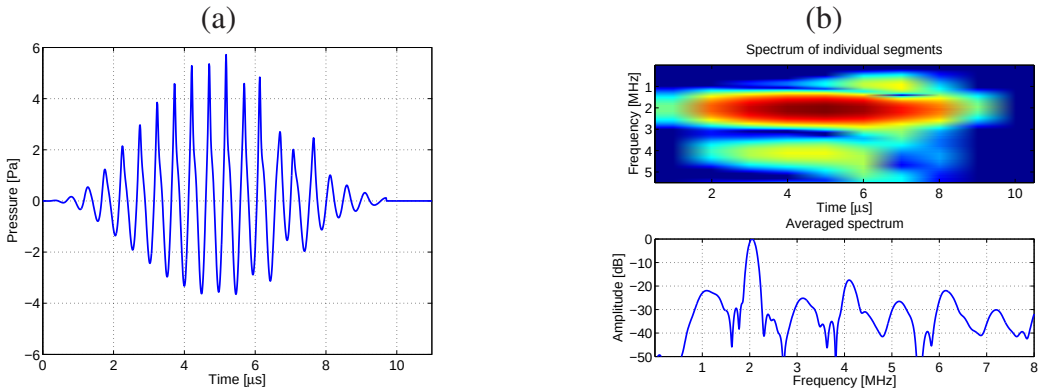

Figure 4.5: Example of scattered pressure (a) and it's corresponding spectrum (b) when using a Hanning shaped driving pulse. Sonazoid is used and the excitation is a 20 cycles Hanning shaped signal with a center frequncy of 2 MHz and an acoustic pressure of 525 kPa.

4.2.2 Dependence on overpressure

In this section, the simulation results achieved when changing the ambient overpressure will be shown. Fig. 4.6 shows an example of how the scattered spectrum changes, when the ambient pressure is the only parameter that is changed from one simulation to another. The example is for Levovist when driven by a rectangular pulse with 32 cycles and an acoustic pressure of 800 kPa. In Fig. 4.6 (a), the scattered spectrum is shown when no pressure is seen and Fig. 4.6 (b) shows the spectrum when an overpressure of 25 kPa is applied. Comparing the two spectra, a

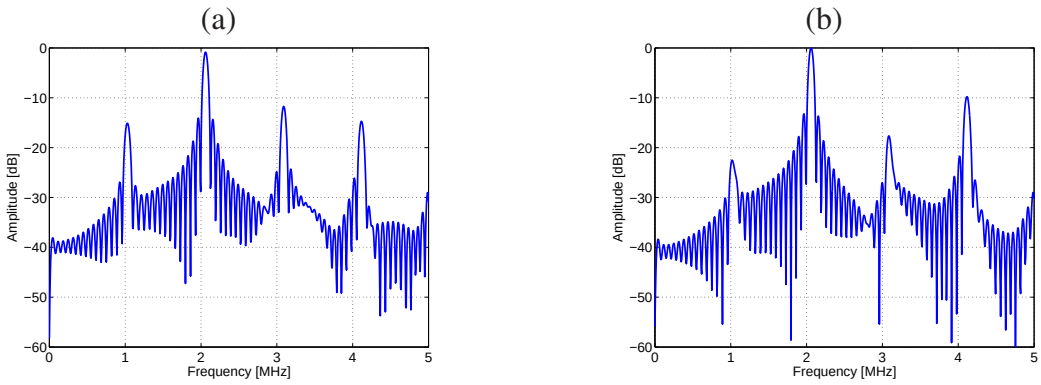

Figure 4.6: Example of spectrum of scattered response from excitation of microbubble corresponding to Levovist. The driving pulse is a 32 cycles rectangular shaped signal with a center frequncy of $f_c = 2$ MHz and an acoustic pressure of $P_{ac} = 800$ kPa. (a) is when no overpressure is applied and (b) shows the response when a overpressure of 25 kPa is applied.

clear reduction of the subharmonic component at 1 MHz is observed. Looking at the fundamental at 2 MHz and the second harmonic component at 4 MHz, it is seen that these increases when overpressure is applied. In fact, this is a clear tendency from many of the simulations.
Fig. 4.7 shows the effect on the subharmonic component when the pulse length is varied. It displays the energy of the subharmonic component when using the same setup as used to create Fig. 4.6. There is a clear tendency for all pulse lengths that the energy decreases as the over-

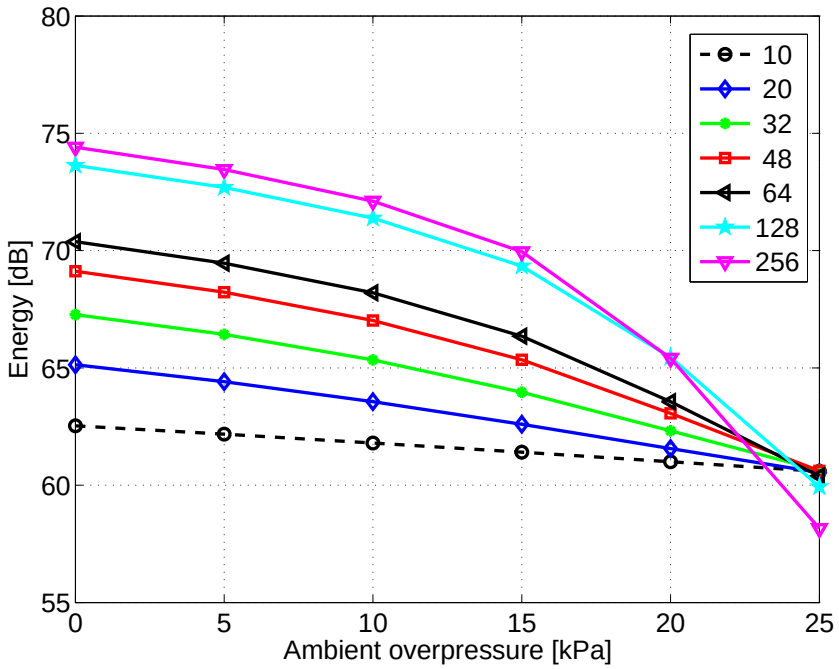

Figure 4.7: Energy of the subharmonic component scattered by Levovist when using a rectangular shaped driving pulse with an acoustic pressure of 800 kPa. The energy is displayed as a function of ambient pressure and each curve in the plot represents a different number of cycles in the driving pulse as indicated by the legend.

pressure is increased. Furthermore, the total decrease in energy also seems to be dependent on the number of cycles in the driving pulse. However, Fig. 4.7 also indicates that the decrease is

not completely linear in all cases. For easy comparison of the change in energy for the different simulation setups, Fig. 4.8 shows the energy of the three frequency components as function of ambient overpressure when each simulation has been normalized to their respective maximum. Looking at the results for the fundamental, it is seen that this component is not affected by

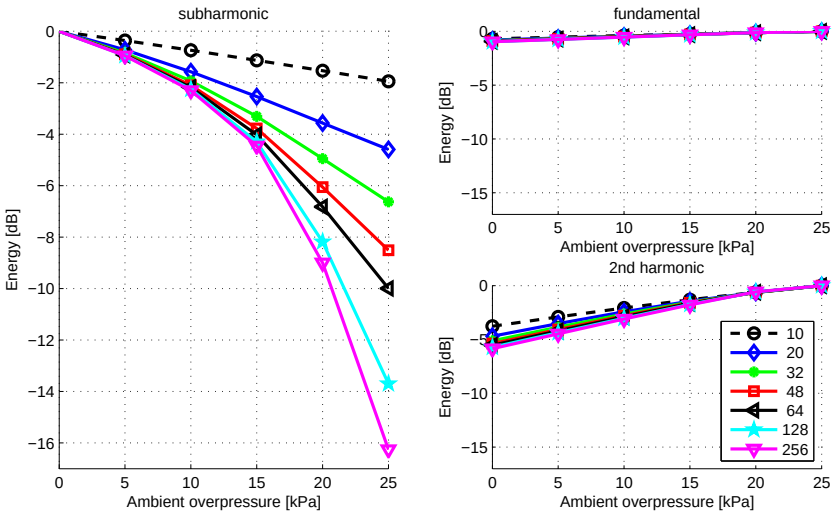

Figure 4.8: Decrease in energy of respective frequency components scattered by Levovist when using a rectangular shaped driving pulse with an acoustic pressure of 800 kPa. The energy is displayed as a function of ambient pressure and each curve in the plots represents a different number of cycles in the driving pulse as indicated by the legend.

ambient pressure changes. The second harmonic seems to be affected and increases about 5 dB, slightly dependent on the pulse length. This increase is quiet in contradiction to the experiments by Shi et al. [69], who excited Levovist in the growth stage using a 64 cycles rectangular pulse. They found that the second harmonic decreases by 1.8 dB over the same ambient pressure interval. When examining the subharmonic in Fig. 4.8, a highly pulse length dependent decrease is observed. As the number of pulse cycles is increased, the reduction in energy also increases. However, the decrease becomes less linear as the pulse length increases. For the driving pulse with 64 cycles, a decrease of 9.9 dB is found. This is in very good agreement with the experimental results by Shi et al. [69], who measured a reduction of 9.6 dB.
Fig. 4.9 shows the ambient pressure sensitivity of the subharmonic component when the ambient pressure is increased from 0 to 25 kPa. The sensitivity corresponds to the absolute reduction divided by 25 and is shown as a function of the acoustic pressure and number of pulse cycles. Fig. 4.9, thereby, summarizes 252 of the most promising simulations of Levovist. Furthermore, to get a measure of the linearity between the energy of the subharmonic component and the overpressure, a straight line has been fitted using linear regression for each simulation setup, when only the overpressure is changed. Next, the correlation coefficient, r, has been calculated to see how well a linear relationship between subharmonic energy and ambient overpressure can be assumed. The respective correlation coefficients are shown to the right in Fig. 4.9.
Fig. 4.9 shows very clearly two characteristics: The optimal driving pressure is 775 kPa, which is in the upper end of the growth stage of the subharmonic component. Furthermore, the sensitivity is increased as the driving pulse length is increased. This indicates, unfortunately, that a compromise between axial resolution and pressure sensitivity exists. The correlation coefficients to the right in Fig. 4.9 indicate a very good linearity. In fact, it can be seen that the two

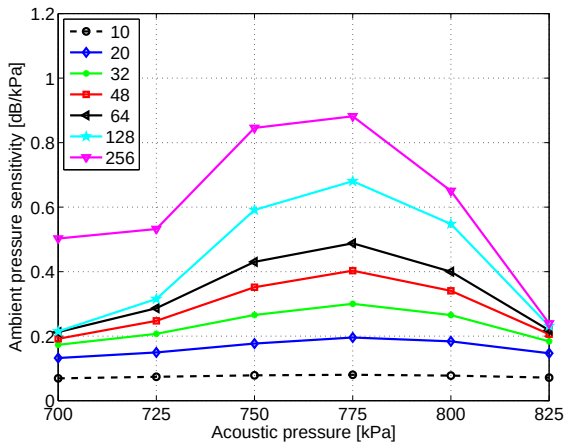

N_c	P_{ac} 700	725	750	775	800	825
10	1.00	1.00	1.00	1.00	1.00	1.00
20	1.00	1.00	1.00	1.00	1.00	0.99
32	1.00	1.00	0.99	1.00	0.99	0.99
48	1.00	1.00	0.99	1.00	0.98	0.98
64	1.00	0.99	0.99	1.00	0.97	0.98
128	0.99	0.99	0.97	0.99	0.95	0.97
256	1.00	1.00	0.97	0.99	0.93	0.97

Correlation coefficients

Figure 4.9: Ambient pressure sensitivity of the subharmonic component for Levovist when the ambient pressure is increased from 0 to 25 kPa. The sensitivity is shown as a function of acoustic pressure and number of cycles in the rectangular driving pressure. To the right, the respective correlation coefficients, when using a linear regression model, are shown.

lowest coefficients are actually for the two simulations in Fig. 4.8 with 256 and 128 cycles, respectively. The rest of the coefficients are all equal to or above $r = 0.97$. The maximum sensitivity for Levovist was achieved using a rectangular pulse of 256 cycles with a driving pressure of 775 kPa. Using this setting, a reduction of the subharmonic was simulated to be 22.0 dB ($r = 0.99$) giving a pressure sensitivity of 0.88 dB/kPa. For a shorter driving pulse with 64 cycles, the best pressure sensitivity was found to be 0.49 dB/kPa ($r = 1.0$).

Examining the results for Sonazoid gives the same indications as for Levovist, although the results are not as symmetric around a certain acoustic pressure. However, once again there is a clear tendency that a specific acoustic pressure in the upper end of the growth stage will optimize the ambient pressure sensitivity. Furthermore, the simulations also indicate the same relation between sensitivity and pulse length. The findings for Sonazoid are summarized in Fig. 4.10, which is the same as Fig. 4.9 for Levovist. Using a rectangular driving pulse with

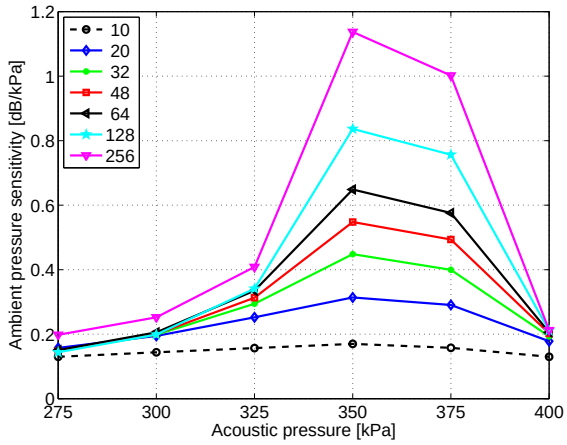

N_c	P_{ac} 275	300	325	350	375	400
10	1.00	1.00	1.00	1.00	1.00	1.00
20	0.99	1.00	1.00	1.00	0.99	0.99
32	1.00	0.99	0.99	0.99	0.98	0.99
48	1.00	0.99	0.99	0.99	0.97	0.99
64	1.00	0.99	0.98	0.99	0.96	0.98
128	1.00	0.99	0.98	0.97	0.94	0.98
256	1.00	1.00	0.98	0.96	0.90	0.98

Correlation coefficients

Figure 4.10: Ambient pressure sensitivity of the subharmonic component for Sonazoid when the ambient pressure is increased from 0 to 25 kPa. It is shown as a function of acoustic pressure and number of cycles in the rectangular driving pressure.

256 cycles, a maximum pressure sensitivity of 1.14 dB/kPa ($r = 0.96$) was found. For a driving pulse with 64 cycles, the best sensitivity was found to be 0.65 dB/kPa with a linear correlation coefficient of $r = 0.99$.

4.3 Conclusion

A simulation study consisting of 7200 simulations has been carried out to investigate and optimize the subharmonic response sensitivity to ambient pressure changes. Two different types of ultrasound contrast agents, corresponding to Levovist and Sonazoid, were simulated. While the parameters of the microbubbles were kept fixed, the parameters describing the driving pulse and ambient overpressure were changed in each simulation. The initial simulations showed that the subharmonic component is more easily generated using a rectangular shaped driving pulse compared to a Hanning shaped signal. For the case of Levovist, it was not possible to generate the subharmonic using the Hanning shaped excitation even for very high acoustic driving pressures. This dissimilarity in responses makes a study of the differences in shell properties of Levovist and Sonazoid interesting. Investigations of the subharmonic energy as function of ambient overpressure showed two tendencies very clearly: The amount of reduction in energy of the subharmonic component is dependent on acoustic driving pressure and peaks when the acoustic pressure is in the upper end of the growth stage. Second, the investigations also showed a clear relation between the amount of energy reduction and length of the driving pulse.

4.3.1 Future perspectives

Since an ultrasound contrast agent does not consist of microbubbles of exactly the same size, it would be interesting to investigate the behavior and accuracy when simulating a population of bubbles. Therefore, a new parameter study should include a distribution of bubbles with slightly different properties. As a start, the radius of the bubbles could vary according to the size distribution known for most contrast agents. For the specific agents, Levovist is known for a wide population of bubble sizes while the third generation agent Sonazoid has more uniform bubbles. In this way, the importance of a narrow size distribution could be investigated.

CHAPTER

FIVE

Experimental measurements

This Chapter describes the experiments which have been carried out in the laboratory during this thesis. The measurements carried out in this project have all been phantom experiments, meaning the contrast agent has been injected into a chamber filled with either water or saline. As all the experiments have been carried out using the same measurement setup and signal processing, this is presented in Section 5.1 before presenting the two different types of measurements and corresponding results. The purpose of the first type of measurement was to investigate the microbubble response as a function of the amplitude of the excitation pulse. This is presented in Section 5.2. The second type of measurement has investigated the ambient pressure sensitivity by subjecting the microbubbles to different hydrostatic overpressures. The measurement procedure and achieved results of this experiment is presented in Section 5.3. Chapter 5 ends with a small summarizing discussion including suggestions for future interesting investigations.

5.1 Experimental measurement setup

To investigate the ambient pressure sensitivity of a contrast agent, a measurement setup consisting of a sealed chamber with functionality for controlling the pressure inside is required. Fig. 5.1 and Fig. 5.2 show a block diagram and a photo of the experimental setup, which has been designed to carry out the measurements in this thesis. The setup can be divided into four parts and the last three of these are described in further details in the following subsections. The first part is a single standard PC equipped with connections for ethernet and serial communication running Matlab (The MathWorks Inc., Natick, MA) under Linux. This is the main part used to control the experiment regarding timing, ultrasound acquisition, and ambient pressure regulation. The next part is used for the ultrasound acquisition, which is carried out using the experimental ultrasound scanner RASMUS [87]. This part is controlled from the PC through an ethernet connection. For the acquisition, a single array transducer is connected to the RASMUS system. This is a unique solution for this type of contrast agent experiment as the literature usually has presented a setup using a single element transducer [75, 76] or a separate transmitter and receiver. Thus, Shi et al. 1999 [69] explain that the advantage of utilizing a separate transmitter and receiver is that the scattered response is limited to come from the microbubbles in the confocal region of the two transducers. However, a setup consisting of two transducers will most likely never work in a clinical environment as it will be difficult for the doctors to control. And the need of two transducers will also put a limitation to the possible areas that can be monitored. The third part concerns the measuring chamber. The phantom is airtight and contains the contrast agent that is injected into either degassed water or saline.

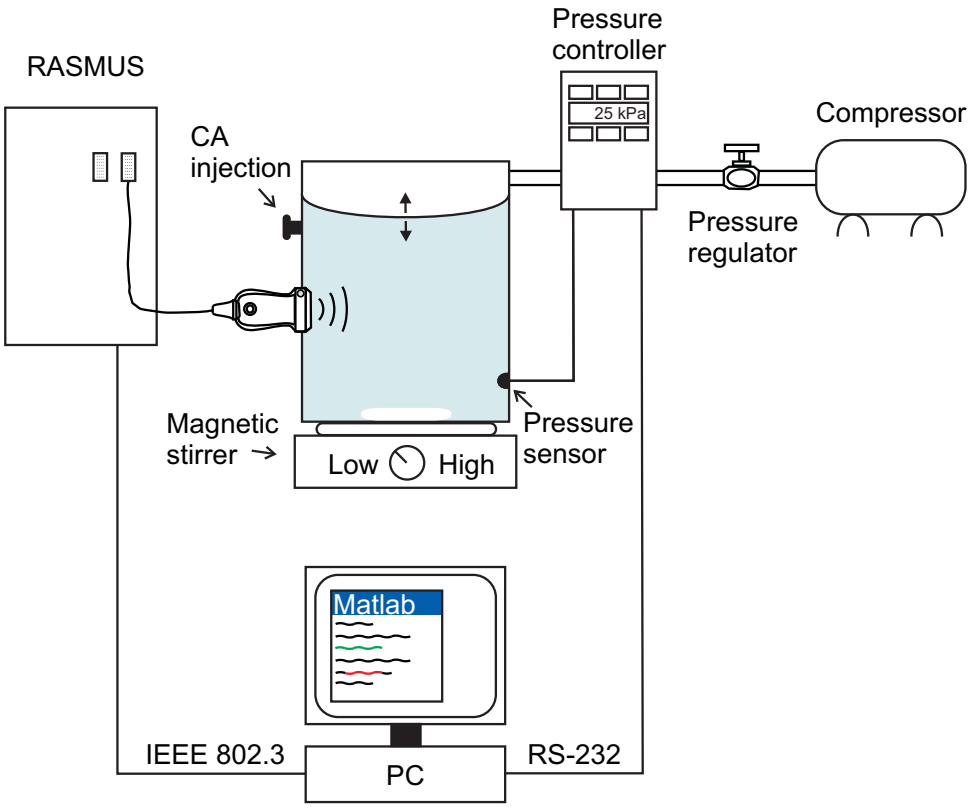

Figure 5.1: Block diagram of the measurement setup. The left part shows the ultrasound acquisition part. The right part illustrates the pressure management system.

To keep the bubbles in motion, the chamber is placed on a magnetic stirrer. The final part is for regulating the ambient pressure inside the chamber. This is adjusted automatically by a pressure controller, which is managed from the PC through a RS-232 serial connection.

5.1.1 Ultrasound acquisition

The Remotely Accessible Software configurable Multi-channel Ultrasound Sampling (RASMUS) system is a real-time ultrasound scanner specifically designed for research purposes. It is capable of controlling a 128-element transducer. Having full control of the transducer makes it possible to design unique transmission sequences. In transmission, it is possible to control all 128 elements at once, while 64 channels can be sampled at a time through a two-to-one multiplexing system in receive. It can store 16 GBytes of raw ultrasound data with a sampling frequency of 40 MHz and a precision of 12 bits for offline processing, which is essential in experiments like these. An acquisition sequence is set up and controlled through a Matlab interface on the control PC. For the experiments in this thesis, a single 64 element phased array transducer (BK Medical, Herlev, Denmark) is connected to the RASMUS system. The transducer was selected based on a preliminary study investigating the frequency bandwidth of four suitable transducers available in the laboratory. The study and corresponding considerations can be seen in Appendix A, while the two-way impulse response and frequency spectrum of the chosen transducer is depicted in Fig. 5.3. The transducer is a prototype from BK Medical and was mainly selected over the other suitable candidates, in respect to the bandwidth, because of its physical small size. As can be seen, the frequencies at 2 MHz and 4 MHz

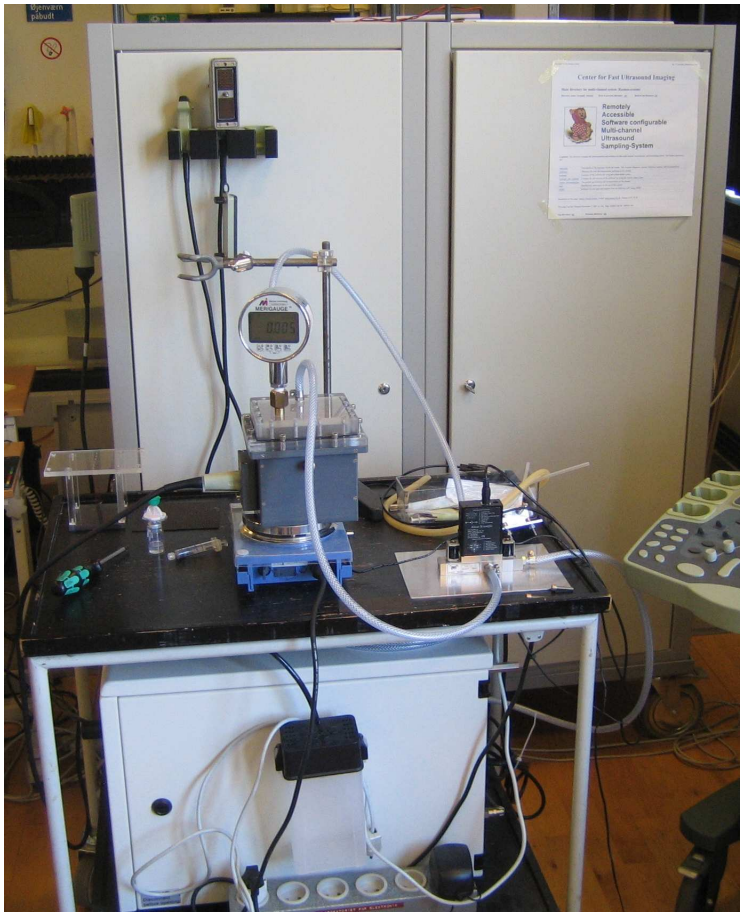

Figure 5.2: Picture of the measurement setup in the laboratory. The compressor, measurement chamber, magnetic stirrer, pressure controller, and connecting tubes are placed on the table in front of the experimental ultrasound system, RASMUS, covering the background. Also, a vial with contrast agent from SonoVue can be seen to the left on the table.

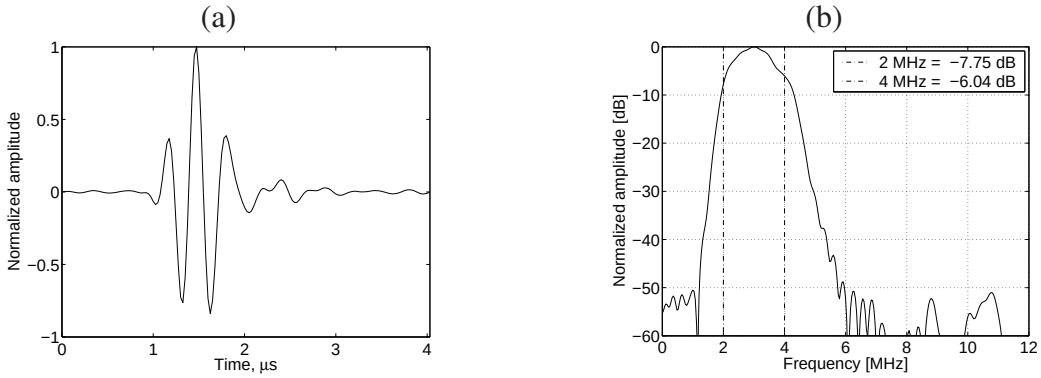

Figure 5.3: Two-way impulse response (a) and the corresponding frequency spectrum (b) of the selected transducer, which is a prototype from BK Medical. It has a center frequency of 3 MHz and a -6 dB bandwidth of 60 percent.

are almost attenuated the same without being attenuated too much. This makes the transducer very suitable for the measurements involving non-linear contrast agents, since both the fundamental and subharmonic component can be acquired. The most important properties of the

transducer are listed in Table 5.1, while the complete specifications can be seen in Table A.1 in Appendix A.

Parameter	Designation
Transducer type	Phased array
No. elements	64
Center frequency	3 MHz
Bandwidth (-6 dB)	60 %
Pitch	0.26 mm

Table 5.1: Properties of the selected transducer.

5.1.2 Measurement chamber

The measuring chamber is airtight and consists of two parts separated by a rubber membrane. A photo of the actual design and a corresponding illustration sketching the dimensions can be seen in Fig. 5.4 and Fig. 5.5, respectively. The bottom part is made of rigid PVC (polyvinyl chloride), which is a robust plastic material. The inner walls are coated with acoustic damping material with a thickness of 1 cm used to reduce ultrasound reflections from prior emissions. Inside, the chamber measures 7.9x7.9x9.7 cm (WxLxH) yielding an inner volume of 605 ccm, which is filled with either water or saline. The sides of the chamber has three sealed holes. One is for connecting the transducer and the other two are inlets for fast injection of contrast agent and a sensor to monitor the pressure inside the chamber, respectively. To fix the transducer, a holder is sealed to the side by four bolts. A rubber pad is furthermore put in between the holder and the phantom to keep the chamber airtight. The lid is fixed to the bottom part by eight bolts ensuring a steady and firm hold. It is made of acrylic plastic and has two inlets. One inlet is for a pressure gauge (3900 MeriGauge, Meriam Process Technologies, Ohio), which can be used for manual observation of the pressure. The other inlet is used to regulate the pressure by inflating and exhaling compressed air. To prevent the inflated air to be mixed with the bubbles injected into the liquid, a 1 mm thick rubber membrane is placed in between the two chamber parts. To ensure a constant pressure all over, and to prevent a large ripple when adjusting the pressure, a cavity with a dead volume of 12.5 ccm has been hollowed out in the lid. The magnetic stirrer IKA RCT (IKA-Werke GmbH & Co. KG, Staufen, Germany) is used to move a magnetic stick placed at the bottom of the measurement chamber. In this way, the microbubbles are kept in motion, thereby, preventing aggregation during the measurement [88]. The stick has a cylindric shape with a length of 5 cm and a diameter of 0.8 cm.

5.1.3 Ambient pressure regulation

The pressure is managed by a custom designed dual valve pressure controller PCD4-10PSIG (Alicat Scientific, Tucson, AZ). It is used to automatically measure and control the pressure inside the chamber. The regulation is done by opening one valve at a time. One of the valves is used to increase the pressure inside the chamber and another is used to release the pressure. The second valve, which is also managed by the controller, eliminates the need for an extra hole in the chamber (bleed port) and a corresponding relief valve. The pressure controller has been customized to have an external pressure sensor, which makes it possible to measure the

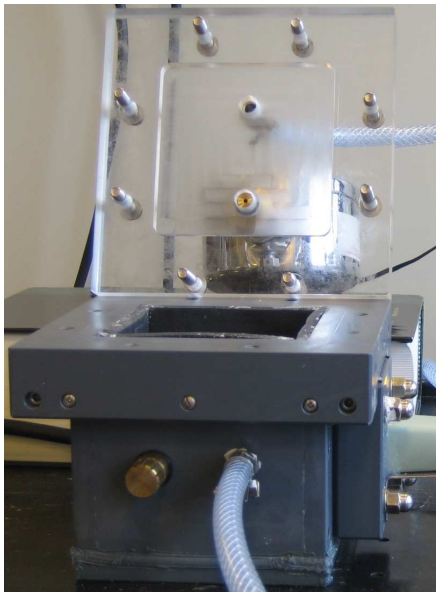

Figure 5.4: Picture of the two parts constituting the measurement chamber. To see the cavity and inlets in the lid, the rubber membrane separating the two parts has been removed.

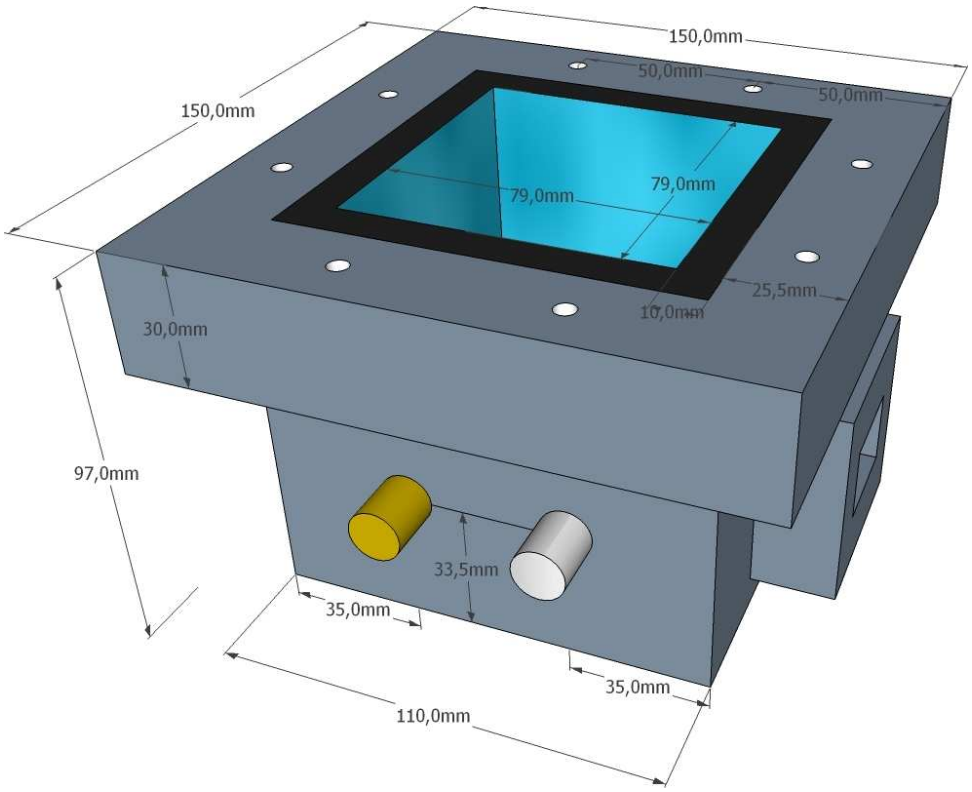

Figure 5.5: Drawing illustrating the dimensions of the bottom part of the measurement chamber used in the experiments. The phantom is made of rigid PVC and has inlets for injection of contrast agent, the transducer, and remote observation of the pressure.

pressure inside the bottom part of the measurement chamber instead of above the membrane. For this, the external sensor is connected to one of the inlets on the side of the chamber using a 1/8” plastic tube. The controller is furthermore fully programmable in real-time through a RS-232 serial interface connected to the PC. To communicate with the controller unit, a software library for Matlab has been developed and an overview of the available routines is given in Appendix B. The compressed air, which is inflated when the pressure should be increased, is generated by a silent oil-less compressor OF301-4M (Jun-Air International A/S, Nørresundby, Denmark). It provides a feed pressure of 4 bar, which is reduced to a constant feed pressure of 2 bar using a separate precision regulator from ATD Tools (Wentzville, MO).

5.1.4 Calibration of the acoustic pressure

The acoustic pressure or amplitude of the emitted ultrasound is an important property when using contrast agents in general. If the acoustic pressure is too high, the bubbles will rupture and the gas will quickly dissolve into the blood [30, 89]. Furthermore, as will become clear in Section 5.2, the acoustic pressure has to exceed a threshold before the subharmonic component is generated [90]. Therefore, a hydrophone has been used to measure the acoustic pressure of the selected transducer when connected to the RASMUS system. The driving pulse had the same shape and focal point as the one used for the experiments which will be described in Section 5.2 and 5.3. For the measurement, the XYZ Translation System [91] available at CFU was used. This provides accurate control of the hydrophone position relative to the transducer during the measurements. The acoustic pressure was measured at 11 points around the focal point along the acoustic axis of the transducer where the pressure is at its maximum. To get an overview of the entire transducer field, a simulation has, furthermore, been performed. The simulation was carried out using the simulation toolbox Field II [92, 93] using the same transducer setup and excitation parameters as in the measurement. The result of the simulation is shown in Fig. 5.6 (a). As the simulation only gives a qualitative indication of the pressure field,

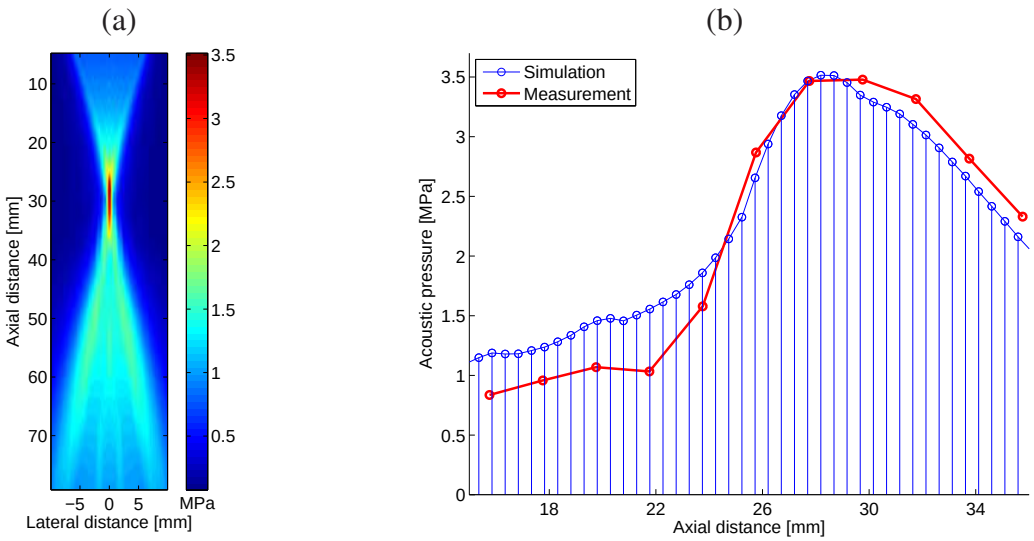

Figure 5.6: (a) Simulation of the emitted pressure field when using the transducer setup described in Section 5.1.1 and a steered excitation pulse with an axial focus in 30 mm. (b) Comparison of the simulation and corresponding measurement of the acoustic pressure. The simulation is an extraction of the center line in the image in (a).

it has been scaled to the maximum acoustic pressure of the transducer, which was measured using the hydrophone. As can be seen in Fig. 5.6 (a), most of the energy is centered around focus in $z = 30$ mm as expected. A comparison of the simulation along the horizontal line yielding the highest pressure and the measurement using the hydrophone can be seen in Fig. 5.6 (b). From Fig. 5.6 (b), the simulation and the measurement is seen to have the same shape but with a deviation in the amplitudes. One possible explanation for the deviation could be that the measurement was not carried out exactly along the acoustic axis. Another reason could be the missing information on the transducer parameters as the transducer is a prototype without any data sheet. When looking more closely to Fig. 5.6 (b), the peak pressure is seen to occur 1.5 mm before the desired focal depth in $z = 30$ mm. The small displacement can probably be explained by the amplitude term, $p_0(r)$, in the equation for the acoustic pressure of a spherical wave, which is given by [94]

$$p(t, r) = p_0(r) \cdot e^{j(\omega t - kr)}\,, \tag{5.1}$$

where r is the radial distance and $k = \frac{2\pi}{\lambda}$ is the wave number. The acoustic pressure amplitude is usually given by $p_0(r) = \frac{1}{r}$. This means that, as the wave propagates away from the transducer and spreads out, the acoustic pressure is reduced because the energy of the wave must be constant. Therefore, it is possible that a summation of all the emitted waves from every single transducer element gives rise to a higher acoustic pressure in a point just before the focal point. As an acoustic pressure of 3.5 MPa (Mechanical Index = 1.75) is guaranteed to destroy all the microbubbles, the requirement for the measurement investigating the response as a function of driving pressure (Section 5.2) is fulfilled.

5.1.5 Signal processing

As described in Section 5.1.1, the RASMUS system is used to acquire raw ultrasound data. This necessitates that some signal processing must be applied before the data can be used for further investigations. This Subsection describes the standard processing steps which are applied to data acquired in the measurements described in Section 5.2 and Section 5.3. Furthermore, to make the estimates more robust, the energy of the fundamental and subharmonic component is chosen as a measure instead of the peak amplitude. Therefore, this Subsection ends with a discussion of how data is extracted and used to estimate the power density spectra.

Filtration

To increase the signal-to-noise ratio, all noise should be removed from the acquired data. This is carried out using a filter, which allows all expected frequencies to pass and attenuates everything else. According to [94, page 161], the filter, which maximizes the ratio peak instantaneous power and mean noise power, has the following transfer function:

$$H_m(f) = G_a R_s^*(f) \cdot e^{-j2\pi f t_1}, \tag{5.2}$$

where G_a is a constant (usually set to 1) and $R_s(f)$ is the spectrum of the received signal when noise is not present. In traditional ultrasound imaging, the expected frequencies correspond to the frequency spectrum of the reflected pulse when compensating for the distortion caused by the transducer. Therefore, a matched filter is normally designed by convolving the emitted pulse by the two-way impulse response of the transducer. However, in this case one of the purposes

is to utilize the non-linear response of the contrast agent, which a matched filter would remove. From Fig. 5.3 (b), which shows the frequency spectrum of the transducer, it can be seen that the transducer has a limited bandwidth and only allows for two consecutive harmonics at 2 and 4 MHz to pass. Therefore, the filter used in this thesis attenuates all other frequencies but the fundamental at 4 MHz and the first subharmonic at 2 MHz. To keep the design simple, the current filter does not take the frequency spectrum of the transducer into account. Instead, it is simply designed from the emitted pulse. An example of one of the filters can be seen in

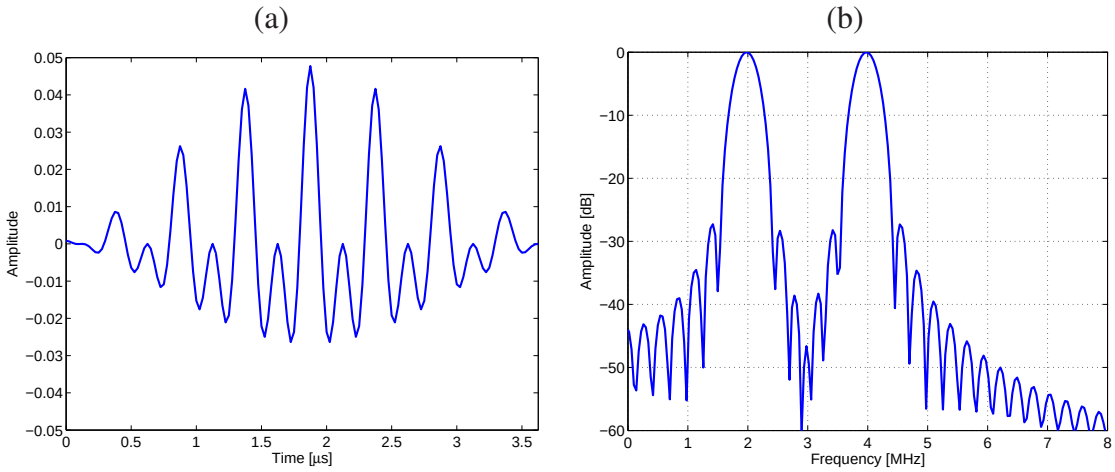

Figure 5.7: Example of one of the filters used for the measurements involving a non-linear contrast agent. (a) shows the filter in the time domain while (b) shows the corresponding frequency spectrum.

Fig. 5.7. It is designed to have a -6 dB bandwidth corresponding to a 10 percent cosine tapered excitation pulse with a center frequency of 4 MHz and 10 cycles.

Focusing in receive

When data is acquired from a single emission, it is done by sampling data from each transducer element separately. Since a single point in space will scatter sound spherically, all transducer elements will not receive the reflection from a point at the same time due to the shape of the transducer. To compensate for this, the received data must be focused toward the desired point of listening. This is carried out by applying individual delays to the signals received by each element. When the individual signals have been delayed properly, they can all be summed to form a single signal representing the result of an emission. Besides the steering of the listening beam, a weighting of the individual elements also takes place. This is called apodization and usually a window is used to favor the center elements while more or less neglecting the signals received at the outermost elements. In stead of using the same weighting at all depths, dynamic apodization can be used. This is used to keep a constant F-number, which is defined as

$$F_{\#} = \frac{z}{d},$$

where z is the distance from the transducer and d is the size of the active aperture, which can be explained as the number of elements not weighted with 0. Having a constant and low $F_{\#}$ ensures a good spatial resolution. In this thesis, a dynamic apodization with a $F_{\#} = 2$ and a

Hamming window is used for all data being beamformed. The delay and sum process in receive is also called beamforming. At CFU, a toolbox called the beamformation toolbox, BFT2 [95], has been developed to ease up this task. As a final thing, it should be noted that the beamformed data is scaled according to the output of the analog-to-digital converter (ADS 807, Burr-Brown, Tucson, AZ) in the RASMUS system, which has a peak-to-peak voltage of 2 V. The data has, thereby, been scaled by a factor of $2\ \mathrm{V}/4096$ before further processing.

Matters on accuracy and resolution for spectral estimation

The ultimate perspective of this approach is to develop a method that could present blood pressure values in a region in the body in real time as we know from flow estimation today. This requires that some considerations regarding the selection of data for estimating the power density spectrum (PDS) is made when implementing the approach. Therefore, this subsection briefly presents the compromise that exists between accuracy and axial resolution. The power spectrum of a stationary random process is defined as the Fourier transform of the autocorrelation sequence:

$$P_x = \int_{-\infty}^{+\infty} R_x(\tau) \exp(-2\pi f \tau)\, d\tau, \tag{5.3}$$

where R_x is the autocorrelation function defined as

$$R_x = E\{x(t)\, x(t+\tau)\}. \tag{5.4}$$

When a limited number of samples is used for the estimation, the spectral resolution will be degraded. As extracting a limited number of samples can be compared to multiplying the data set by a rectangular window, the spectral resolution will be smoothened by a factor equal to the spectral width of the window used for data extraction. The spectral resolution when using a rectangular window is approximately

$$\Delta f = \frac{f_s}{N}, \tag{5.5}$$

where f_s is the sampling frequency and N is the number of samples used for estimating the periodogram. Assuming a fundamental frequency of $f_0 = 4$ MHz, which implies a subharmonic component at $f_{sub} = 2$ MHz, a minimum spectral resolution of $\Delta f = 1$ MHz is sufficient to ensure separation of the two components in the estimate of the PDS. Using a sampling frequency of $f_s = 40$ MHz, this necessitates a minimum of $N = 40$ samples.
As the periodogram, denoted $\hat{P}_x(f)$, is based on a limited number of samples, it is only an estimate of the true PDS. The variance of the periodogram is [96]

$$\sigma^2\left\{\hat{P}_x(f)\right\} \approx P_x^2(f)\left[1 + \left(\frac{\sin 2\pi f N}{N \sin 2\pi f}\right)^2\right], \tag{5.6}$$

which is seen to be proportional to the square of its power spectrum even for large numbers of N. To reduce the variance, the average of a number of periodograms can be used according to Bartlett's method [97]. The periodogram averaging can be carried out over consecutive emissions or by using independent data segments from a single emission, which in turn will reduce the axial resolution. This disadvantage can, however, be reduced by letting the segments overlap as suggested by Welch [98]. Using L data segments for estimating the periodograms, the variance is approximately reduced to

$$\sigma^2\left\{\hat{P}_x(f)\right\} \approx \frac{1}{L} P_x^2(f). \tag{5.7}$$

To get an expression of the relative uncertainty for the estimation of $\hat{P}_x(f)$, the normalized variance can be defined as [99]

$$\mathcal{V} = \frac{\sigma^2\left\{\hat{P}_x(f)\right\}}{E^2\left\{\hat{P}_x(f)\right\}}, \tag{5.8}$$

which for the rectangular window gives

$$\mathcal{V} = \frac{1}{L}. \tag{5.9}$$

From (5.9), it is possible to determine the number of periodograms necessary to obtain a specific relative accuracy. For example, if a normalized variance of 5 % is desired, $L = 20$ independent data segments should be used for the estimation of the power density spectrum. Assuming a sound speed in water of $c = 1480$ m/s, an axial distance of $\Delta z = LN/f_s \cdot c = 29.6$ mm of data would, thereby, be required for a single accurate estimate. This would give a very coarse axial resolution if data were acquired in a single emission. Instead, data could be acquired over 10 emissions, yielding a spatial resolution of 3.0 mm. In the experiments to be presented in Section 5.2 and 5.3, 50 acquisitions are carried out in each measurement. In this way, five independent estimates can be used to calculate a mean and standard deviation.

5.2 Dependence on acoustic pressure

The acoustic pressure or amplitude of the emitted ultrasound is an important property when using contrast agents in general. As mentioned before, the bubbles will rupture and the gas quickly dissolve into the blood if the acoustic pressure is too high [89]. Moreover, the acoustic pressure has to exceed a threshold before the subharmonic component is generated [90]. This Section describes the experiments which have been carried out to investigate the fundamental and subharmonic response when the driving pressure is varied. The first part of Section 5.2 is based on the same measurement as presented in the paper [80] available in Appendix D.4. The results are, however, presented in a slightly different way, which makes it more suitable to comment on the observed trends. Furthermore, as four, more or less, similar experiments have been carried out, the last part of Section 5.2 shows the results of another measurement, which has not been presented elsewhere.

5.2.1 Method

To measure the behavior of the fundamental and subharmonic component as a function of the acoustic driving pressure, the setup presented in Section 5.1 was used, although the functionality for regulating the ambient pressure was not needed. For both measurements, approximately 0.5 ml of the contrast agent SonoVue (Bracco, Milano, Italy) was injected into 0.6 l of saline. To eliminate air bubbles from the preparation process, the liquid was poured into the chamber the day before the experiment took place. The response was investigated as a function of 14 different acoustic driving pressures in the range from 100 to 900 kPa. In all cases, the excitation pulse was a cosine tapered pulse consisting of 32 cycles with center frequency of 4 MHz. For each acoustic amplitude level, 50 acquisitions were carried out using a pulse repetition frequency of 50 Hz. As 14 acoustic pressures were investigated, the experiment took 14 seconds after an initial waiting period after injection to ensure proper mixing of the microbubbles. The setup parameters for the measurements are summarized in Table 5.2. In the first measurement to be presented, the driving pressure was increased continuously while it was decreased in the second measurement.

Parameter	Designation	Unit
f_0	`4.0`	[MHz]
N_c	`32`	[cycles]
Shape	`10 % cosine tapered`	
P_{ac}	`100 200 300 325 350 375 400 450 485 500 550 600 700 900`	[kPa]
N_{emis}	`50`	[emissions]
f_{prf}	`50`	[Hz]
Contrast agent	`SonoVue, batch 8A008D`	

Table 5.2: Setup parameters for the experiment investigating the dependence on the acoustic driving pressure. The first part concerns the excitation pulse, the second part the emission sequence, and the final part designates the contrast agent used in the experiment. As can be seen, all parameters are the same except for the amplitude of the driving pulse which is either increased or decreased continuously during the experiment.

5.2.2 Results

Fig. 5.8 shows the energy of the fundamental and subharmonic component calculated for each of the 14 different acoustic driving pressures in two different display modes. In Fig. 5.8 (a), the energy is plotted in ordinary scale and includes the standard deviation (STD) of the five estimates at each acoustic pressure level. Although it is not shown here, the normalized variance

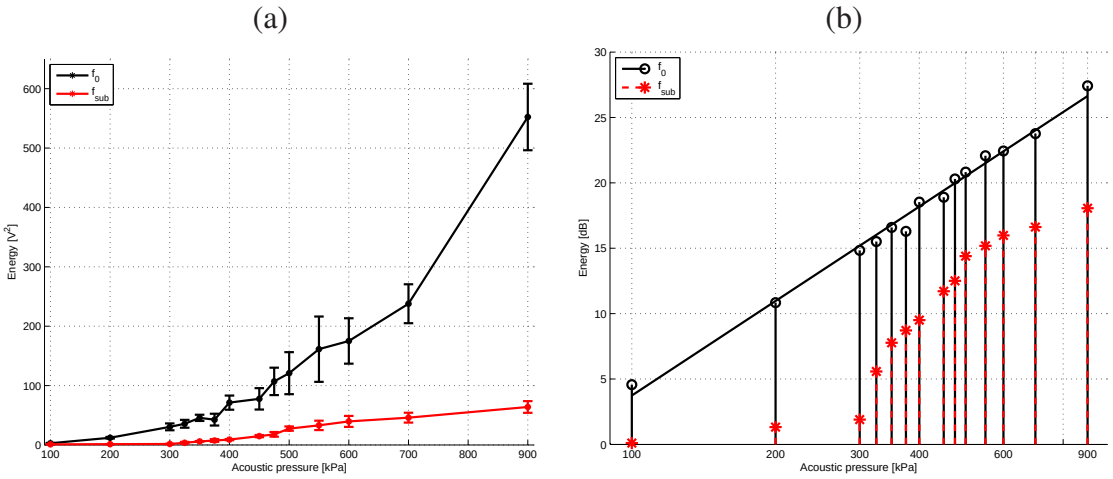

Figure 5.8: Energy of the fundamental and subharmonic component as function of the acoustic driving pressure displayed in (a) ordinary and (b) logarithmic scale, respectively. The solid line in (b) is the power function $f(x) = 3.76 \cdot 10^{-5} \cdot x^{2.4}$ yielding the best regression fit with a correlation coefficient of $R = 0.995$.

is seen to increase slightly with increasing acoustic pressure for the fundamental component. This is not as pronounced for the subharmonic component. Calculating the average normalized variance, it is 0.19 for both frequency components. This is higher than expected from Section 5.1.5. The reason for this is not clear but most likely it is caused by the size distribution of the bubbles. This means that big bubbles, having a large scattering cross-section, will generate more energy than the small bubbles. Other possible reasons could be a too high pulse repetition frequency or too fast stirring causing turbulence. At the high acoustic pressures, disruption of the encapsulated microbubbles and scattering from free bubbles most probably also contributes to deviations in the acoustic response. Fig. 5.8 (a) is primarily included for comparison purpose when discussing the results in Section 5.3. To show the trends more easy, the energy of the respective components is plotted in double logarithmic scale in Fig. 5.8 (b). Looking at the fundamental component, an almost linear relation, in double logarithmic scale, between the energy and the acoustic pressure is observed. Regression analysis on the results for the fundamental component shows that the relation is best described using the power function $f(x) = 3.76 \cdot 10^{-5} \cdot x^{2.4}$, which is shown in Fig. 5.8 as the solid line. In this case, the correlation coefficient is $R = 0.995$. This indicates that the energy of the fundamental component, in logarithmic scale, will increase by a factor of 2.4 when the acoustic pressure is doubled. This also yields that the relation between the amplitude of the fundamental component and the acoustic pressure is 1.2. This is not the same as predicted by theoretical models describing the contrast agent Albunex (Molecular Biosystems Inc., San Diego, CA) [100, 35], which predicts the amplitude of the fundamental component to be proportional to the acoustic pressure, meaning a relation of 1.0. The reason for this is not known, but part of the explanation could be that the model is only accurate for lower acoustic pressures or the different gas cores of Albunex

and SonoVue. A similar measurement, as presented here, has been reported for the contrast agent Optison (at the time Molecular Biosystems Inc., San Diego, CA) [101]. In this case, the fit was divided into two parts. One for acoustic pressures below 1.0 MPa and one for acoustic pressures above, and the relation was found to be 1.0 and 1.3, respectively. When looking at the energy of the subharmonic component, it behaves, somewhat, different from the fundamental. Roughly, the behavior can be split into three parts. In the first part, almost no change in the amount of energy is seen and the subharmonic component is not (or almost not) visible in the corresponding spectra. This part is also known as the occurrence stage. In the experiment summarized in Fig. 5.8, this is observed for acoustic pressures below 300 kPa. For driving pressures between 300 and 500 kPa, a rapid increase ($f\left(x\right) = 1.41 \cdot 10^{-12} \cdot x^{4.9}$, $R = 0.98$) in energy is suddenly observed. This part is often referred to as the growth stage and implies that the subharmonic component gets more and more pronounced in the spectra. For acoustic pressure levels above 500 kPa, the increase in energy decays and this part is known as the saturation stage. At these acoustic pressure levels, a general increase in energy for all frequencies has also been reported, indicating that the bubbles are being disrupted [102, 103, 104]. Unlike before, the interval for subharmonic growth differs quiet much from the results presented in [101], who found the subharmonic growth period of Optison to be around 1.2 and 1.8 MPa when using an excitation frequency of 4 MHz. The explanation for this is most likely found in the different types of contrast agents, which will have varying subharmonic threshold levels depending on the driving frequency. In fact, the growth interval of Optison is reported to be between 400 and 800 kPa when exciting the bubbles at 2 MHz instead [101]. For a third contrast agent, Levovist (Schering AG, Berlin, Germany), the growth interval is reported to be between 300 and 600 kPa when excited at 2 MHz [69].

As the experiment where carried out measuring the response at all acoustic pressures consecutively, the experiment was also performed using the inverse acoustic pressure sequence (decreasing the acoustic pressure from 900 to 100 kPa) to see the effect of this and investigate factors like time dependency. The result of this experiment is summarized in Fig. 5.9, once again displaying the energy of the fundamental and the subharmonic component as a function of the acoustic driving pressure in double logarithmic scale. For this experiment, the STD was the same as before with an average relative STD of 0.21 and 0.19 for the fundamental and subharmonic component, respectively. When first comparing Fig. 5.9 to Fig. 5.8 (b), the behavior of the fundamental and subharmonic component is seen to be almost the same. However, looking more closely, first of all, a difference in the energy level is observed. On average, the difference is 4.5 and 6.4 dB for the fundamental and subharmonic component, respectively. This is likely caused by different amount of contrast agent from the first measurement to the other as no pipette for exact dosing was used in the experiments. Looking at the energy of the fundamental component, the same linear (in double logarithmic scale) pattern as in Fig. 5.8 is seen. Once again, regression analysis has been performed to find the best fit, which is obtained when using the power function $f\left(x\right) = 2.23 \cdot 10^{-5} \cdot x^{2.3}$ yielding a correlation coefficient of $R = 0.996$. This suggests that the relation between the amplitude of the fundamental component and the acoustic excitation pressure is the same as before, which was a factor of 1.2. Looking at the subharmonic component in Fig. 5.9, the occurrence stage is once again observed to be at acoustic pressure levels below 300 kPa. The growth interval and the saturation stage is, however, not as easy to distinguish from each other. Still, the decay in rapid growth occurs around 550 and 600 kPa, which is higher than in the first measurement when increasing the acoustic pressure.

From the results presented in Fig. 5.8 and Fig. 5.9, several things can be concluded. The

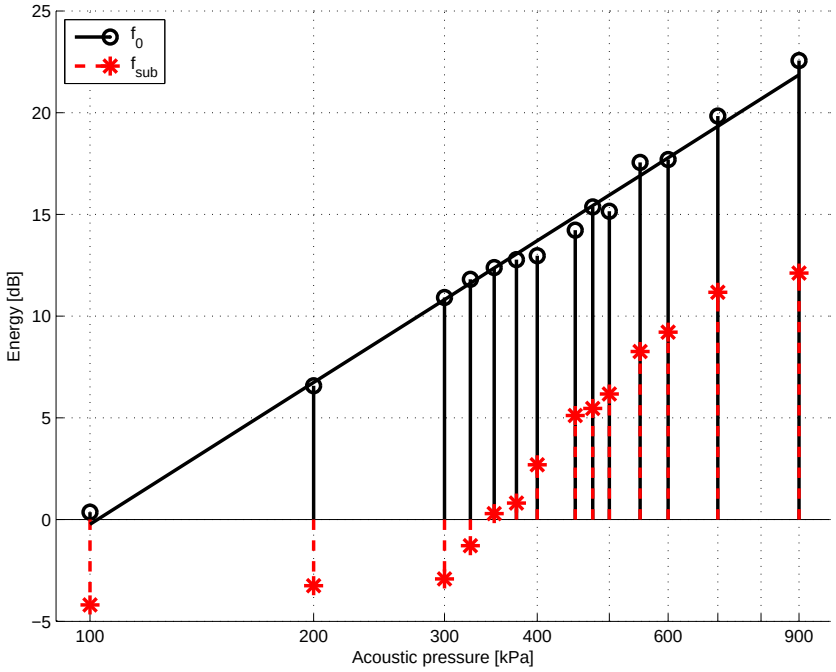

Figure 5.9: Energy of the fundamental and subharmonic component as function of the acoustic driving pressure. The experiment is the same as in Fig. 5.8 but the acoustic pressure sequence was reversed during the experiment. The solid line is the power function $f\,(x) = 9.36 \cdot 10^4 \cdot x^{2.3}$ yielding the best regression fit with a correlation coefficient of $R = 0.996$.

behavior of the fundamental and subharmonic component each have a specific pattern as a function of the acoustic excitation pressure. But the amplitude of the echo response seems to be very dependent on the amount of microbubbles as it varies from one measurement to another. The measurements show that the relationship between the energy of the fundamental response for the current batch of SonoVue and the acoustic driving pressure can be described by a power function with an exponent of 2.4. This fit perfectly covers the entire pressure range of the investigated excitation pressures. The subharmonic component, however, has a more complex behavior in respect to the excitation pressure. For the current batch, the occurrence stage was found to be for acoustic pressures below 300 kPa. The growth period is present at pressure levels between 300 and approximately 500 kPa. Acoustic pressures above this level must be categorized to be within the saturation stage of the subharmonic component. As a final thing, the measurements were, unfortunately, accompanied by a high STD. This is presumably because of the size distribution of the microbubbles, which could indicate a problem obtaining accurate estimates of the ambient pressure using this setup and SonoVue.

5.3 Ambient pressure sensitivity

As described in Chapter 3 and Chapter 4, it is expected that ultrasound contrast agents can be used as pressure sensors because of their compressibility and sensitivity to the ambient pressure. This Section presents the experiments carried out to investigate the ambient pressure sensitivity when utilizing the subharmonic response. The results of two measurements will be presented in Section 5.3.3 and Section 5.3.4, respectively. As the measurements are almost similar and the setup varies only in the acoustic excitation pressure, the measurement procedure of both measurements is described in Section 5.3.1. Section 5.3.2 illustrates how the pressure is managed during an experiment based on the data obtained in the first measurement. The results shown in Section 5.3.3 are based on the measurement first presented in the paper [79], which is available in Appendix D.3. Section 5.3.4 presents the results when using a slightly higher acoustic driving pressure. This measurement and a comparison to the results in [79] has been presented in the conference paper [80] appended in Appendix D.4. In this Section, the results are, however, presented in a slightly different way.

5.3.1 Method

The ambient pressure sensitivity has been investigated using the airtight measurement setup presented in Section 5.1. To ensure the experiment is carried out correctly, a trial protocol has been written and can be seen in Appendix C. It describes the procedure for setting up and initialize the equipment as well as how to prepare and carry out the measurement itself. For each of the measurements to be presented, the same batch of SonoVue as for the initial experiments described in Section 5.2 was used. Each measurement was carried out at once acquiring 50 lines of data at 11 ambient pressure levels using a pulse repetition frequency of 50 Hz. Every 2 seconds, the ambient pressure was increased in steps of 5 kPa until the peak ambient pressure of 25 kPa was reached. This corresponds to the common physiological blood pressure range in the human body. It was then decreased in steps of 5 kPa every 2 seconds. The ambient pressure was allowed 1 second to adjust in between acquisition at each pressure setting. Thereby, the entire measurement lasted 21 seconds and provided two series of scattered ultrasound data at each ambient pressure, except at 25 kPa - one set when increasing the ambient pressure and another set when decreasing the ambient pressure. This procedure is very different from the one used by Shi and colleagues [69, 72] as they replace the liquid and microbubbles in between each measurement and acquire the data at the same time after injection at each ambient pressure level. This will, of course, reduce the time dependency but it is also very far from an *in vivo* situation. So is a static pressure in general like the pressure sequence just described. However, as a first attempt of ambient pressure estimation at CFU, it still resembles a clinical situation more closely as do the setup in general. The emitted ultrasound pulse was a steered beam identical to the one used to investigate the acoustic driving pressure dependent behavior described in Section 5.2. As mentioned, two similar experiments were carried out using an acoustic driving pressure of 485 and 500 kPa, respectively. These acoustic pressure settings were selected based on the experiments described in Section 5.2, which indicated this to be in the upper end of the subharmonic growth stage. The parameters for the two measurements are listed in Table 5.3.

Parameter	Designation	Unit
f_0	`4.0`	[MHz]
N_c	`32`	[cycles]
Shape	`10 % cosine tapered`	
P_{ac}	`485 500`	[kPa]
N_{emis}	`50`	[emissions]
f_{prf}	`50`	[Hz]
P_{ov}	`0 5 10 15 20 25`	
Contrast agent	`SonoVue, batch 8A008D`	

Table 5.3: Setup parameters for the experiment investigating the dependence on the acoustic driving pressure. The first part describes the excitation pulse. The second part is related to the shooting sequence. The third part denotes the ambient pressure settings and the final row lists the contrast agent used for the experiments.

5.3.2 Ambient pressure regulation

During each of the experiments, the ambient pressure inside the chamber was measured and stored continuously every 200 ms. A summary of the ambient pressure management for the first experiment, using an acoustic driving pressure of 485 kPa, is shown in Fig. 5.10 (a). It displays the instantaneous pressure, measured by the sensor inside the chamber, and the desired pressure transmitted from the PC. The time intervals for acquiring the ultrasound data is furthermore indicated by the filled circles. Moreover, the relative deviation, which is defined as the absolute difference between the measured pressure and the desired pressure divided by the desired pressure, is shown in Fig. 5.10 (b). From Fig. 5.10, a high overshoot is seen when

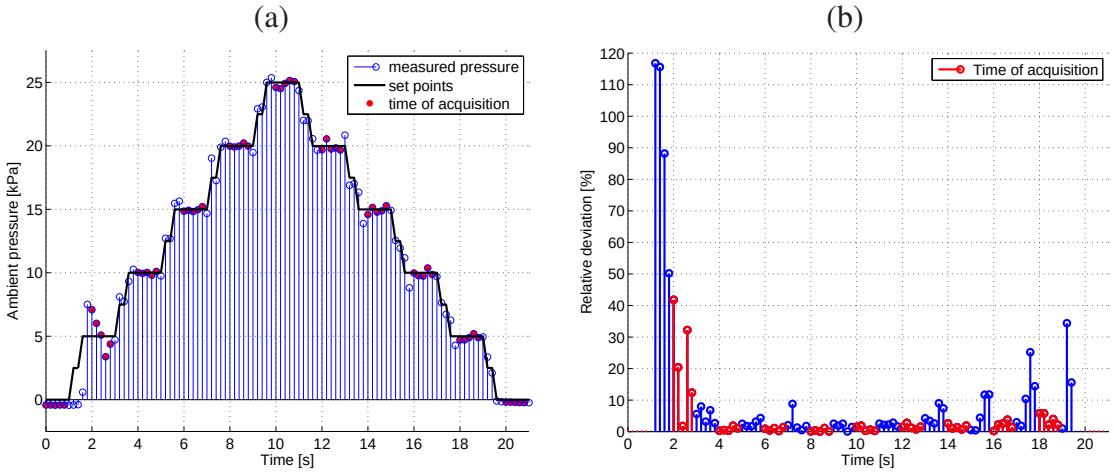

Figure 5.10: Example of the ambient pressure log obtained during an experiment. This is for the measurement with $P_{ac} = 485$ kPa. In (a), the solid thick line indicates the pressure set points transmitted from the PC to the pressure controller. The stems displays the immediate pressure measured inside the chamber at the current time instants. Finally, the dots inside the circles denote the time of ultrasound data acquisition. (b) shows the relative deviation defined as the difference over the desired pressure.

applying an ambient over pressure for the first time. The most likely explanation for this is that the rubber membrane got stuck to the inlet for compressed air. To compensate, the pressure controller increases the feed pressure and, eventually, pushing the membrane downward rather powerfully. This theory is corroborated when looking at the rest of the pressure log, which shows that the measured pressure closely follows the desired pressure. A possible solution to fix the overshoot could be to increase the space between the membrane and the inlet of the feed pressure, which is only 2 mm in the current setup. A larger dead volume (with limitations) would probably also reduce the general ripple when changing the set point and, thereby, refine the precision and speed of the ambient pressure regulation. Disregarding the first set point at 5 kPa, the measured ambient pressure is within 0.5 kPa of the desired set points when acquiring the ultrasound data. The maximum relative deviation in respect to the desired set point is 5.8 %, which is observed during the second measurement at 5 kPa. On average, the relative deviation is 1.5 % at the time of data acquisition.

5.3.3 Acoustic pressure of 485 kPa

Fig. 5.11 (a) and (b) shows the energy including ± 1 standard deviation (STD) of the fundamental and subharmonic component as a function of the ambient pressure and in order of time in respect to the measurement sequence. As 10 acquisition lines are used for each estimate, and 50 emissions are acquired at each ambient pressure, the mean and STD shown in Fig. 5.11 is based on five independent estimates. When looking at the two figures in Fig. 5.11, first of

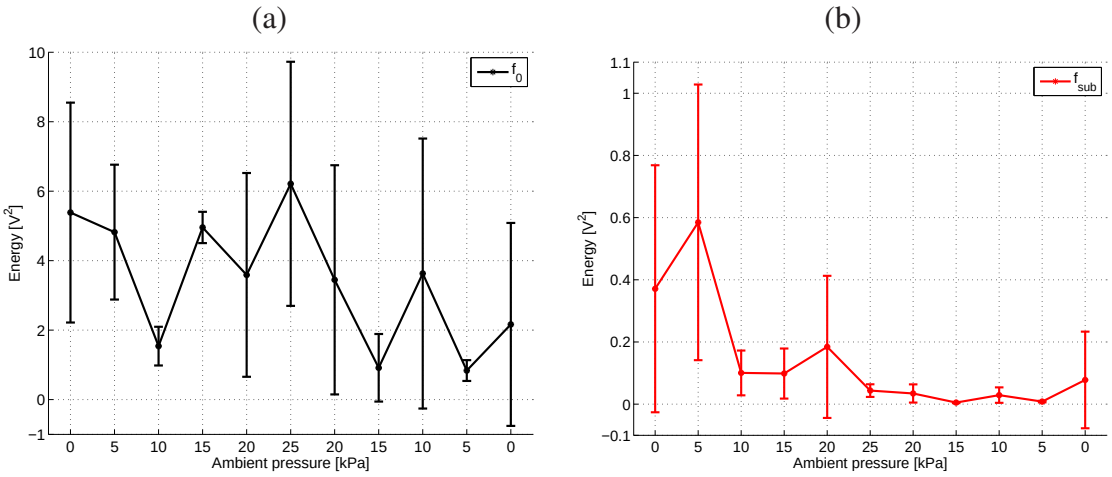

Figure 5.11: Energy of the fundamental (a) and subharmonic (b) component at the 11 ambient pressures settings listed in Table 5.3 when using an acoustic driving pressure of 485 kPa. At each ambient pressure, the mean and STD of five estimates is shown.

all a high STD is observed in both cases. For some estimates it is even higher than the mean value giving an indication of negative energy values, which is clearly wrong. Unfortunately, the high STD has also been presented by Adam et al. [75] who also used a single transducer for the acquisition. When applying a static ambient pressure, they report a STD which is two times greater than the mean value at the beginning of the experiment and 2.5 times the mean after 16 seconds. In this experiment, the relative STD is on avarage 0.69 and 0.86 for the fundamental and subharmonic component, respectively which is approximately four times more than observed in the experiments described in Section 5.2. The high STD must first of all be caused

by the same reasons as mentioned in Section 5.2, being the size distribution, too high acoustic pressure, too high pulse repetition, or too fast stirring. But as the STD has increased further, the ambient pressure must also have an influence. This could be because of small variations in the pressure regulation. When looking at the average energy of the fundamental component displayed in Fig. 5.11 (a), it is seen to vary up and down, hence not indicating any real pattern. Still, two trends can be observed with some conviction. First, when looking at the first six measurement points, constituting the first measurement sequence, the energy is more or less constant. This could indicate that the energy or amplitude of the fundamental component is not very sensitive to the ambient pressure. This would, thereby, support what has previously been reported theoretically [78] and by experiments [69]. Looking at the second measurement sequence made up by the last six measurement points in Fig. 5.11 (a), the energy is seen to decrease even though the ambient pressure is being released. This is most likely caused by bubble dissolution, or even destruction, possibly because of too high acoustic pressure, time dependency, ambient pressure effects, or a combination of these. It is well known that the bubbles will dissolve over time once they are injected into either water or blood because of the gas diffusion processes that take place [40]. Several studies have shown that an increased static pressure causes the attenuation to deteriorate faster than if no over pressure is applied [40, 57]. For clarification it should, in this connection, be noted that cyclic ambient pressure does not seem to have the same degrading effect - at least not when the ambient pressure is varied between 0 Pa and another level within the human physiological blood pressure range [75, 63]. In Fig. 5.11 (b), the energy of the subharmonic component seems to drop from the beginning of the experiment to the end. According to Shi and colleagues [69, 72], this was expected for the first six measurement points. But the fact that the energy continues to drop for at least the next two measurement points ($P_{ov} = [20\ \ 15]$ kPa) could, once again, indicate that the bubbles are being dissolved.

In general when looking at Fig. 5.11 (a) and (b), a fluctuating behavior and indication of bubble dissolution is seen. As the microbubbles will, for a fact, dissolve and change character over time when injected into the circulatory system (e.g. [60]), a more robust measure than solely the energy, or the amplitude for that matter, of the subharmonic component is needed for future implementation. Therefore, the ratio of subharmonic energy to the energy of the fundamental component has been investigated. The reason for this is based on the theoretical findings presented in Chapter 4 and experiments carried out under near-optimal measurement conditions [69], which show that the fundamental component is not affected by ambient pressure changes while the subharmonic is. This indicates that the ratio should be a just as sensitive, but possibly more robust, measure as it reduce factors like bubble concentration, time dependency, and possibly also bubble size considerations. The result when using the relation between the energy of the subharmonic and the fundamental component is shown in Fig. 5.12, which also includes the STD of the five estimates at each ambient pressure setting. Although the STD, relatively, has only reduced slightly compared to Fig. 5.11, a clear trend can now be observed from the two measurement series in Fig. 5.12. As the ambient pressure is increased, the ratio decreases. As the ambient pressure is reduced, the ratio increases once again. Since no ambient pressure dependent behavior could be concluded from Fig. 5.11, the findings in Fig. 5.12, thereby, supports the assumption that the ratio could be a more robust measure. Performing regression analysis on the first measurement sequence, when increasing the ambient pressure, indicates a linear ratio of $a_1 = -0.02/\text{kPa}$ with a correlation coefficient of 0.98. For the second measurement sequence, the relationship between the energy of the subharmonic and fundamental component is also found to change by 0.02/kPa. In this case, the correlation coefficient is 0.88. As the mean STD of the first measurement sequence is $\sigma_1 = 0.15$, the average resolu-

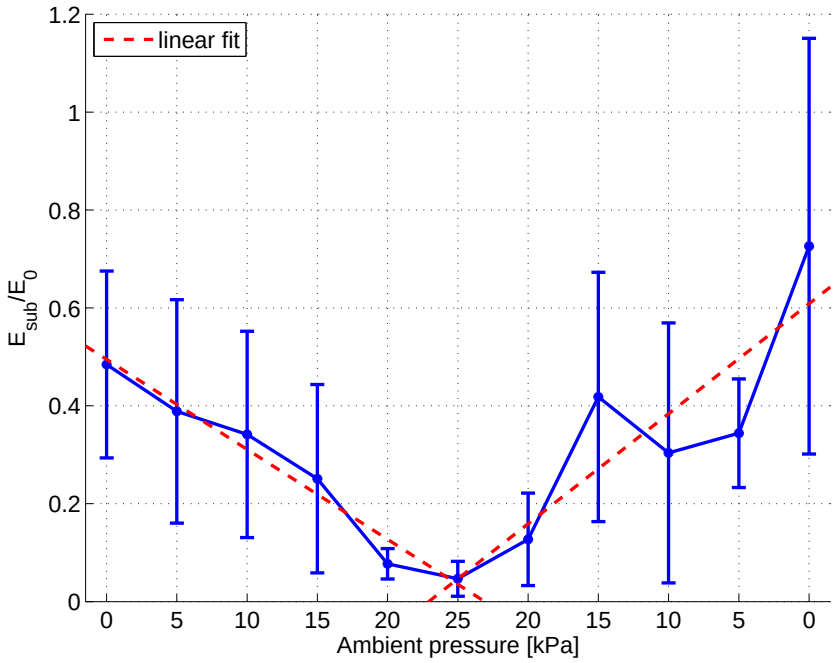

Figure 5.12: Ratio of subharmonic energy to the energy of fundamental component as a function of the ambient pressure and in order of time in respect to the measurement sequence. The dashed lines indicate a linear regression fit, which has been estimated for each of the two measurement sequences, respectively.

tion is $\Delta P_{ov} = \sigma_1/a_1 = \pm 8.1$ kPa. For the second measurement sequence, the resolution is ± 8.8 kPa because of a slightly higher STD on average, $\sigma_2 = 0.20$. As a resolution of 16 kPa almost covers the entire range of the human blood pressure, this is too high to allow for any practical implementation. One reason for the high STD seen in Fig. 5.12 can be because of the size distribution of the microbubbles. Since the bubbles vary in size, they will have different thresholds for generating the subharmonic component [31, 105]. This means that some bubbles will generate more subharmonic energy than others when excited using the same driving pulse. However, this can hardly explain it all and the reasons mentioned when discussing Fig. 5.11 are still relevant. Another open question is why the ratio of the subharmonic to fundamental component is linear and not exponential as expected from the findings by Shi and colleagues [69, 74] and Chapter 4.

5.3.4 Acoustic pressure of 500 kPa

To see the effect of using another acoustic excitation pressure, the experiment was repeated using a driving pressure of 500 kPa. Fig. 5.13 is the same as Fig. 5.11 showing the energy of the fundamental and subharmonic component as a function of the ambient pressure. When looking at the energy of the fundamental component displayed in Fig. 5.13 (a), a different pattern from Fig. 5.11 (a) is seen. First of all, the energy is seen to decrease significantly as the ambient pressure is increased or over time, or a combination of this. The drop in energy continues until the ambient pressure is decreased to above 20 kPa, where an exponential increase ($f(x) = 6.7 \cdot 1.13^x,\ R = 1.0$) is suddenly observed. Comparing the energy of the fundamental component at pressure setting one (0 Pa) and 11 (0 Pa), is does not reach the same level at all at the end of

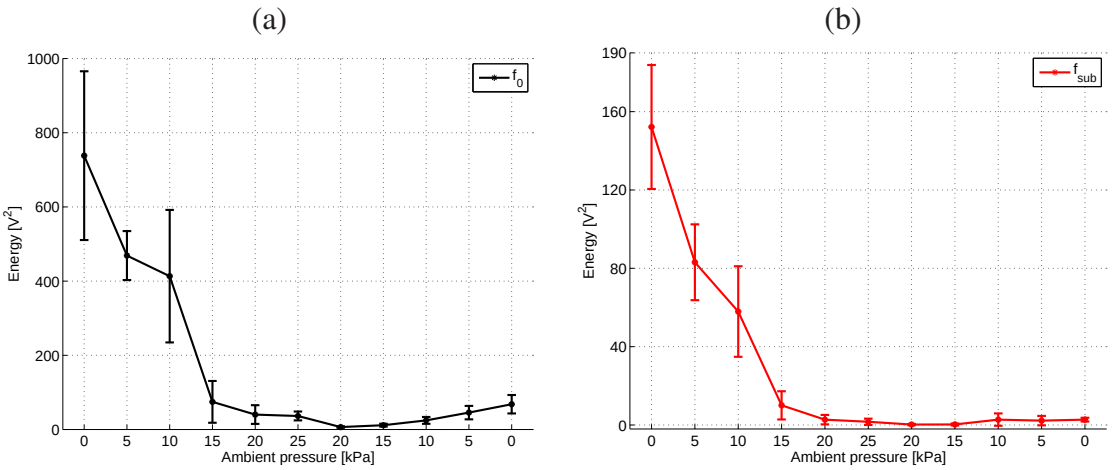

Figure 5.13: Energy of the fundamental (a) and subharmonic (b) component at the 11 ambient pressures settings listed in Table 5.3 when using an acoustic driving pressure of 500 kPa.

the measurement. This indicates that a lot of bubbles have been destroyed most likely due to the high acoustic pressure, but possible also because of the ambient pressure effects mentioned before. The energy of the subharmonic component shown in Fig. 5.13 (b) behaves almost the same as the fundamental, except it does not increase further as the ambient pressure is decreased from 10 to 0 kPa in the second measurement series (pressure setting nine to 11). One explanation for this could be that the size of the bubbles left at this point has reduced and, in that way, makes it more difficult to generate a subharmonic component at 2 MHz. Despite the clear indication of bubble destruction observed in Fig. 5.13, the ratio of subharmonic energy to the energy of the fundamental component has still been investigated like before. The result of this is shown in Fig. 5.14, which displays the relation of the subharmonic energy to the energy of the fundamental component estimated at the respective ambient pressures. Although the effect can be caused by different factors, once again an ambient pressure dependent pattern is observed. In the first measurement series, when the ambient pressure is increased, the ratio decreases, though it is not as linear as before. When the ambient pressure is released again, the ratio increases once again. However, in this case the STD is seen to be higher than the mean value at almost all measurement points. Furthermore, it does not increase at the same rate as it decreases. In the first measurement series, the linear relation is 0.06/kPa with a correlation coefficient of 0.95. This is 3 times more than for the measurement using a lower driving pressure of 485 kPa. Even an increase in sensitivity was expected from the simulation study in Chapter 4, it is questionable if part of this reduction is also caused by bubble disruption. This suspicion is supported when looking at the second measurement series in Fig. 5.14. In this case, the relation is found to increase linearly by 0.01/kPa ($R = 0.92$) as the ambient pressure is decreased. However, despite the high STD, the steep relation observed for the first measurement series yields an average resolution of ± 3.66 kPa. Although this is still at least a factor of 2 too high for blood pressure estimation in the small vessels, it indicates that ambient pressure measurements can be performed using this approach.

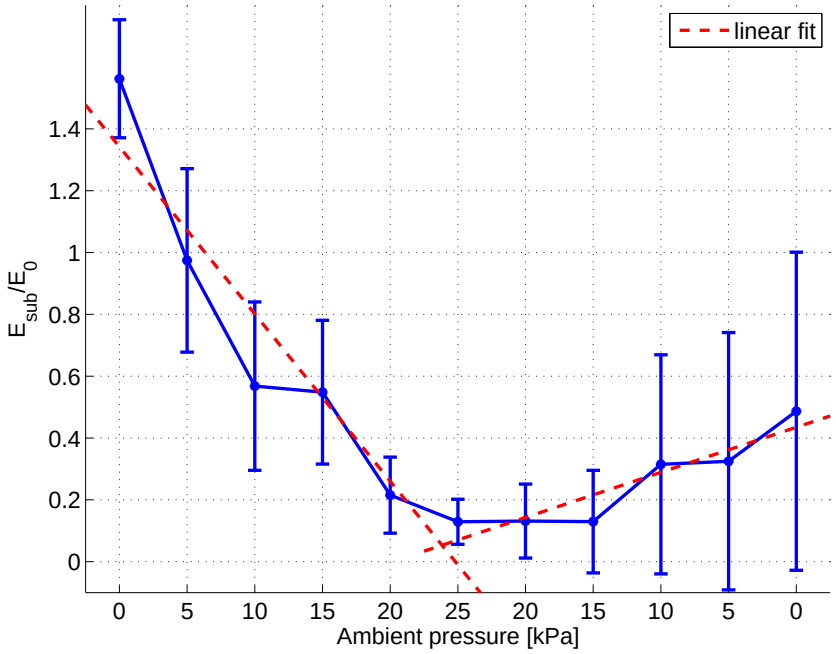

Figure 5.14: Ratio of subharmonic energy to the energy of fundamental component at various ambient pressure levels when using a driving pressure of 500 kPa. The dashed lines indicate the best regression fit for each of the two measurement sequences.

5.4 Closing remarks

The change in energy from one measurement to the other presented in Section 5.2, when investigating the driving pressure, shows that the amount of microbubbles is an important factor. As the exact number of bubbles in a certain region in the body is nearly impossible to control during an entire investigation using contrast agent, this indicates that it will be very difficult to obtain quantitative pressure values with an approach utilizing only the subharmonic response. Furthermore, the behavior of subharmonic energy as a function of ambient pressure presented in Fig. 5.11 (b) and Fig. 5.13 (b) cannot be used to conclude any ambient pressure dependent response at all. Although this can be caused by many different reasons such as the driving pressure, the ambient pressure sequence, or the pulse repetition frequency, it still reveals that a more robust measure than solely the subharmonic response is needed if the subharmonic ambient pressure sensitivity should be utilized *in vivo*. As argued, and demonstrated in Fig. 5.12 and Fig. 5.14, the relation between the subharmonic to the fundamental component seems to be a good alternative. In this way, a linear relation between the contrast agent response and the ambient pressure was obtained. However, the high STD observed in both measurements does not make the approach suitable for *in vivo* studies before more measurements and further investigations have been carried out. First of all, future measurements should demonstrate repeatability of the approach. But as strong indications of bubble rupture is seen for the second measurement at 500 kPa, lower driving pressures should be used. On reflection, the excitation pressures should not have been selected as close to each other as they were in the first place when the purpose is to investigate if it affects the ambient pressure sensitivity. Any future experiment should, therefore, use acoustic pressures corresponding to the beginning and reasonable close to the end of the growth interval, respectively. Despite of this, a clear differ-

ence was in fact observed. Also, similar measurements should be carried out to investigate the effects of the driving pulse length, which, from the study described in Chapter 4, also seems to be an important factor. Future experiments should also investigate other ambient pressure measurement sequences, once again to test repeatability and the robustness of the approach. A cyclic ambient pressure sequence should also be considered to mimic the human blood pressure more closely. Regarding steps to investigate the STD, it is expected, when considering the measurements in Section 5.2, it will reduce when using a lower acoustic pressure. Other attempts should investigate factors like pulse repetition frequency, speed of magnetic stirrer, and attention should be paid when the ambient pressure scheme is changed. Furthermore, contrast agents with different physical properties like size distribution and resonance frequency should be investigated. Finally, if the ambient pressure sensitivity cannot be improved, one of the other measurement techniques described in Chapter 3 should be investigated using the designed measurement setup. Two of these techniques could be the ones based on measuring the disappearance time or the resonance frequency shift, respectively. Measuring the dissolution time by means of bubble destruction will, however, prevent continuous monitoring over the traditional life time of a contrast agent when injected into the circulatory system. Moreover, the mechanisms when destroying the bubbles using a too high acoustic pressure is not yet fully understood and accompanied with a small risk of producing jets [106], which can cause damage to the vessel walls. Finally, as the disappearance time depends on the initial bubble size, the size distribution needs to be very narrow. Also, a small bubble size will put a limitation to the pressure renge and resolution as the bubbles will dissolve more quickly.

CHAPTER

SIX

Conclusion

Currently, there exist no reliable approach for estimating the blood pressure locally in the body non-invasively. The purpose of this PhD project has been to investigate ambient pressure sensitivity of an ultrasound contrast agent. In this context, three subjects have been addressed in this thesis.

A literature study investigated and summarized the various approaches which have been presented since the idea of using bubbles as pressure sensors was first presented in 1977. Common for all methods is that they use a technique to measure a change in either resonance frequency, disappearance time, or subharmonic amplitude. Within the last decade, approaches for detecting the last two properties have shown promising results.

To investigate the sensitivity of the subharmonic response to ambient pressure changes, a parameter study consisting of 7200 simulations was performed. While the parameters of the microbubbles were fixed, the parameters describing the excitation pulse and ambient overpressure were changed in each simulation. Investigations of the subharmonic energy as function of ambient overpressure showed two clear tendencies: The amount of reduction in energy of the subharmonic component is dependent on the acoustic driving pressure and peaks when the acoustic pressure is in the upper end of the growth stage. Second, the investigation also showed a clear relation between the amount of energy reduction and length of the driving pulse. Simulations of Levovist indicate a linear change in energy of the subharmonic component as a function of ambient overpressure. Changing the overpressure from 0 to 25 kPa indicates a pressure sensitivity of 0.49 and 0.88 dB/kPa for a rectangular driving pulse with 64 and 256 cycles, respectively. For Sonazoid, the sensitivity was found to be 0.65 and 1.14 dB/kPa when using the same excitation pulses as for Levovist.

The main emphasis of this PhD project has been to carry out experimental measurements. This necessitated the design and establishment of equipment at CFU for measurements with contrast agent and control of the ambient pressure. As the ultimate objective is to carry out *in vivo* measurements, the experimental setup has been designed to resemble a realistic clinical situation. Different designs and settings for managing the ambient pressure have been tested during the project and a suitable setup now seems to exist. The setup consists of a sealed and airtight chamber with connections for a single array transducer and inlets for automatic regulation of the ambient pressure and easy injection of the contrast agent. The acquisition of raw ultrasound data and management of the ambient pressure is controlled from a single standard PC. Except from an overshoot in the very beginning, the ambient pressure regulation is fast and has a relative deviation from the desired pressure of 1.5 %.

Initial measurements of the response of SonoVue as a function of the excitation pressure

showed two characteristic things. The relationship between the energy of the fundamental component and the driving pressure can accurately be described by a power function having a coefficient of 2.4. The subharmonic response, on the other hand, must be divided into the three characteristic stages, and the growth interval of the current batch was found to be between 300 and approximately 500 kPa.

The ambient pressure sensitivity of SonoVue was measured using an acoustic pressure of 485 and 500 kPa, respectively. The measurement procedure provided two separate sequences for each acoustic driving pressure, one when increasing the ambient pressure and another when decreasing the ambient pressure. The results clearly showed that the amplitude of the subharmonic component cannot be used as a measure using the specific setup. However, when using the ratio of the subharmonic energy to the energy of the fundamental component, a clear ambient pressure dependent pattern was found. When increasing the hydrostatic ambient pressure from 0 to 25 kPa, the relation decreases linearly by 0.02/kPa and 0.06/kPa with correlation coefficients of 0.98 and 0.95 using an excitation pressure of 485 and 500 kPa, respectively. When decreasing the ambient pressure in steps of 5 kPa, the relation increases linearly once again. The increase is 0.02/kPa and 0.01/kPa with linear correlation coefficients of 0.88 and 0.92 for driving pressures of 485 and 500 kPa, respectively. Unfortunately, the standard deviation is currently too high to allow for any practical implementation. The best accuracy was found to be ± 3.66 kPa, which was obtained for the first measurement sequence using an excitation pressure of 500 kPa.

Bibliography

[1] B. B. Goldberg, *Ultrasound contrast agents*. London: Martin Dunitz Ltd., 1996.

[2] L. Hoff, *Acoustic Characterization of Contrast Agents for Medical Ultrasound Imaging*. Kluwer Academic Publishers, 2001.

[3] H. Becher and P. N. Burns, *Handbook of Contrast Echocardiography: Left ventricular function and myocardial perfusion*. Berlin: Springer, 2000.

[4] E. Quaia, *Contrast Media in Ultrasonography: Basic Principles and Clinical Applications*. Berlin: Springer, 2005.

[5] C. E. Brennen, *Cavitation and bubble dynamics*. New York: Oxford University Press, Inc., 1995.

[6] T. G. Leighton, *The acoustic bubble*. London: Academic Press, 1997.

[7] J. C. Hogg, "Neutrophil kinectics and lung injury," *Physiological Review Letters*, vol. 67, pp. 1249–1295, 1987.

[8] W. F. Ganong, *Review of Medical Physiology*. Prentice Hall, 1991.

[9] E. M. Agency, "European public assessment report (epar) sonovue," European Medicines Agency, 7 Westferry Circus, Canary Wharf, London, Tech. Rep., 2007.

[10] A. Bouakaz, S. Frigstad, F. J. ten Cate, and N. de Jong, "Super harmonic imaging: a new imaging technique for improved contrast detection," *Ultrasound Med. Biol.*, vol. 28, Issue 1, pp. 59–68, 2002.

[11] P. D. Krishna, P. M. Shankar, and V. L. Newhouse, "Subharmonic generation from ultrasonic contrast agents," *PMB*, vol. 44, Issue 3, pp. 681–694, 1999.

[12] W. T. Shi, F. Forsberg, A. L. Hall, R. Y. Chiao, J.-B. Liu, S. Miller, K. E. Thomenius, M. A. Wheatley, and B. B. Goldberg, "Subharmonic imaging with microbubble contrast agents: initial results," *Ultrasonic Imaging*, vol. 21, Issue 2, pp. 79–94, 1999.

[13] E. Chérin, J. Brown, S.-E. Måsøy, H. Shariff, R. Karshafian, R. W. P. N. Burns, and S. F. Foster, "Radial modulation imaging of microbubble contrast agents at high frequency," *Ultrasound Med. Biol.*, vol. 34 Issue 6, pp. 949–962, 2008.

[14] S.-E. Måsøy, O. Standal, P. Nasholm, T. F. Johansen, B. Angelsen, and R. Hansen, "Surf imaging: In vivo demonstration of an ultrasound contrast agent detection technique," *IEEE Trans. Ultrason., Ferroelec., Freq. Contr.*, vol. 55, Issue 5, pp. 1112–1121, 2008.

[15] R. Gramiak and P. M. Shah, "Echocardiography of the aortic root," *Invest. Radiol.*, vol. 3, pp. 356–366, 1968.

[16] F. W. Kremkau, R. Gramiak, E. L. Carstensen, P. M. Shah, and D. H. Kramer, "Ultrasonic detection of cavitation at catheter tips," *Am. J. Roentgen. Rad. Therapy and Nuclear Medicine*, vol. 110, Issue 1, pp. 177–183, 1970.

[17] M. C. Ziskin, A. Bonakdarpour, D. P. Weinstein, and P. R. Lynch, "Contrast agents for diagnostic ultrasound," *Invest. Radiol.*, vol. 7, Issue 6, pp. 500–505, 1972.

[18] A. A. Bove, M. C. Ziskin, and W. L. Mulchin, "Ultrasonic detection of in-vivo cavitation and pressure effects of high-speed injections through catheters," *Invest. Radiol.*, vol. 4, Issue 4, pp. 236–240, 1969.

[19] B. A. Carroll, R. J. Turner, E. G. Tickner, D. B. Boyle, and S. W. Young, "Gelatin encapsulated nitrogen microbubbles as ultrasonic contrast agents," *Invest. Radiol.*, vol. 15, pp. 260–266, 1980.

[20] S. B. Feinstein, P. M. Shah, R. J. Bing, S. Meerbaum, E. Corday, B. L. Chang, G. Santillan, and Y. Fujibayashi, "Microbubble dynamics visualized in the intact capillary circulation," *J. Am. Coll. Cardiol.*, vol. 4, Issue 3, pp. 595–600, 1984.

[21] A. Bouakaz and N. de Jong, "Wfumb safety symposium on echo-contrast agents: Nature and types of ultrasound contrast agents," *Ultrasound Med. Biol.*, vol. 33, no. 2, pp. 187–196, 2007.

[22] F. Fobbe, O. Ohnesorge, M. Reichel, O. Ernst, R. Schuermann, and K. Wolf, "Transpulmonary contrast agent and color-coded duplex sonography: first clinical experience," *Radiol.*, vol. 185, p. 142, 1992.

[23] B. B. Goldberg, J. B. Liu, P. N. Burns, D. A. Merton, and F. Forsberg, "Galactose-based intravenous sonographic contrast agent: experimental studies," *J. Ultrasound Med.*, vol. 12, pp. 463–470, 1993.

[24] R. Schlief, "Echo enhancement: agents and techniques - basic principles," in *Adv. Echo-Contrast*, vol. 4, 1994, pp. 5–19.

[25] C. Marelli, "Preliminary clinical experience in cardiology with sonazoid," *Am. J. Cardiol.*, vol. 86, Issue 4, Part Supplement 1, pp. 10–13, 2000.

[26] G. M. Lanza, K. D. Wallace, M. J. Scott, C. K. Sheehan, W. P. Cacheris, D. H. Christy, A. M. Sharkey, J. G. Miller, and S. A. Wickline, "Initial description and validation of a novel site targeted ultrasonic contrast agent," in *CIRCULATION*, vol. 92, Issue 8, Suppl. 1, 1995, pp. I–260.

[27] G. M. Lanza, K. D. Wallace, M. J. Scott, W. P. Cacheris, D. R. Abendschein, D. H. Christy, A. M. Sharkey, J. G. Miller, P. J. Gaffney, and S. A. Wickline, "A novel site-targeted ultrasonic contrast agent with broad biomedical application," in *CIRCULATION*, vol. 94, Issue 12, 1996, pp. 3334–3340.

[28] A. L. Beart, *Encyclopedia of Diagnostic Imaging*. Berlin: Springer, 2008.

[29] M. Minnaert, "On musical air-bubbles and the sound of running water," *Philos. Mag.*, vol. 16, pp. 235–248, 1933.

[30] A. Bouakaz, M. Versluis, and N. de Jong, "High-speed optical observations of contrast agent destruction," *Ultrasound Med. Biol.*, vol. 31, Issue 3, pp. 391–399, 2005.

[31] A. Eller and H. G. Flynn, "Generation of subharmonics of order one-half by bubble in a sound field," *J. Acoust. Soc. Am.*, vol. 46, pp. 722–727, 1969.

[32] Lord Rayleigh, "On the pressure developed in a liquid during the collapse of a spherical cavity," *Philos. Mag.*, vol. 34, pp. 94–98, 1917.

[33] M. S. Plesset, "The dynamics of cavitation bubbles," *J. Appl. Mech.*, vol. 16, pp. 277–282, 1949.

[34] N. de Jong and L. Hoff, "Ultrasound scattering properties of albunex microspheres," *Ultrasonics*, vol. 31, pp. 175–181, 1993.

[35] C. C. Church, "The effects of an elastic solid surface layer on the pulsations of gas bubbles," *J. Acoust. Soc. Am.*, vol. 97, pp. 1510–1521, 1995.

[36] K. E. Morgan, J. S. Allen, P. A. Dayton, J. Chomas, A. Klibanov, and K. W. Ferrara, "Experimental and theoretical evaluation of microbubble behavior: effect of transmitted phase and bubble size," *IEEE Trans. Ultrason., Ferroelec., Freq. Contr.*, vol. 47, pp. 1494–1509, 2000.

[37] N. de Jong, P. J. A. Frinking, A. Bouakaz, M. Goorden, T. Schourmans, X. Jingping, and F. Mastik, "Optical imaging of contrast agent microbubbles in an ultrasound field with a 100-mhz camera," *Ultrasound Med. Biol.*, vol. 26 Issue 3, pp. 487–492, 2000.

[38] P. Marmottant, S. van der Meer, M. Emmer, M. Versluis, N. de Jong, S. Hilgenfeldt, and D. Lohse, "A model for large amplitude oscillations of coated bubbles accounting for buckling and rupture," *J. Acoust. Soc. Am.*, vol. 118, pp. 3499–3505, 2005.

[39] N. de Jong, F. J. ten Cate, C. T. Lancée, J. R. T. C. Roelandt, and N. Bom, "Principles and recent developments in ultrasound contrast agents," *Ultrasonics*, vol. 29, pp. 324–330, 1991.

[40] N. de Jong, F. J. ten Cate, W. B. Vletter, and J. R. T. C. Roelandt, "Quantification of transpulmonary echocontrast effects," *Ultrasound Med. Biol.*, vol. 19, no. 4, pp. 279–288, 1993.

[41] A. Prosperetti, "Application of the subharmonic threshold to the measurement of the damping of oscillating gas bubbles," *J. Acoust. Soc. Am.*, vol. 61, pp. 11–16, 1977.

[42] D. H. Evans, W. N. McDicken, R. Skidmore, and J. P. Woodcock, *Doppler Ultrasound, Physics, Instrumentation, and Clinical Applications*. New York: John Wiley & Sons, 1989.

[43] A. C. Burton, *Physiology and Biophysics of the Circulation*, 2nd ed. Chicago: Year Book Medical Publishers, 1972.

[44] A. L. Strauss, F. J. Roth, and H. Rieger, “Noninvasive assessment of pressure gradients across iliac artery stenoses: duplex and catheter correlative study,” *J. Ultrasound Med.*, vol. 12, pp. 17–22, 1993.

[45] H. Baumgartner, H. Schima, G. Tulzer, and P. Kuehn, “Effect of stenosis geometry on the doppler-catheter gradient relation in vitro: A manifestation of pressure recovery,” *J. Am. Coll. Cardiol.*, vol. 21, Issue 4, pp. 1018–1025, 1993.

[46] A. K. Reddy, G. E. Taffet, S. Madala, L. H. Michael, M. L. Entman, and C. J. Hartley, “Noninvasive blood pressure measurement in mice using pulsed doppler ultrasound,” *Ultrasound Med. Biol.*, vol. 29, pp. 379–385, 2003.

[47] W. M. Fairbank and M. O. Scully, “A new noninvasive technique for cardiac pressure measurements: resonant scattering of ultrasound from bubbles,” *IEEE Trans. Biomed. Eng.*, vol. 24, pp. 107–110, 1977.

[48] J. C. Devin, “Survey of thermal, radiation and viscous damping of pulsating air bubbles in water,” *J. Acoust. Soc. Am.*, vol. 31, pp. 1654–1667, 1959.

[49] B. Hök, “A new approach to noninvasive manometry: Interaction between ultrasound and bubbles,” *Med. Biol. Eng. Comp.*, vol. 19, pp. 35–39, 1981.

[50] V. L. Newhouse and P. M. Shankar, “Bubble size measurements using the nonlinear mixing of two frequencies,” *J. Acoust. Soc. Am.*, vol. 75 (5), pp. 1473–1477, 1984.

[51] P. M. Shankar, J. Y. Chapelon, and V. L. Newhouse, “Fluid pressure measurement using bubbles insonified by two frequencies,” *Ultrasonics*, vol. 24, pp. 333–336, November 1986.

[52] T. Tamura, K. Chihara, K. Shirae, K. Ishihara, T. Nagakura, J. Tanouchi, and A. Kitabatake, “Dynamic pressure measurement using two-frequency ultrasound,” in *Jpn. J. Appl. Phys.*, 1989, pp. 211–213.

[53] K. Ishihara, A. Kitabatake, J. Tanouchi, K. Fujii, M. Uematsu, Y. Yoshida, T. Kamada, T. Tamura, K. Chihara, , and K. Shirae, “New approach to noninvasive manometry based on pressure dependent resonant shift of elastic microcapsules in ultrasonic frequency characteristics,” *Jpn. J. Appl. Phys.*, vol. 27-1, pp. 125–127, 1988.

[54] J. Mottley, E. C. Everbach, K. Q. Schwarz, R. Schlief, and R. S. Meltzer, “Decay of ultrasound integrated backscatter from a saccharide contrast agent is accelerated by increased pressure,” in *CIRCULATION*, vol. 82, 1990, pp. 139–140.

[55] J. R. Shapiro, S. A. Reisner, G. S. Lichtenberg, and R. S. Meltzer, “Intravenous contrast echocardiography with use of sonicated albumin in humans systolic disappearance of left ventricular contrast after transpulmonary transmission,” *J. Am. Coll. Cardiol.*, vol. 16, Issue 7, pp. 1603–1607, 1990.

[56] R. Shandas, D. J. Sahn, G. Bales, T. Elkadi, K.-K. Yau, and M. Gharib, “Persistence of albunex (alb) ultrasound contrast agent in-vitro study of the effects of pressure and acoustic power on particle size and the duration of contrast and doppler enhancement,” in *CIRCULATION*, vol. 82, Issue 4, Suppl. III, 1990, p. 95.

[57] C. Vuille, M. Nidorf, R. L. Morrissey, J. B. Newell, A. E. Weyman, and M. H. Picard, "Effect of static pressure on the disappearance rate of specific echocardiographic contrast agents," *J. Acoust. Soc. Echocar.*, vol. 7, Issue 4, pp. 347–354, 1994.

[58] S. Gottlieb, A. Ernst, and R. S. Meltzer, "Effect of pressure on echocardiographic videodensity from sonicated albumin: An in vitro model," *J. Ultrasound Med.*, vol. 14, Issue 2, pp. 109–116, 1995.

[59] A. A. Brayman, M. Azadniv, M. W. Miller, and R. S. Meltzer, "Effect of static pressure on acoustic transmittance of albunex microbubble suspensions," *J. Acoust. Soc. Am.*, vol. 99, no. 4, pp. 2403–2408, 1996.

[60] N. de Jong and F. J. ten Cate, "New ultrasound contrast agents and technological innovations," *Ultrasonics*, vol. 34, Issue 2-5, pp. 587–590, 1996.

[61] R. Schlief and H. Poland, "Ultrasonic manometry process in a fluid by means of microbubbles, U. S. Patent 5,195,520," March 1993.

[62] A. Bouakaz, P. J. A. Frinking, N. de Jong, and N. Bom, "Noninvasive measurement of the hydrostatic pressure in a fluid-filled cavity based on the dissappearance time of micrometer-sized free gas bubbles," *Ultrasound Med. Biol.*, vol. 25, no. 9, pp. 1407–1415, 1999.

[63] L. Hoff and P. C. Sontum, "Acoustic characterisation of nycomed's nc100100 contrast agent," in *Proc. IEEE Ultrason. Symp.*, 1998, pp. 1799–1802.

[64] ——, "Acoustic properties of shell-encapsulated, gas-filled ultrasound contrast agents," in *Proc. IEEE Ultrason. Symp.*, 1996, pp. 1441–1444.

[65] L. Hoff, P. C. Sontum, and J. M. Hovem, "Oscillations of polymeric microbubbles: Effect of the encapsulating shell," *J. Acoust. Soc. Am.*, vol. 107 (4), pp. 2272–2280, 2000.

[66] A. Bouakaz, P. J. A. Frinking, and N. de Jong, "Noninvasive pressure measurement using microbubble contrast agent and wavelet transforms," *Proc. IEEE Ultrason. Symp.*, pp. 1907–1910, 2000.

[67] P. J. A. Frinking, N. de Jong, and E. I. Céspedes, "Scattering properties of encapsulated gas bubbles at high ultrasound pressures," *J. Acoust. Soc. Am.*, vol. 105 (3), pp. 1989–1996, 1999.

[68] E. G. Tickner, J. I. Jackson, and R. E. Short, "Ultrasound-based pressure measurement using bubble decay," in *Proc. IEEE Ultrason. Symp.*, 2001, pp. 1663–1667.

[69] W. T. Shi, F. Forsberg, J. S. Raichlen, and L. Needleman, "Pressure dependence of subharmonic signals from contrast microbubbles," *Ultrasound Med. Biol.*, vol. 25, pp. 275–283, 1999.

[70] W. T. Shi, F. Forsberg, B. B. Goldberg, and J. S. Raichlen, "Method and system for pressure estimation using subharmonic signals from microbubble-based ultrasound contrast agents, U. S. Patent 6,302,845," March 1999.

[71] F. Forsberg, J.-B. Liu, W. T. Shi, J. Furuse, M. Shimizu, and B. B. Goldberg, "In vivo pressure estimation using subharmonic contrast microbubble signals: Proof of concept," *IEEE Trans. Ultrason., Ferroelec., Freq. Contr.*, vol. 52, pp. 581–583, 2005.

[72] L. M. Leodore, F. Forsberg, and W. T. Shi, "In vitro pressure estimation obtained from subharmonic contrast microbubble signals," *Proc. IEEE Ultrason. Symp.*, 2007.

[73] ——, "Subharmonic contrast microbubble signals for noninvasive pressure estimation: an in vitro study," in *CIRCULATION*, vol. 116, Issue 16, Suppl. S, 2007, p. 646.

[74] F. Forsberg, J. Dave, V. G. Halldorsdottir, L. M. Leodore, F. Lin, A. L. Hall, and K. Thomenius, "Applying real-time noninvasive pressure estimation obtained from subharmonic contrast microbubble signals," in *Proc. IEEE Ultrason. Symp.*, 2008, pp. 1694–1697.

[75] D. Adam, M. Sapunar, and E. Burla, "On the relationship between encapsulated ultrasound contrast agent and pressure," *Ultrasound Med. Biol.*, vol. 31, pp. 673–686, 2005.

[76] D. Razansky, Y. Ganor, M. Sapunar, E. Kimmel, and D. Adam, "Estimation of ambient pressure changes using nonlinear acoustic preoperties of ultrasound contrast agents," in *Proc. IEEE Ultrason. Symp.*, 2005, pp. 858–861.

[77] K. S. Andersen and J. A. Jensen, "Simulation of microbubble response to ambient pressure changes," in *Proc. SPIE - Medical Imaging 2008: Ultrasound Imaging and Signal Processing*, vol. 6920, Feb. 2008, p. 692016.

[78] ——, "Ambient pressure sensitivity of microbubbles investigated through a parameter study," *J. Acoust. Soc. Am.*, Submitted Dec. 2008.

[79] ——, "In vitro measurement of ambient pressure changes using a realistic clinical setup," in *Proc. IEEE Ultrason. Symp.*, Nov. 2008, pp. 1096–1099.

[80] ——, "Non-invasive estimation of blood pressure using ultrasound contrast agents," in *Int. Congr. Ultrason.*, Jan. 2009.

[81] L. Trilling, "The collapse and rebound of a gas bubble," *J. Applied Phys.*, vol. 23, pp. 14–17, 1952.

[82] J. B. Keller and M. Miksis, "Bubble oscillations of large amplitude," *J. Acoust. Soc. Am.*, vol. 68, pp. 628–633, 1980.

[83] S. Hilgenfeldt and D. Lohse, "The acoustics of diagnostic microbubbles: dissipative effects and heat deposition," *Ultrasonics*, vol. 38, pp. 99–104, 2000.

[84] N. de Jong, L. Hoff, and N. Bom, "Absorption and scatter of encapsulated gas filled microspheres: theoretical considerations and some measurements," *Ultrasonics*, vol. 30, pp. 95–103, 1992.

[85] J.-F. Yu, D. Zhang, X.-F. Gong, Y.-J. Gong, Z.-M. Zhu, and X.-M. Liu, "Frequency dependences of sound attenuation and phase velocity in suspensions containing encapsulated microbubbles," *Chin. Phys. Lett.*, vol. 22, no. 4, pp. 892–895, 2005.

[86] W. Lauterborn and E. Cramer, "Subharmonic route to chaos observed in acoustics," *Phys. Rev. Letters*, vol. 47, pp. 1445–1448, 1981.

[87] J. A. Jensen, O. Holm, L. J. Jensen, H. Bendsen, H. M. Pedersen, K. Salomonsen, J. Hansen, and S. Nikolov, "Experimental ultrasound system for real-time synthetic imaging," in *Proc. IEEE Ultrason. Symp.*, vol. 2, 1999, pp. 1595–1599.

[88] P. A. Dayton, J. S. Allen, and K. W. Ferrara, "The magnitude radiation force on ultrasound contrast agents," *J. Acoust. Soc. Am.*, vol. 112, pp. 2183–2192, 2002.

[89] J. E. Chomas, P. Dayton, J. A. K. Morgan, and K. W. Ferrara, "Mechanisms of contrast agent destruction," *IEEE Trans. Ultrason., Ferroelec., Freq. Contr.*, vol. 48 Issue 1, pp. 232–248, 200.

[90] E. Biagi, L. Breschi, E. Vannacci, and L. Masotti, "Subharmonic emissions from microbubbles: Effect of the driving pulse shape," *IEEE Trans. Ultrason., Ferroelec., Freq. Contr.*, vol. 53, pp. 2174–2182, Nov. 2006.

[91] M. H. Pedersen, K. L. Gammelmark, J. E. Wilhjelm, C. T. Bøgh, J. A. Jensen, and U. Junghans, *XYZ Translation System Software Manual*, 1st ed., Center for Fast Ultrasound Imaging, Technical University of Denmark, DK-2800 Lyngby, August 2003.

[92] J. A. Jensen, "Field: A program for simulating ultrasound systems," *Med. Biol. Eng. Comp.*, vol. 10th Nordic-Baltic Conference on Biomedical Imaging, Vol. 4, Supplement 1, Part 1, pp. 351–353, 1996b.

[93] J. A. Jensen and N. B. Svendsen, "Calculation of pressure fields from arbitrarily shaped, apodized, and excited ultrasound transducers," *IEEE Trans. Ultrason., Ferroelec., Freq. Contr.*, vol. 39, pp. 262–267, 1992.

[94] J. A. Jensen, *Estimation of Blood Velocities Using Ultrasound: A Signal Processing Approach*. New York: Cambridge University Press, 1996.

[95] S. Gustavsson and J. Kortbek, "Users guide for the beamformation toolbox ii, release 5.0," Ørsted•DTU, Technical University of Denmark, Lyngby, Denmark, Tech. Rep., 2005.

[96] J. G. Proakis and D. G. Manolakis, *Digital Signal Processing*. New York: Macmillian Inc., 1988.

[97] M. S. Bartlett, "Smoothing periodograms from time series with continuous spectra," *Nature (London)*, vol. 161, pp. 686–687, May 1948.

[98] P. D. Welch, "The use of fast Fourier transform for the estimation of power spectra: A method based on time averaging over short, modified periodograms," *IEEE Trans. Au. Electroacous.*, vol. AU-15, pp. 70–73, 1967.

[99] M. H. Hayes, *Statistical Digital Signal Processing and Modeling*. New York: John Wiley & Sons, 1996.

[100] N. de Jong, R. Cornet, and C. T. Lancée, "Higher harmonics of vibrating gas-filled microspheres. part one: Simulations," *Ultrasonics*, vol. 32, pp. 447–453, 1994.

[101] W. T. Shi and F. Forsberg, "Ultrasonic characterization of the nonlinear properties of contrast microbubbles," *Ultrasound Med. Biol.*, vol. 26, pp. 93–104, 2000.

[102] N. de Jong, "Improvements in ultrasound contrast agents," *IEEE Eng. Med. Biol. Mag.*, vol. 15, pp. 72–82, 1996.

[103] P. A. Dayton, K. Morgan, A. L. Klibanov, G. Brandenburger, and K. W. Ferrara, "Simultaneous optical and acoustical observation of contrast agents," *Proc. IEEE Ultrason. Symp.*, pp. 1583–1591, 1997.

[104] W. T. Shi, F. Forsberg, and H. Oung, "Spectral broadening in conventional and harmonic doppler measurements with gaseous contrast agents," *Proc. IEEE Ultrason. Symp.*, pp. 1575–1578, 1997.

[105] E. A. Neppiras, "Subharmonic and other low-frequency emission from bubbles in sound-irradiated liquids," *J. Acoust. Soc. Am.*, vol. 46, Issue 3, pp. 587–601, 1969.

[106] M. Postema, A. van Wamel, C. T. Lancée, and N. de Jong, "Ultrasound-induced encapsulated microbubble phenomena," *Ultrasound Med. Biol.*, vol. 30, pp. 827–840, 2004.

[107] N. Oddershede, "Variable structures for CFU data," Ørsted•DTU, Technical University of Denmark, Tech. Rep., 2005.

APPENDIX

A

Measurement of impulse responses

Before any other measurement can be carried out, a transducer must be selected. To do this, the impulse response of different transducers must be measured. However, before measuring the impulse response of a transducer, it shall meet some requirements. Since it should be possible to observe the subharmonic signal having a frequency half the emitted one, the transducer must not attenuate neither f_0 nor $\frac{1}{2}f_0$ too much. Therefore, it is desired that the transducers to choose from have a center frequency between 2 and 4 MHz.
In this thesis, the two-way impulse response of the transducer is found in stead of the one-way impulse response. To estimate the two-way impulse response, a Gaussian distributed signal with zero mean is emitted towards the bottom of the single wire phantom. The received signal is given by

$$y(t) = h(t) * x(t) * h(t) \,, \tag{A.1}$$

where $h(t)$ is the one-way impulse response of the transducer and $x(t)$ is the emitted signal. Defining the two-way impulse response as $h_{tw}(t) = h(t) * h(t)$ and convolving the received signal with the time reversed of the emitted signal gives

$$\big(x(t) * h_{tw}(t)\big) * x(-t) = R_x(\tau) * h_{tw}(t) \,, \tag{A.2}$$

where $R_x(\tau)$ is the autocorrelation function of $x(t)$. Assuming $x(t)$ is white noise with zero mean gives the autocorrelation function as a Delta function:

$$R_x(\tau) = \delta(t) \,. \tag{A.3}$$

This means that convolving the received signal with the time reversed of the emitted signal yields

$$h_{tw}(t) * \delta(t) = h_{tw}(t) \,, \tag{A.4}$$

assuming the emitted signal is ideal white noise.
In total, four transducers at CFU have been found to meet the requirements on center frequency and bandwidth described above. Table A.1 lists the specifications of these transducers and the frequency spectra of the transducers are shown in Fig. A.1. As it can be seen, all the transducers attenuates the frequencies at 1 MHz 40 dB or more. This necessitates that the center frequency is set to $f_0 = 4$ MHz. Having determined the center frequency, and thereby, the subharmonic frequency, both BK Type 1 and the prototype transducer, BK Type 3, seem to be suitable. The reason why the prototype is selected is mainly because of its physical small size.

ID	f0	Type	BW	Elements	Pitch	Kerf	Height	Elev. foc.	Conv. rad.
		MHz	% (6 dB)		mm	mm	mm	mm	mm
BK Type 1	3.5	Convex	61	128	0.525	?	13	60	?
BK Type 2	4	Convex	65	128	0.245	0.070	10	70	29.5
Sound Techn. Type 1	3.5	Phased	?	128	0.220	?	15	85	0
BK Type 3[1]	3	Phased	60	64	0.260	?	13	80	0

Table A.1: Specifications of considered transducers.

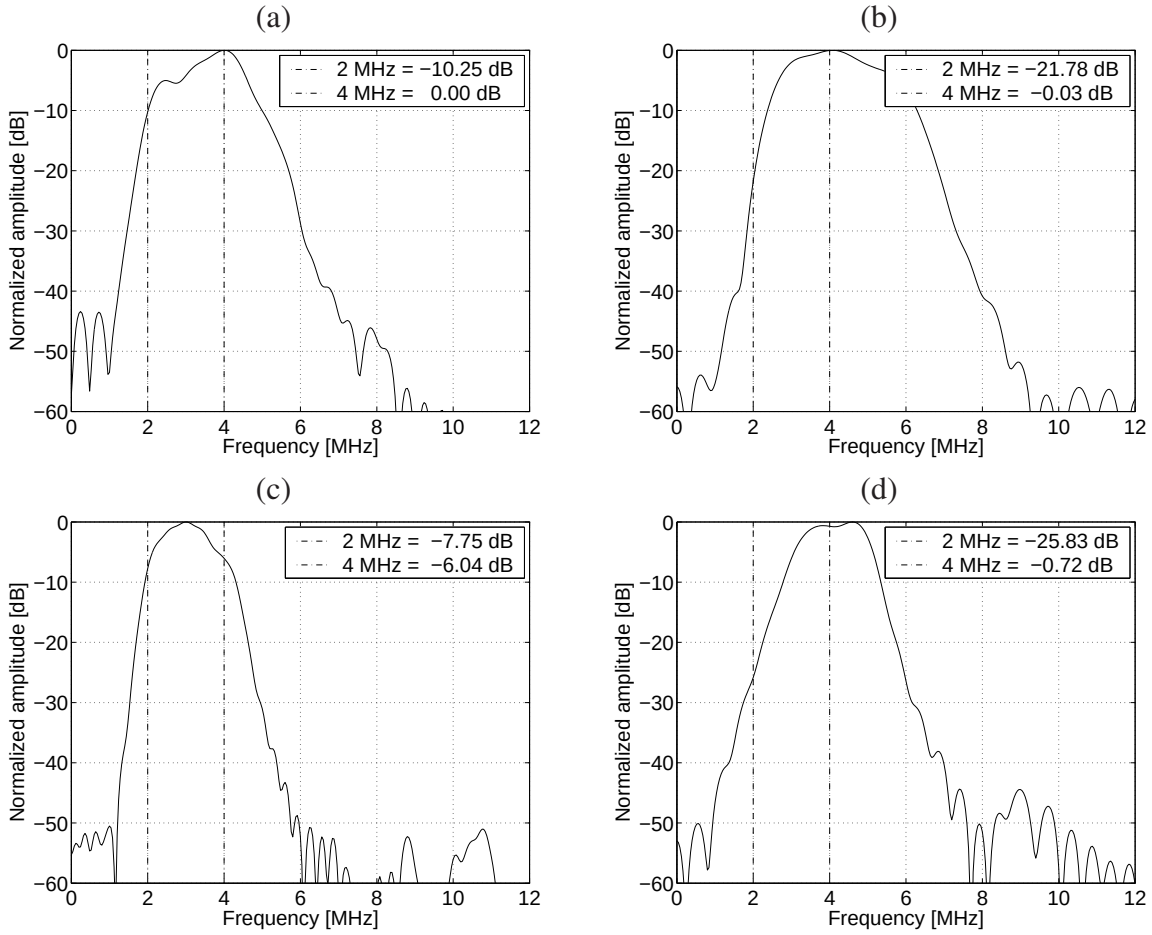

Figure A.1: Frequency spectra of various transducers. BK Type 1 (a), BK Type 2 (b), BK Type 3 (c), and Sound Technology Type 1(d). They have all been calculated from the two-way impulse responses measured using the bottom of the single wire phantom.

[1]Since this transducer is a prototype, it has not been possible to find all the specifications. In fact, some of the information have been taken from a specification sheet belonging to another prototype transducer. The impulse responses are, however, very similar and it is assumed that the transducer is a prior prototype to the selected, before it was putted in a standard BK Medical case.

APPENDIX

B

Pressure controller library

Function	Description
pc_abort	Fast approach to transmit 0 as pressure set-point.
pc_adjust_differential	Adjusts the differential term of the controller.
pc_adjust_integral	Adjusts the I gain of the controller.
pc_adjust_proportional	Adjusts the proportional term of the controller.
pc_assign_new_adress	Changes the adress of the unit connected to a specified COM port.
pc_change_pressure	Sends desired pressure (set point) to the pressure controller.
pc_fix_improper_termination	Fast way to establish communication and transmit 0 Pa as set-point.
pc_flush_buffer	Empties the buffer by throwing all available bytes away.
pc_get_pressure	Reads pressure and set point from controller.
pc_manual	Gives an example of how to use the library.
pc_mode	Changes information mode of pressure controller to either streaming (0) or polling (1) mode.
pc_read	Universal function used to read information from the controller.
pc_setup_rs232	Opens COM port and changes streaming mode to polling mode.
pc_tare	Tares (zeros) the pressure gauge.
pc_terminate	Terminates and closes the communication.
pc_validate_control	Separate script used to test communication and adjustment of the pressure automatically.
pc_write	Universal function which can be used to send any string to the pressure controller.

Table B.1: Short description of available functions designed to communicate with the pressure controller.

APPENDIX

C

Trial protocol for measurements

Version 3.0

This document describes the procedure and necessary equipment for an ultrasound measurement using the experimental scanner RASMUS [87], a contrast agent, and the inflatable phantom (ver 5.2) designed at CFU.

C.1 List of Equipment

The following equipment must be present to carry out the measurement.

- A PC running Linux and Matlab.
- The experimental scanner RASMUS.
- BK-2-ZE-0741 phased array prototype transducer.
- Inflatable phantom (ver 5.2).
- 1 liter of demineralized water or saline.
- Tools for tighten the lid of the phantom.
- Compressor: Jun-Air OF301-4M.
- Dual Valve Pressure Controller: Custom designed Alicat Scientific PCD4-10PSIG.
- Precision pressure regulator: ATD Tools
- Contrast agent.
- Syringe for injection of the contrast agent, e.g. G21.
- Magnetic stirrer.
- Magnetic stick (50 mm) for the magnetic stirrer.
- MATLAB measurement scripts organized as described in Section C.4.

C.2 Setting up the Equipment

Before a measurement can be started, the following steps must be carried out in the order given below.

Preparing the RASMUS System

1. Turn on the RASMUS system and the desired PC for controlling the measurement. The PC must have a LAN connection and a serial COM port.
2. Connect to ”recv” and ”rasmusxmit” using the ’ssh’ command.
3. Run ’sys_master_control’ on both units.
4. Start a MATLAB session (#1) on the main PC.

Preparing the Experimental Setup

1. Attach the transducer to the phantom.
2. Put the magnetic stick at the bottom of the phantom.
3. At least 24 hours before experiment, pour demineralized water or saline into the phantom.
   Ensure the tube connecting the pressure controller sensor port and the measurement chamber is also filled.
4. Connect the extension cord to the power supply and verify that the compressor, magnetic stirrer, and pressure controller is turned on.
5. Verify that the stirrer can invoke the magnetic stick in the phantom.
6. Ensure the feed pressure of the compressor is set to 4 bar.
7. Ensure the precision regulator is adjusted to 2 bar.
8. Start another MATLAB session (#2) on the main PC.
9. Invoke the function ”pc_setup_rs232” in session #2 to establish contact to the pressure controller.
10. Verify connection has been establish using the function ”pc_get_pressure”.
11. Tare (zero) the pressure sensor using the command ”pc_tare”.
12. Ensure the following terms are adjusted properly by invoking the respective functions ”pc_adjust_...”: Differential (1500), Integral (31), Proportional (65535).
13. *Optional:*
    If the manual pressure gauge is fixed on the lid of the phantom, tare it by press and release ”MIN/MAX” and ”DAMP” at the same time.

14. Fix the lid to the lower part of phantom.
15. Put ambient pressure to the chamber using the function ”pc_change_pressure”.
16. Release the pressure back to 0 Pa.

C.3 Measurement Procedure

Prior to injection of the contrast agent, it is necessary to ensure that everything works as intended. This section outlines the preparation procedure. Besides the procedure for verification of the equipment, a manual for handling the contrast agent is also given. The following items list the necessary things to do before the agent can be injected.

1. Adjust the script ”main_rasmus_...” to perform an initial measurement for adjusting the TGC (Time Gain Compensation). This is done by a boolean (*adjust_TGC*) in the script.
2. Setup the RASMUS system using MATLAB session #1 (initiate the script ”main_rasmus_...”).
3. Turn on low-voltage amplifiers.
4. Turn on high-voltage amplifiers.
5. Insert the contrast agent and wait approximately 1 minute for proper dispersion.
6. Adjust the TGC by performing a number of test measurements.
7. When satisfied, ensure the same start time (*start_time_stamp*) is given in the two control measurement script, ”main_rasmus_...” and ”manage_pressure_script.m”.
8. Initiate the script ”main_rasmus_...” with the boolean *adjust_TGC* set to 0.
9. Start ”manage_pressure_script.m” in MATLAB session #2 immediately after.

Handling of Contrast Agent

The following items are guidelines on how to handle the contrast agent Optison. It is a free translation from Danish of selected items listed on page 23 in the product information regarding Optison.

- Remove the vial from the refrigerator and let it obtain room temperature.
- Turn and rotate the vial carefully in approximately three minutes for complete re-suspension of the micro spheres.
- Complete re-suspension will turn op as a white uniform color without any material on the surface of the plug and the vial.
- OPTISON should gently be drawn into the syringe within one minute after re-suspension.
- OPTISON will separate when left in the syringe and needs to be suspended before use.

- Suspend the micro spheres in the syringe before injection by holding the syringe horizontally between the palms and quickly roll it back and forth for at least 10 seconds.
- Inject the suspension through the syringe with a maximum injection rate of 1.0 ml/s.
- Immediately before injection, a visual inspection is compulsory to ensure full suspension of the micro spheres.

Terminating the RASMUS System

When the measurement has been carried out, the RASMUS system must be terminated properly. The ordered steps below outlines the procedure.

1. Turn off high-voltage amplifiers.
2. Turn off low-voltage amplifiers.
3. When all data has been stored, end 'sys_master_control' on "recv" and "rasmusxmit" by typing 'Ctrl'+'c'.
4. End secure shell sessions using the 'exit' command.

5a. Log in to "recv" on the PC next to RASMUS and type 'poweroff'.

5b. Log in to "rasmusxmit" at the PC next to RASMUS and type 'poweroff'.

6. Turn off the RASMUS system.

C.4 Description of necessary measurement scripts

The following type of Matlab scripts are necessary to perform a measurement. The examples listed is the names of the scripts which were used for a measurement on 31 November 2008.

Main script , e.g. "main_rasmus_20081131.m"
: This is the main script used to set up a measurement using the RASMUS system. It is used to call sub-scripts which initializes measurement parameters, prepares RASMUS for measurement, controlling the timing of the entire experiment, and saves data.

Initialize parameters , e.g. "initialize_params_ver_1p2.m"
: Handles the main initialization of various parameters used to set up the RASMUS system. The initialization should be organized in proper structures according to the common variable structure at CFU [107].

Define emission sequence , e.g. "define_shooting_seq_32cycles.m"
: This script is used to define parameters regarding emission and reception during a measurements using RASMUS. In this script, the excitation waveforms (shape and length of emission pulse, virtual focal points) and shooting sequence should be defined.

Manage pressure script , e.g. ”manage_pressure_script_ver2p1.m”

This script is used to manage the pressure inside the inflatable phantom during a measurement using RASMUS.

APPENDIX

D

Papers

D.1 K. S. Andersen and J. A. Jensen, Simulation of microbubble response to ambient pressure changes, *Progress in Biomedical Optics and Imaging - Proceedings of SPIE 2008*

This paper was published in *Progress in Biomedical Optics and Imaging - Proceedings of SPIE 2008, Issue Vol.6920, 2008*. Conference title: *Medical Imaging 2008: Ultrasonic Imaging and Signal Processing. Issue Vol.6920, Page no. 692016-1-12*.

Simulation of microbubble response to ambient pressure changes

Klaus Scheldrup Andersen and Jørgen Arendt Jensen

Center for Fast Ultrasound Imaging, Ørsted•DTU,
Technical University of Denmark, Kgs. Lyngby, Denmark

ABSTRACT

The theory on microbubbles clearly indicates a relation between the ambient pressure and the acoustic behavior of the bubble. The purpose of this study was to optimize the sensitivity of ambient pressure measurements, using the subharmonic component, through microbubble response simulations. The behaviour of two different contrast agents was investigated as a function of driving pulse and ambient overpressure, p_{ov}. Simulations of Levovist using a rectangular driving pulse show an almost linear reduction in the subharmonic component as p_{ov} is increased. For a 20 cycles driving pulse, a reduction of 4.6 dB is observed when changing p_{ov} from 0 to 25 kPa. Increasing the pulse duration makes the reduction even more clear. For a pulse with 64 cycles, the reduction is 9.9 dB. This simulation is in good correspondence with measurement results presented by Shi et al. 1999, who found a linear reduction of 9.6 dB. Further simulations of Levovist show that also the shape and the acoustic pressure of the driving pulse are very important factors. The best pressure sensitivity of Levovist was found to be 0.88 dB/kPa. For Sonazoid, a sensitivity of 0.71 dB/kPa has been found, although the reduction is not completely linear as a function of the ambient pressure.

Keywords: Ultrasound contrast agent, simulation of microbubbles, ambient pressure estimation

1. INTRODUCTION

Local blood pressure measurements provide important information on the state of health of the organs in the human body and can be used to diagnose severe heart, lung, and kidney diseases. The pressure is currently measured locally in arteries and organs by means of a pressure catheter. As this is an invasive technique, it is inconvenient to the patient, there is a risk of infection, and the catheter will inevitably introduce changes to the blood flow and, thereby, the pressure. Therefore, many attempts to find a noninvasive procedure have been made. When evaluating new approaches for noninvasive local blood pressure measurements, the sensitivity is a crucial factor. Although, the human blood pressure varies between 0 and approximately 25 kPa (1 kPa = 7.5 mmHg), it should still be possible to distinguish pressure differences as low as 1-3 kPa to measure the blood pressure in the small veins and arteries. One noninvasive approach that has been suggested is to perform Doppler echocardiography using a simplified modification of the Bernoulli equation.[1,2] This method was, however, concluded not to yield reproducible or reliable results by Straus et al.[3] Another type of approach, which is still being investigated, is to combine microbubbles injected into the blood and diagnostic ultrasound.

It is well known that bubbles in a fluid can be used for measurement of pressure gradients due to their size dependent oscillations. Since the introduction of ultrasound contrast agents (UCAs), many approaches on how to exploit their ambient pressure sensitivity have been presented. One of the first to propose noninvasive measurement of cardiac pressure using an UCA were Fairbank and Scully[4] in 1977. They claimed that the acoustic properties of the microbubbles change when the size of the bubbles changes. To measure these changes, they suggested the use of resonance excitation. However, due to the large size distribution of the first generation UCAs containing free bubbles, their results were inconclusive. Other suggestions from that time are by Hok[5] in 1981 and Newhouse and Shankar[6,7] in 1986. Newhouse and Shankar showed theoretically and experimentally

Further author information:
Klaus Scheldrup Andersen:
E-mail: ksa@oersted.dtu.dk, Telephone: +45 4525 3898,
Address: Ørsted•DTU, Bldg. 349, Technical University of Denmark, DK-2800 Kgs. Lyngby, Denmark

that accurate bubble size measurements are possible using a double frequency technique for determination of the sum and difference frequencies. The rapid dissolution time after injection of the free air bubbles prevented, however, any practical implementation.

With the introduction of the more stable second generation UCAs, the circulation system can now be used to transport the encapsulated microbubbles to the region of interest. This has initiated new attempts to exploit the ambient pressure dependent acoustic properties that the high compressible air and gas bubbles possess. Bouakaz et al.[8] presented in 1999 an approach for measuring the disappearance time of free bubbles, which were generated at the region of interest by rupturing the contrast agent microbubbles using a low-frequency high acoustic amplitude pulse. From *in vitro* experiments they concluded the approach to have a resolution of 6.7 kPa (50 mmHg). Later, they suggested the resolution could be improved by using larger bubbles or by using wavelet processing or a combination of this.[9] No *in vivo* results or further investigations have, however, been presented using this approach yet. Around the same time, Shi et al.[10] observed from experiments that the subharmonic component of Levovist is highly sensitive to ambient pressure changes compared to the fundamental and the second harmonic component. They reported a 9.9 dB linear decrease of the peak amplitude of the subharmonic component when increasing the ambient hydrostatic pressure from 0 to 24.8 kPa (186 mmHg). Furthermore, they found that the ambient pressure-induced reduction was highest when the acoustic excitation pressure was around the growth stage of the subharmonic, which occurs when the acoustic driving pressure causes the subharmonic component to increase rapidly from background noise level to be clearly visible in the spectrum. Recently, the same group have presented similar results for Sonazoid, which was found to have an average decrease of 13.3 dB.[11] Furthermore, in 2005 the same group presented *in vivo* results for proof of concept of the capabilities of the subharmonic response.[12] As the measurements were performed directly on the abdominal cavity and the aorta by incision of two dogs, this can hardly be characterized as noninvasive. However, the results still showed that the subharmonic component decreased as the ambient pressure increased and, thereby, indicated the subharmonic response of UCAs can be used for ambient pressure measurements. Also in 2005, Adam et al.[13] investigated microbubbles' response to cyclic ambient pressure changes by mimicking left ventricular pressure changes. They found that the subharmonic response correlated best with the cyclic changes compared to the fundamental and second harmonic, but also observed a transient delay before this correlation occured. In spite of all these promising measurement results, the mechanism of the complex and highly nonlinear UCAs is, however, not fully understood. This necessitates use of modeling to improve existing techniques and create new ones to exploit the capabilities of UCAs optimally.

Modeling the acoustics of bubbles in a fluid is a still ongoing investigation, which was initiated by Lord Rayleigh[14] in 1917 who studied damages to ship propellers due to bubble cavitation. In 1933, Minnaert[15] explained the characteristic resonance frequency of free bubbles when he did a theoretical and experimental study of bubbles' emission of sound. Since then, several modifications to the existing models and new theoretical models on how to predict the behavior of an oscillating bubble have been presented. Most models are based on modifications of the Rayleigh-Plesset[16] equation and are capable of handling shell encapsulating bubbles. This includes the models used by de Jong and Hoff[17] and Church.[18] Other models are based on the modified Herring equation to describe the radial motion (e.g. Morgan et al.[19]). Recently, Vos et al.[20] proposed a novel approach for investigation of full populations of microbubbles' behavior in acoustic fields, also based on the modified Herring equation. The study, furthermore, included a new method to estimate the viscoelastic shell properties of UCAs. Existing methods for this based on the Rayleigh-Plesset equation has been suggested by de Jong et al.[17,21] and described further by Hoff.[22]

Despite the growing number of experiments within hydrostatic pressure measurements, no real parameter study investigating the response of microbubbles in respect to ambient pressure changes has been performed until now. The purpose of this study was to optimize the sensitivity of pressure measurements through bubble response simulations investigating the complex mechanisms for subharmonic generation. This was carried out by an extensive number of simulations of two commercial UCAs. Since the study focused on the effect of the driving pulse, the parameters of the microbubbles were fixed in all simulations whereas several different settings regarding the excitation pulse were varied.

This paper is organized as follows: Section 2 presents the choice of simulation model and parameters used for the investigation. Furthermore, it also describes the processing of the simulated response. The achieved results

are presented and discussed in Section 3. Finally, the investigation is summarized by a conclusion in Section 4.

2. THEORY AND METHOD

The investigation has been performed using the Matlab (The Math Works Inc., Natick, Mass., USA) environment. To carry out the simulations, the free simulation program Bubblesim by Hoff[22] is used. Bubblesim is a toolbox that calculates the oscillation and scattered echo for a specified contrast agent microbubble and excitation pulse. It numerically solves a second order ordinary differential equation (ODE) that has been combined from a set of equations, each equation modeling different parts (bubble, shell, and surrounding liquid) of the system that makes up a contrast agent microbubble. In Bubblesim, the following four different models are implemented: The Rayleigh-Plesset[16] (R-P) model, the Trilling[23] model, the Keller-Miksis[24] model, and a modified version of the R-P model, which is an intermediate model of the R-P on one side and the Trilling and Keller-Miksis models on the other. The largest disadvantage of the R-P model is that it does not include radiation damping, which is energy loss caused by radiation of sound. This is accounted for in the Trilling and the Keller-Miksis models, which both include a finite but constant speed of sound in the liquid. However, both the Trilling and Keller-Miksis model has a risk of becoming numerical unstable when the bubble wall velocity becomes comparable to the speed of sound (acoustic Mach numbers, $M = \dot{R}/c$, around unity). This happens for high oscillation amplitudes and causes the models to have an unphysical negative inertia. Instead, Hilgenfeldt et al.[25] have used a modified version of the R-P model that includes the radiation damping term from the Trilling and Keller-Miksis models. This version is implemented in Bubblesim and the model selected for the parameter investigation. It was chosen because of its numerical stability, which is important when doing many simulations spanning a wide range of variable changes. The modified R-P model is[22]

$$\rho R\ddot{R} + \frac{3}{2}\rho\left(\dot{R}\right)^2 - p_L + p_{ov} + p_{ac}\left(t\right) - \frac{R}{c}\cdot\dot{p_L} = 0, \tag{1}$$

where ρ is the surrounding liquid density, R is the bubble radius, $\dot{R} = \frac{dR}{dt}$ denotes derivation w.r.t. time t, p_L is the pressure at the bubble surface, p_{ov} is the static background overpressure, p_{ac} is the driving acoustic pressure, and c is the speed of sound. The first term describes the pressure as function of the bubble wall acceleration, whereas the second term describes the pressure as a function of the bubble wall velocity. $p_\infty = p_{ov} + p_{ac}$ is the background pressure describing the pressure in the liquid far from the bubble surface. p_L includes contributions from the gas, the viscosity, and the effects of the shell encapsulating the bubble. Finally, the last term including $\dot{p_L} = \frac{dp_L}{dt}$ is the one accounting for the radiation damping. Any numerical solver can be used to solve the ODE in (1). Examples are the Runge-Kutta algorithm of order 4 and 5 (`ODE45`) and the multistep ODE solver of variable order from 1 to 5 (`ODE15s`), which are both available in Matlab as a standard. In this study, the solver of variable order has been selected as it should be more reliable and stable for solving situations where the differential equation becomes stiff.[22] This occurs for example when the bubble radius changes slowly during the expansion phase but goes through very fast changes in radius and velocity under compression. The choices on simulation model and numerical solver, as well as other general setup parameters, for the simulations in this study are summarized in Table 1.

Parameter	Designation
ODE solver	`ODE15s`
Simulation model	`Modified Rayleigh-Plesset`
Thermal damping	`Isothermal`
Liquid	`Water`

Table 1. List of simulation parameters regarding general setup of Bubblesim.

In its standard form, Bubblesim has a flexible graphical user interface, which makes it easy to perform single simulations for minor investigations. In this study, a batch mode has been created for two reasons: It gives a bit more control and, more importantly, it makes it possible to perform multiple simulations automatically, which is essential in a parameter study like this. Furthermore, one modification has been made to Bubblesim. In its

original form, it is not possible to change the ambient overpressure parameter denoted p_{ov} in (1). Since this is crucial, when investigating microbubbles' sensitivity to ambient pressure changes, this feature has been enabled by small modifications to the source code.

While the bubble size distribution can be determined with a multisizer, it is somewhat more difficult to specify the parameters related to the surrounding shell of today's UCA microbubbles. One way to do this is to perform a combination of experiments and model fitting as described by de Jong and associates.[17,21,22] This will, however, only give an estimate of proper designations and usually an interval for some of the parameters is given. The procedure has been used by Yu et al.[26] and Hoff[22] to estimate suitable parameters for the commercial contrast agents Levovist (Schering AG, Berlin, Germany) and Sonazoid (GE Healthcare, Oslo, Norway), respectively. The values used in this investigation were fixed for all simulations and are listed in Table 2. Before a simulation

Contrast agent	Bubble Radius [μm]	Shell Thickness [nm]	Shear Modulus [MPa]	Shear Viscosity [Pa s]
Levovist	3.0	6.0	80	1.3
Sonazoid	3.2	4.0	52	0.99

Table 2. List of the parameters used to describe the two different types of bubbles for the simulations in Bubblesim.

can be carried out, a driving pulse must be selected. Since the emphasis of this study was to optimize the subharmonic sensitivity to ambient pressure changes as a function of the excitation pulse, a large number of different driving pulses were examined. The driving pulse was generated based on four different characteristics being the center frequency, f_c, the number of pulse cycles, N_c, the maximum acoustic pressure, p_{ac}, and the shape of the pulse. The possible designations used for the investigation are listed in the upper part of Table 3. As can be seen from Table 3, 30 different settings for the acoustic pressure is used. This was decided to ensure determination of the growth stage of the subharmonic component with a reasonable precision. Although an acoustic pressure of 950 kPa will probably destroy the microbubbles in real measurements, the high values were selected to cover the entire range of subharmonic growth and saturation. The bottom row of Table 3 lists the designations of the ambient overpressures which were used in the simulations. As can be seen, the range covers the interval between 0 and 25 kPa in steps of 5 kPa. In this way, the most common human blood pressure values are covered. Combining all the parameters in Table 3 gives a total of 3600 different simulations for each contrast agent.

Parameter	Designation	Unit
f_c	`2.0`	[MHz]
N_c	`1 2 5 10 20 32 48 64 128 256`	[cycles]

p_{ac}	`100 150 200 250 300 350 375 400 425 450`
	`475 500 525 550 575 600 625 650 675 700`
	`725 750 775 800 825 850 875 900 925 950`
		[kPa]

Pulse shape	`'rectangular' 'hanning'`	
p_{ov}	`0 5 10 15 20 25`	[kPa]

Table 3. List of parameter designations used in combination with the contrast agents listed in Table 2. Combining all settings gives 3600 simulations in total for each agent.

When Bubblesim has completed a simulation, the simulated scattered pressure is returned and the Fourier transformation is applied. Next, a search for the fundamental (f_0), the first subharmonic ($\frac{1}{2}f_0$), and the second harmonic ($2f_0$) component is performed and the energy of each component is calculated. The center frequencies of the harmonic bands were selected as multiples of the emitted center frequency, f_c. It should, however, be denoted that initial simulations show that the frequency of the subharmonic component shifts slightly as the acoustic driving pressure is increased! The energy has been chosen over the peak amplitude since this is a more

robust measure. The bandwidth to calculate the energy within was selected as the −10 dB bandwidth of the excitation pulse.

3. RESULTS AND DISCUSSION

This section presents some of the results obtained through the simulation study. First, the fundamental, the subharmonic, and the second harmonic dependence on acoustic pressure will be presented. This is a natural step for two reasons: First of all, generation of the subharmonic component must be ensured before looking into the ambient pressure dependency. Another reason is to see at which acoustic pressures the growth stage of the subharmonic occurs for the two types of microbubbles. Along with this investigation, the scattered spectra have been examined to ensure useful responses and proper selection of the bandwidth intervals to calculate the energy of the respective frequency components within. Since these results are rather trivial and takes up a lot of space, only a few selected spectra are presented in this section. In the last part of this section, the influence of ambient overpressure will be examined.

3.1 Dependence on Acoustic Pressure

Fig. 1 shows the energy of the subharmonic, the fundamental, and the second harmonic component of Sonazoid as a function of acoustic pressure when a rectangular driving pulse for a different number of cycles is used. Examining the subharmonic component, three characteristic stages are clearly observed. In the occurrence stage, which occurs for acoustic pressures below 350 kPa, the subharmonic is around the noise level and hence insignificant. For acoustic pressures in the interval between 350 kPa and 450 kPa, the subharmonic increases rapidly and this part can be characterized as the growth stage. When increasing the acoustic pressure further, the growth eases off and can be compared to the saturation stage observed in measurements. This pattern is the same for pulses of other length than displayed here, although the subharmonic component can not be distinguished from the fundamental for driving pulses smaller than 5 cycles. Looking at the fundamental, it behaves somewhat different from what was expected. For pressures below 350 kPa it increases linearly as expected according to measurement experiments. Then it almost does not change until the driving pressure reaches 800 kPa, where it suddenly increases rapidly until an acoustic pressure around 875 kPa. At these levels, the corresponding spectra look more noisy, which is also supported by looking at the second harmonic component. In this connection, however, the second harmonic behaves less linear as function of driving pressures, although the pattern is more or less the same as for the fundamental. This chaotic behavior at high acoustic pressure levels predicted in the simulations is actually in good correspondence with experimental results of free bubbles achieved by Lauterborn and Cramer.[27] One explanation for the little change of the fundamental between 350 and 800 kPa could be that some of the increased energy is transferred to the subharmonic and ultraharmonics, which at these driving levels are observed in the spectra.
When the shape of the driving pulse is changed by applying a Hanning window, especially the fundamental and partly the second harmonic changes behavior as can be seen in Fig. 2. Using this type of driving pulse, the increase is more constant as the acoustic pressure is increased. The chaotic behavior is, however, still observed for very high acoustic pressures. Regarding the subharmonic component, the three stages pattern is the same as observed for the rectangular driving pulse, although the interval of the growth period seems to have increased a little. This makes sense since less energy is transmitted using a Hanning shaped driving pulse compared to a rectangular signal of the same acoustic strength.

The results for the simulations of Levovist as a function of acoustic pressure using a rectangular driving pulse is shown in Fig. 3 (a). Once again, the three stages behavior of the subharmonic component is observed. However, now the growth stage first occurs in the interval from 600 to 900 kPa. Although the increase in Energy is the same, the interval is much higher than experimental results achieved by Shi et al.,[10] who observed it to be between 300 and 600 kPa for Levovist using a 64 cycles rectangular driving pulse with a center frequency of 2 MHz. The fundamental and second harmonic more closely resembles the obtained measurement results, although the simulated saturation is not as pronounced in the measurements. The simulations of Levovist using a Hanning shaped excitation pulse indicates it is very hard to generate the subharmonic component for this type of driving pulse, see Fig. 3 (b). In fact, the subharmonic component is hardly visible in any of the spectra, not

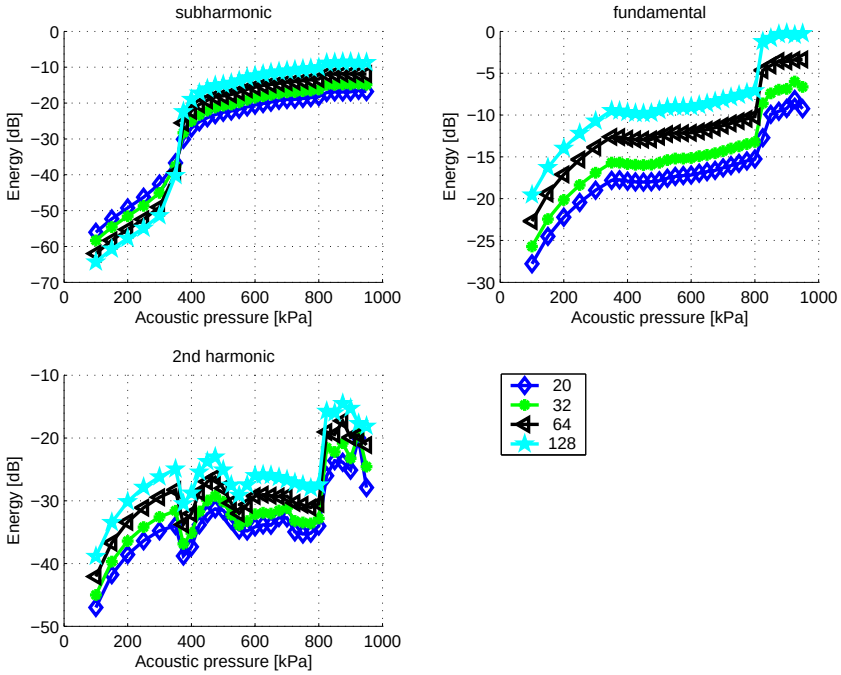

Figure 1. Energy as a function of acoustic pressure for Sonazoid. The driving pulse is a rectangular shaped sinusoidal. Upper left graph shows the subharmonic behavior, upper right shows the first harmonic, and lower left presents the behavior of the second harmonic component. Each curve represent a different number of cycles in the driving pulse as displayed in the legend to the lower right in the figure.

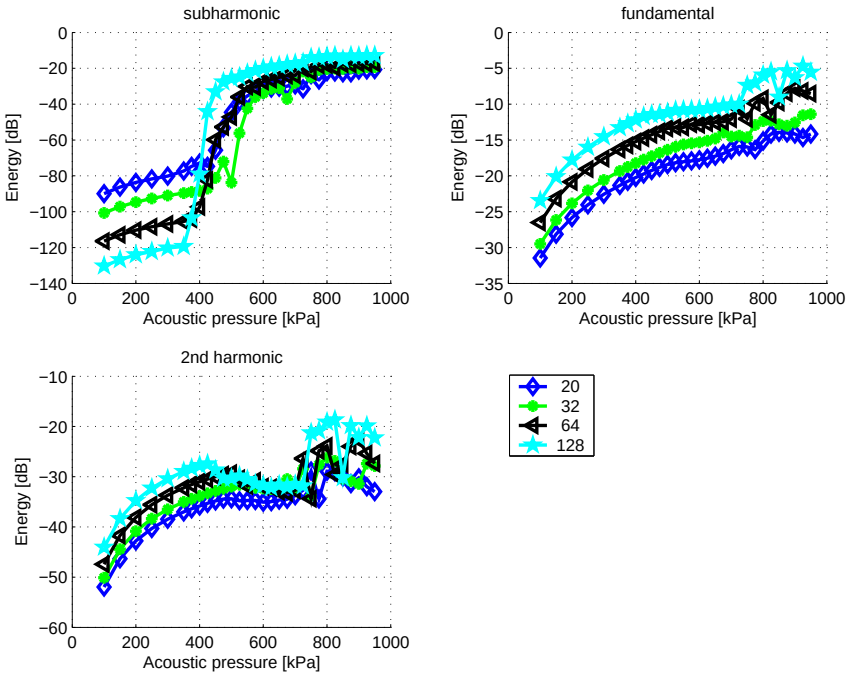

Figure 2. Energy as a function of acoustic pressure for Sonazoid. The driving pulse is a Hanning shaped sinusoidal. Upper left graph shows the subharmonic behavior, upper right shows the first harmonic, and lower left presents the behavior of the second harmonic component. Each curve represent a different number of cycles in the driving pulse as displayed in the legend to the lower right in the figure.

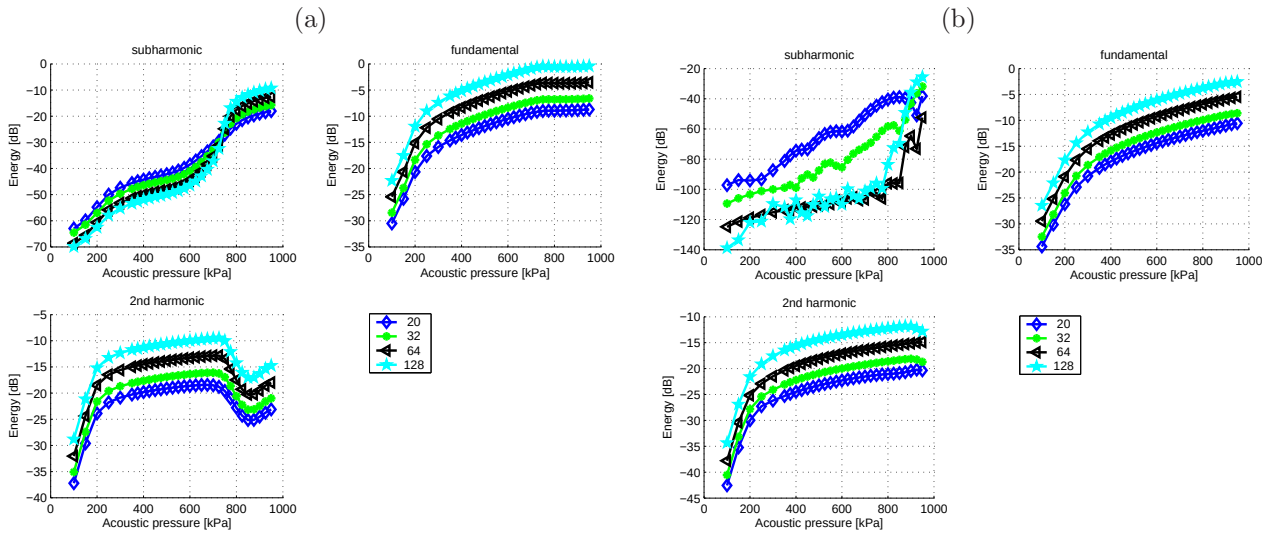

Figure 3. Energy as a function of acoustic pressure for Levovist. The driving pulse is a rectangular shaped (a) and Hanning shaped (b) sinusoidal, respectively. Upper left graph shows the subharmonic behavior, upper right shows the first harmonic, and lower left presents the behavior of the second harmonic component. Each curve represent a different number of cycles in the driving pulse as displayed in the legend to the lower right in the figure.

even a the very high driving pressures. Regarding the fundamental and second harmonic component, they are similar to what was observed using the rectangular driving pulse.

Except, possibly, for the last setup, common for all the simulations is that the subharmonic component has a threshold and is present only above a certain acoustic pressure. This observation was also reported by Prosperetti[28] who examined this experimentally on free bubbles and, as mentioned, by Shi et al.[10] One difference between the simulations and the measurements is, however, that the simulated threshold seems to be higher than the measured. A reason for this can be the selection of the shell parameters for Levovist as the simulated threshold of Sonazoid is comparable to the measured threshold of Levovist. In contrast to the threshold behavior of the subharmonic, the higher harmonics seems to be present to various degrees for all driving pressures.
Finally, one interesting observation regarding the scattered pressure, when using the Hanning shaped driving pulse for excitation of Sonazoid, should be noted. When the driving pressure is increased to a level where the subharmonic is generated, the scattered response suddenly changes characteristics halfway in the pulse as shown in Fig. 4 (a). In the first half, the traditional harmonic distortion is clearly observed but no subharmonics. Halfway in the signal, the characteristic oscillation at twice the driving period is seen and continues for the rest of the scattered response. As can be seen from the corresponding spectrum in Fig. 4 (b), this is what gives rise to the sub- and ultraharmonics.

3.2 Dependence of Overpressure

In this subsection, the simulation results achieved when changing the ambient overpressure will be shown. Fig. 5 shows an example of how the scattered spectrum changes, when the ambient pressure is the only parameter that is changed from one simulation to another. The example is for Levovist when driven by a rectangular pulse with 32 cycles and an acoustic pressure of 800 kPa. In Fig. 5 (a), the scattered spectrum is shown when no pressure is seen and Fig. 5 (b) shows the spectrum when an overpressure of 25 kPa is applied. Comparing the two spectra, a clear reduction of the subharmonic component at 1 MHz is observed. Looking at the fundamental at 2 MHz and the second harmonic component at 4 MHz, it is seen that these increases when overpressure is applied. In fact, this is a clear tendency from many of the simulations.
To see the effect on the subharmonic component when the pulse length is varied, Fig. 6 has been created. It displays the energy of the subharmonic component when using the same setup as used to create Fig. 5. As can be seen, there is a clear tendency for all pulse lengths that the energy decreases as the overpressure is increased.

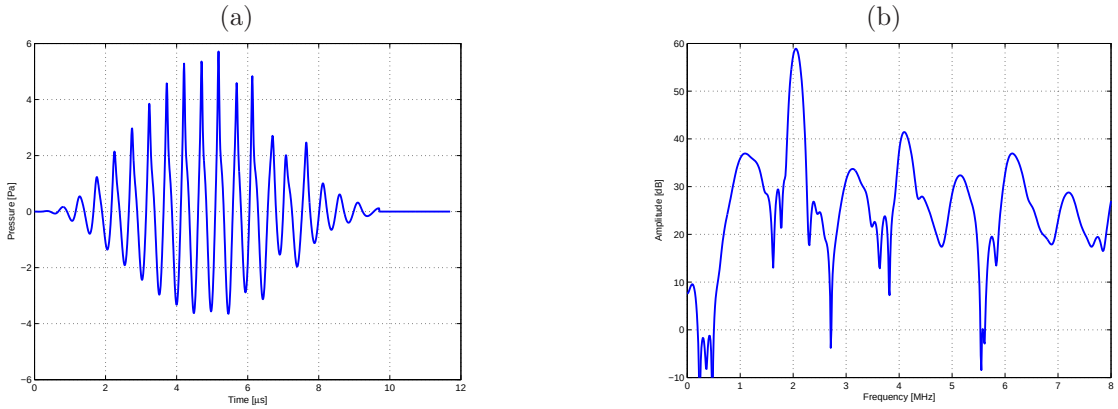

Figure 4. Example of scattered pressure (a) and it's corresponding spectrum (b) when using a Hanning shaped driving pulse. The bubble corresponds corresponds to Sonazoid and the excitation is a 20 cycles Hanning shaped signal with a center frequncy of 2 MHz and an acoustic pressure of 525 kPa.

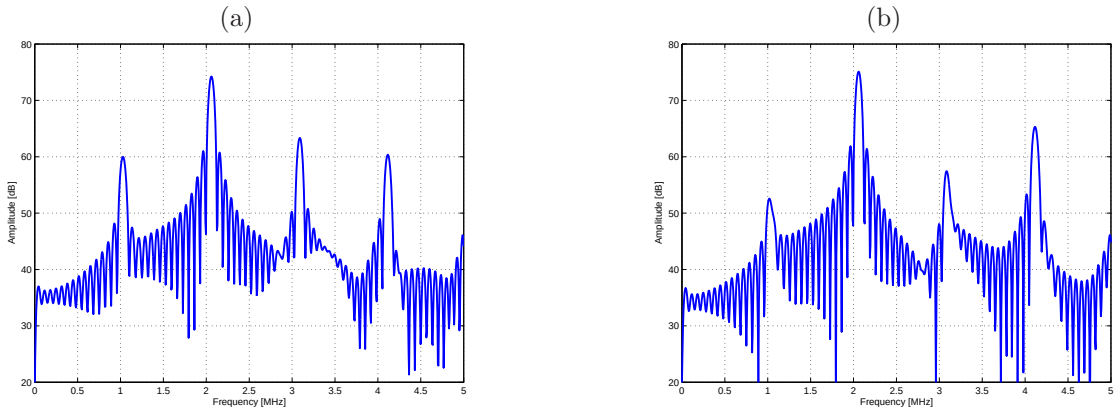

Figure 5. Example of spectrum of scattered response from excitation of microbubble corresponding to Levovist. The driving pulse is a 32 cycles rectangular shaped signal with a center frequncy of $f_c = 2$ MHz and an acoustic pressure of $P_{ac} = 800$ kPa. (a) is when no overpressure is applied and (b) shows the response when a overpressure of 25 kPa is applied.

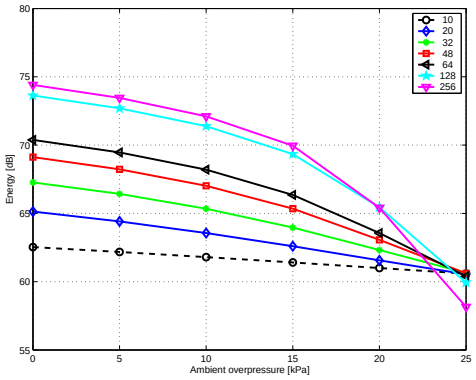

Figure 6. Energy of the subharmonic component scattered by Levovist when using a rectangular shaped driving pulse with an acoustic pressure of 800 kPa. The energy is displayed as a function of ambient pressure and each curve in the plot represents a different number of cycles in the driving pulse as indicated by the legend.

Furthermore, the total decrease in energy also seems to be dependent on the number of cycles in the driving pulse. However, Fig. 6 also indicates that the decrease is not completely linear in all cases. For easy comparison of the change in energy for the different simulation setups, Fig. 7 shows the energy of the three frequency components as function of ambient overpressure when each simulation has been normalized to their respective maximum. Looking at the results for the fundamental, it is seen that this component is not affected by ambient pressure

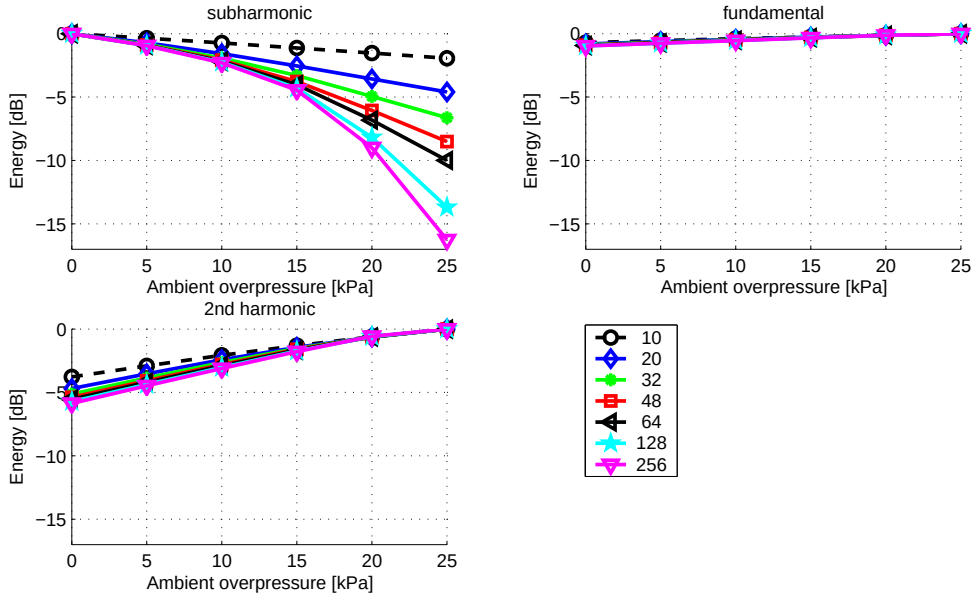

Figure 7. Decrease in energy of respective frequency components scattered by Levovist when using a rectangular shaped driving pulse with an acoustic pressure of 800 kPa. The energy is displayed as a function of ambient pressure and each curve in the plots represents a different number of cycles in the driving pulse as indicated by the legend.

changes. The second harmonic seems to be affected and increases about 5 dB, slightly dependent on the pulse length. This increase is quiet in contradiction to the experiments by Shi et al.,[10] who excited Levovist in the growth stage using a 64 cycles rectangular pulse. They found that the second harmonic slightly decreases by 1.8 dB over the same ambient pressure interval. When examining the subharmonic in Fig. 7, a highly pulse length dependent decrease is observed. As the number of pulse cycles is increased, the reduction in energy also increases. However, the decrease becomes less linear as the pulse length increases. For the 64 cycles pulse, a decrease of 9.9

dB is simulated. Opposite to the other results, this is in very good correspondence to the experimental results achieved by Shi et al.,[10] who measured a reduction of 9.6 dB.
Fig. 8 shows the absolute reduction of the subharmonic when the ambient pressure is increased from 0 to 25 kPa. The reduction is shown as a function of the acoustic pressure and number of pulse cycles and Fig. 8, thereby, summarizes 42 of the most promising simulations of Levovist. Furthermore, to get a measure of the linearity between the energy of the subharmonic component and the overpressure, a straight line has been fitted using linear regression for each simulation setup, when only the overpressure is changed. Next, the correlation coefficient, r, has been calculated to see how well a linear relationship between subharmonic energy and ambient overpressure can be assumed. The respective correlation coefficients are shown to the right in Fig. 8. Fig. 8

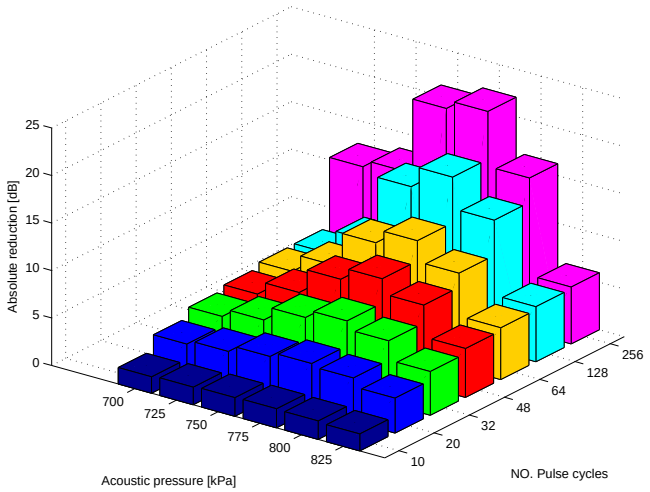

N_c \ P_{ac}	700	725	750	775	800	825
10	1.73	1.85	1.96	2.01	1.94	1.79
20	3.30	3.74	4.42	4.90	4.59	3.67
32	4.32	5.17	6.64	7.51	6.63	4.60
48	4.79	6.18	8.79	10.07	8.51	5.15
64	5.31	7.17	10.75	12.20	9.94	5.46
128	5.37	7.88	14.78	17.01	13.70	5.79
256	12.57	13.30	21.14	22.04	16.26	5.99

Absolute reduction [dB]

N_c \ P_{ac}	700	725	750	775	800	825
10	1.00	1.00	1.00	1.00	1.00	1.00
20	1.00	1.00	1.00	1.00	1.00	0.99
32	1.00	1.00	0.99	1.00	0.99	0.99
48	1.00	1.00	0.99	1.00	0.98	0.98
64	1.00	0.99	0.99	1.00	0.97	0.98
128	0.99	0.99	0.97	0.99	0.95	0.97
256	1.00	1.00	0.97	0.99	0.93	0.97

Correlation coefficients

Figure 8. Absolute reduction of the subharmonic component for Levovist when the ambient pressure is increased from 0 to 25 kPa. The reduction is shown as a function of acoustic pressure and number of cycles in the rectangular driving pressure. To the right, the respective correlation coefficients, when using a linear regression model, are shown.

shows very clearly two characteristics: The optimal driving pressure is 775 kPa, which is in the upper end of the growth stage of the subharmonic component. Furthermore, Fig. 8 shows that the reduction is increased as the driving pulse length is increased. This indicates, unfortunately, that a compromise between axial resolution and pressure sensitivity exists. The correlation coefficients to the right in Fig. 8 indicate a very good linearity. In fact, it can be seen that the two lowest coefficients are actually for the two simulations in Fig. 7 with 256 and 128 cycles, respectively. The rest of the coefficients are all equal to or above $r = 0.97$. The maximum reduction for Levovist was achieved using a rectangular pulse of 256 cycles with a driving pressure of 775 kPa. Using this setting, a reduction of the subharmonic was simulated to be 22.0 dB ($r = 0.99$) giving a pressure sensitivity of 0.88 dB/kPa. For a shorter driving pulse with 64 cycles, the best pressure sensitivity was found to be 0.49 dB/kPa ($r = 1.0$).

Examining the results for Sonazoid gives, more or less, the same indications as for Levovist, although the results are not as clear. A high reduction is only seen for a single acoustic driving pressure (400 kPa). For driving pressures below 400 kPa, the subharmonic disappears when the ambient pressure is increased. For driving pressures between 425 and 800 kPa, the subharmonic is very clear in all the spectra examined. In spite of that, the subharmonic is almost not affected by ambient pressure changes. Still, for the acoustic driving pressure of 400 kPa, the same relation between energy reduction and pulse length is observed. The findings for Sonazoid are summarized in Fig. 9, which is the same as Fig. 8 for Levovist. Reasons for the less clear behavior of Sonazoid can be the selection of driving frequency or, possibly, the selection of fixed shell parameters as the shear modulus and shear viscosity were presented as a range by Hoff.[22]

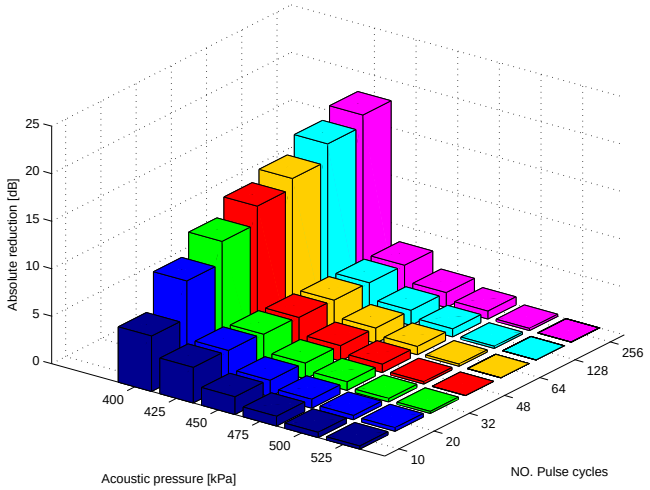

N_c	P_{ac} 400	425	450	475	500	525
10	5.83	3.74	1.87	1.03	0.55	0.33
20	9.75	3.65	1.73	0.94	0.45	0.37
32	12.04	3.48	1.66	0.89	0.36	0.22
48	13.87	3.37	1.62	0.87	0.25	0.01
64	14.90	3.31	1.60	0.86	0.22	0.00
128	16.67	3.27	1.58	0.85	0.23	0.00
256	17.83	3.24	1.57	0.84	0.23	0.00

Absolute reduction [dB]

N_c	P_{ac} 400	425	450	475	500	525
10	0.99	0.97	0.97	0.97	0.94	0.72
20	0.96	0.97	0.98	0.98	0.98	0.63
32	0.93	0.97	0.98	0.98	0.87	0.23
48	0.90	0.97	0.98	0.98	0.61	-0.25
64	0.89	0.98	0.98	0.98	0.32	-0.55
128	0.86	0.98	0.99	0.98	-0.10	-0.78
256	0.85	0.98	0.99	0.98	-0.30	-0.83

Correlation coefficients

Figure 9. Reduction of the subharmonic component for Sonazoid when the ambient pressure is increased from 0 to 25 kPa. The reduction is shown as a function of acoustic pressure and number of cycles in the rectangular driving pressure.

4. CONCLUSION

A simulation study consisting of 7200 simulations has been carried out to optimize the subharmonic response sensitivity to ambient pressure changes. Two different types of ultrasound contrast agents, corresponding to Levovist and Sonazoid, were simulated. While the parameters of the microbubbles were kept fixed, the parameters describing the driving pulse and ambient overpressure were changed in each simulation.

Preliminary investigations showed that the subharmonic component is more easily generated using a rectangular shaped driving pulse compared to a Hanning shaped signal. For the case of Levovist, it was not possible to generate the subharmonic even for very high acoustic driving pressures. This can possibly be solved by using a different driving frequency but the dissimilar responses still makes a study of the differences in shell properties of Levovist and Sonazoid interesting.

Investigations of the subharmonic energy as function of ambient overpressure showed two tendencies very clearly: The amount of reduction in energy of the subharmonic component is dependent on acoustic driving pressure and peaks when the acoustic pressure is in the upper end of the growth stage. Second, the investigations also showed a clear relation between amount of energy reduction and the length of the driving pulse. Simulations of Sonazoid indicate that the simulation parameters, perhaps, not were the best suited for this bubble setup. For Levovist, however, an excellent linear change in energy of the subharmonic component as a function of ambient overpressure was found. Changing the overpressure from 0 to 25 kPa indicates a pressure sensitivity of 0.49 and 0.88 dB/kPa for a rectangular driving pulse with 64 and 256 cycles, respectively.

ACKNOWLEDGMENTS

The authors wish to thank Lars Hoff for making Bubblesim public available. This work was supported by grant 26-04-0024 from the Danish Science Foundation, the Technical University of Denmark, and by B-K Medical Aps.

REFERENCES

1. D. H. Evans, W. N. McDicken, R. Skidmore, and J. P. Woodcock, *Doppler Ultrasound, Physics, Instrumentation, and Clinical Applications*, John Wiley & Sons, New York, 1989.
2. A. C. Burton, *Physiology and Biophysics of the Circulation*, Year Book Medical Publishers, Chicago, 2nd ed., 1972.
3. A. L. Strauss, F. J. Roth, and H. Rieger, "Noninvasive assessment of pressure gradients across iliac artery stenoses: duplex and catheter correlative study," *J. Ultrasound Med.* **12**, pp. 17–22, 1993.

4. W. M. Fairbank and M. O. Scully, "A new noninvasive technique for cardiac pressure measurements: resonant scattering of ultrasound from bubbles," *IEEE Trans. Biomed. Eng.* **24**, pp. 107–110, 1977.
5. B. Hok, "A new approach to noninvasive manometry: Interaction between ultrasound and bubbles," *Med. Biol. Eng. Comp.* **19**, pp. 35–39, 1981.
6. P. M. Shankar, J. Y. Chapelon, and V. L. Newhouse, "Fluid pressure measurement using bubbles insonified by two frequencies," *Ultrasonics* **24**, pp. 333–336, November 1986.
7. V. L. Newhouse and P. M. Shankar, "Bubble size measurements using the nonlinear mixing of two frequencies," *J. Acoust. Soc. Am.* **75**(5), pp. 1473–1477, 1984.
8. A. Bouakaz, P. J. Frinking, N. de Jong, and N. Bom, "Noninvasive measurement of the hydrostatic pressure in a fluid-filled cavity based on the dissappearance time of micrometer-sized free gas bubbles," *Ultrasound Med. Biol.* **25**(9), pp. 1407–1415, 1999.
9. A. Bouakaz, P. J. Frinking, and N. de Jong, "Noninvasive pressure measurement using microbubble contrast agent and wavelet transforms," *Proc. IEEE Ultrason. Symp.* , pp. 1907–1910, 2000.
10. W. T. Shi, F. Forsberg, J. S. Raichlen, and L. Needleman, "Pressure dependence of subharmonic signals from contrast microbubbles," *Ultrasound Med. Biol.* **25**, pp. 275–283, 1999.
11. L. M. Leodore, F. Forsberg, and W. T. Shi, "*In vitro* pressure estimation obtained from subharmonic contrast microbubble signals," *Proc. IEEE Ultrason. Symp.* , 2007.
12. F. Forsberg, J.-B. Liu, W. T. Shi, J. Furuse, M. Shimizu, and B. B. Goldberg, "In vivo pressure estimation using subharmonic contrast microbubble signals: Proof of concept," *IEEE Trans. Ultrason., Ferroelec., Freq. Contr.* **52**, pp. 581–583, 2005.
13. D. Adam, M. Sapunar, and E. Burla, "On the relationship between encapsulated ultrasound contrast agent and pressure," *Ultrasound Med. Biol.* **31**, pp. 673–686, 2005.
14. Lord Rayleigh, "On the pressure developed in a liquid during the collapse of a spherical cavity," *Philos. Mag.* **34**, pp. 94–98, 1917.
15. M. Minnaert, "On musical air-bubbles and the sound of running water," *Philos. Mag.* **16**, pp. 235–248, 1933.
16. M. S. Plesset, "The dynamics of cavitation bubbles," *J. Appl. Mech.* **16**, pp. 277–282, 1949.
17. N. de Jong and L. Hoff, "Ultrasound scattering properties of albunex microspheres," *Ultrasonics* **31**, pp. 175–181, 1993.
18. C. C. Church, "The effects of an elastic solid surface layer on the pulsations of gas bubbles," *J. Acoust. Soc. Am.* **97**, pp. 1510–1521, 1995.
19. K. E. Morgan, J. S. Allen, P. A. Dayton, J. Chomas, A. Klibanov, and K. Ferrara, "Experimental and theoretical evaluation of microbubble behavior: effect of transmitted phase and bubble size," *IEEE Trans. Ultrason., Ferroelec., Freq. Contr.* **47**, pp. 1494–1509, 2000.
20. H. J. Vos, F. Guidi, E. Boni, and P. Tortoli, "Method for microbubble characterization using primary radiation force," *IEEE Trans. Ultrason., Ferroelec., Freq. Contr.* **54**(7), pp. 1333–1345, 2007.
21. N. de Jong, L. Hoff, and N. Bom, "Absorption and scatter of encapsulated gas filled microspheres: theoretical considerations and some measurements," *Ultrasonics* **30**, pp. 95–103, 1992.
22. L. Hoff, *Acoustic Characterization of Contrast Agents for Medical Ultrasound Imaging*, Kluwer Academic Publishers, 2001.
23. L. Trilling, "The collapse and rebound of a gas bubble," *J. Applied Phys.* **23**, pp. 14–17, 1952.
24. J. B. Keller and M. Miksis, "Bubble oscillations of large amplitude," *J. Acoust. Soc. Am.* **68**, pp. 628–633, 1980.
25. S. Hilgenfeldt, D. Lohse, and M. Zomack, "Heat deposition in microbubble ultrasound contrast agents," in *Ultrasonics International 99 joint with 1999 World Congress on Ultrasonics*, Copenhagen, Denmark, 1999.
26. J.-F. Yu, D. Zhang, X.-F. Gong, Y.-J. Gong, Z.-M. Zhu, and X.-M. Liu, "Frequency dependences of sound attenuation and phase velocity in suspensions containing encapsulated microbubbles," *Chin. Phys. Lett.* **22**(4), pp. 892–895, 2005.
27. W. Lauterborn and E. Cramer, "Subharmonic route to chaos observed in acoustics," *Phys. Rev. Letters* **47**, pp. 1445–1448, 1981.
28. A. Prosperetti, "Application of the subharmonic threshold to the measurement of the damping of oscillating gas bubbles," *J. Acoust. Soc. Am.* **61**, pp. 11–16, 1977.

D.2 K. S. Andersen and J. A. Jensen, Ambient pressure sensitivity of microbubbles investigated through a parameter study, *Journal of the Acoustical Society of America*, submitted for possible publication

This paper is based on [77] in Appendix D.1 and has been submitted for consideration for possible publication in the *Journal of the Acoustical Society of America* on December 1, 2008. An associate editor has been assigned the task of handling the manuscript and it is currently being investigated with the advice of external reviewers.

Ambient pressure sensitivity of microbubbles investigated through a parameter study

Klaus Scheldrup Andersen and Jørgen Arendt Jensen
Center for Fast Ultrasound Imaging, Department of Eletrical Engineering, Technical University of Denmark, Build. 348, 2800 Kgs. Lyngby, Denmark

(Dated: February 5, 2009)

Measurements on microbubbles clearly indicate a relation between the ambient pressure and the acoustic behavior of the bubble. The purpose of this study was to optimize the sensitivity of ambient pressure measurements, using the subharmonic component, through microbubble response simulations. The behavior of two microbubbles corresponding to two different contrast agents was investigated as a function of driving pulse and ambient overpressure, p_{ov}. Simulations of Levovist using a rectangular driving pulse show an almost linear reduction in the subharmonic component as p_{ov} is increased. For a 20 cycles driving pulse, a reduction of 4.6 dB is observed when changing p_{ov} from 0 to 25 kPa. Increasing the pulse duration makes the reduction even more clear. For a pulse with 64 cycles, the reduction is 9.9 dB. This simulation is in good correspondence with measurement results presented in the literature. Further simulations of Levovist show that also the shape and the acoustic pressure of the driving pulse are very important factors. The best pressure sensitivity of Levovist was found to be 0.88 dB/kPa. For Sonazoid, a sensitivity of 1.14 dB/kPa has been found, although the reduction is not completely linear as a function of the ambient pressure.

PACS numbers: 43.80.Vj, 43.25.Yw

I. INTRODUCTION

Local blood pressure measurements provide important information on the state of health of the organs in the human body and can be used to diagnose severe heart, lung, and kidney diseases. The pressure is currently measured locally in arteries and organs by means of a pressure catheter. As this is an invasive technique, it is inconvenient to the patient, there is a risk of infection, and the catheter will inevitably introduce changes to the blood flow and, thereby, the pressure. Therefore, many attempts to find a noninvasive procedure have been made. When evaluating new approaches for noninvasive local blood pressure measurements, the sensitivity is a crucial factor. Although, the human blood pressure varies between 0 and approximately 25 kPa (1 kPa = 7.5 mmHg), it should still be possible to distinguish pressure differences as low as 1-3 kPa to measure the blood pressure in the small veins and arteries. One noninvasive approach that has been suggested is to perform Doppler echocardiography using a simplified modification of the Bernoulli equation[1,2]. This method was, however, concluded not to yield reproducible or reliable results by Straus et al.[3]. Another type of approach, which is still being investigated, is to combine microbubbles injected into the blood and diagnostic ultrasound.

Bubbles in a fluid can be used for measurement of pressure gradients due to their size dependent oscillations[4–6]. Since the introduction of ultrasound contrast agents (UCAs), many approaches on how to exploit their ambient pressure sensitivity have been presented. One of the first to propose noninvasive measurement of cardiac pressure using an UCA were Fairbank and Scully[4] in 1977. They claimed that the acoustic properties of the microbubbles change when the size of the bubbles changes. To measure these changes, they suggested the use of resonance excitation. However, due to the large size distribution of the first generation UCAs containing free bubbles, their results were inconclusive. Other suggestions from that time are by Hok[5] in 1981 and Newhouse and Shankar[6,7] in 1986. Newhouse and Shankar showed theoretically and experimentally that accurate bubble size measurements are possible using a double frequency technique for determination of the sum and difference frequencies. The rapid dissolution time after injection of the free air bubbles prevented, however, any practical implementation.

With the introduction of the more stable second generation UCAs, the circulation system can now be used to transport the encapsulated microbubbles to the region of interest. This has initiated new attempts to exploit the ambient pressure dependent acoustic properties that the high compressible air and gas bubbles possess. Bouakaz et al.[8] presented in 1999 an approach for measuring the disappearance time of free bubbles, which were generated at the region of interest by rupturing the contrast agent microbubbles using a low-frequency high acoustic amplitude pulse. From *in vitro* experiments they concluded the approach to have a resolution of 6.7 kPa (50 mmHg). Later, they suggested the resolution could be improved by using larger bubbles or by using wavelet processing or a combination of this[9]. No *in vivo* results or further investigations have, however, been presented using this approach yet. Around the same time, Shi et al.[10] observed from experiments that the subharmonic component of Levovist is highly sensitive to ambient pressure changes compared to the fundamental and the second harmonic component. They reported a 9.9 dB linear decrease of the peak amplitude of the subharmonic component when increasing the ambient hydrostatic pressure from 0 to 24.8 kPa (186 mmHg). Furthermore, they found that the ambient pressure-induced reduction was highest when the

acoustic excitation pressure was around the growth stage of the subharmonic, which occurs when the acoustic driving pressure causes the subharmonic component to increase rapidly from background noise level to be clearly visible in the spectrum. Recently, the same group have presented similar results for Sonazoid, which was found to have an average decrease of 13.3 dB[11]. Furthermore, in 2005 the same group presented *in vivo* results for proof of concept of the capabilities of the subharmonic response[12]. As the measurements were performed directly on the abdominal cavity and the aorta by incision of two dogs, this can hardly be characterized as noninvasive. However, the results still showed that the subharmonic component decreased as the ambient pressure increased and, thereby, indicated the subharmonic response of UCAs can be used for ambient pressure measurements. Also in 2005, Adam et al.[13] investigated microbubbles' response to cyclic ambient pressure changes by mimicking left ventricular pressure changes. They found that the subharmonic response correlated best with the cyclic changes compared to the fundamental and second harmonic, but also observed a transient delay before this correlation occurred. In 2008, Andersen and Jensen presented a new experimental setup, which more realistic resembles a clinical setting using a single array transducer[14]. The setup was used to measure the ambient pressure sensitivity of SonoVue and confirmed the previous findings revealing a pressure sensitivity of 0.42 dB/kPa. The same group has also investigated the dependence on the acoustic driving pressure experimentally[15]. However, the driving pressure was selected too high causing bubble destruction and the investigation was, therefore, inconclusive.

Modeling the acoustics of bubbles in a fluid is a still ongoing investigation, which was initiated by Lord Rayleigh[16] in 1917 who studied damages to ship propellers due to bubble cavitation. In 1933, Minnaert[17] explained the characteristic resonance frequency of free bubbles when he did a theoretical and experimental study of bubbles' emission of sound. Since then, several modifications to the existing models and new theoretical models on how to predict the behavior of an oscillating bubble have been presented. Most models are based on modifications of the Rayleigh-Plesset[18] equation and are capable of handling shell encapsulating bubbles. This includes the models used by de Jong and Hoff[19] and Church[20]. Other models are based on the modified Herring equation to describe the radial motion (e.g. Morgan et al.[21]). Recently, Vos et al.[22] proposed a novel approach for investigation of full populations of microbubbles' behavior in acoustic fields, also based on the modified Herring equation. The study, furthermore, included a new method to estimate the viscoelastic shell properties of UCAs. Existing methods for this based on the Rayleigh-Plesset equation has been suggested by de Jong et al.[19,23] and described further by Hoff[24].

Despite the growing number of experiments within hydrostatic pressure measurements, no real parameter study investigating the response of microbubbles in respect to ambient pressure changes has been performed until now. The purpose of this study is to optimize the sensitivity of pressure measurements through bubble response simulations investigating the complex mechanisms for subharmonic generation. This is carried out by an extensive number of simulations of two commercial UCAs. Since the study focus on the effect of the driving pulse, the parameters of the microbubbles are fixed in all simulations whereas several different settings regarding the excitation pulse were varied. Some part of this work has been presented at the 2008 SPIE Medical Imaging Symposium[25].

This paper is organized as follows: Section II presents the choice of simulation model and parameters used for the investigation. Furthermore, it also describes the processing of the simulated response. The achieved results are presented and discussed in Section III. Finally, the investigation is summarized by a conclusion in Section IV.

II. THEORY AND METHOD

The investigation has been performed using the Matlab (The Math Works Inc., Natick, Mass., USA) environment. To carry out the simulations, the free simulation program Bubblesim by Hoff[24] is used. Bubblesim is a toolbox that calculates the oscillation and scattered echo for a specified contrast agent microbubble and excitation pulse. It numerically solves a second order ordinary differential equation (ODE) that has been combined from a set of equations, each equation modeling different parts (bubble, shell, and surrounding liquid) of the system that makes up a contrast agent microbubble. In Bubblesim, the following four different models are implemented: The Rayleigh-Plesset[18] (R-P) model, the Trilling[26] model, the Keller-Miksis[27] model, and a modified version of the R-P model, which is an intermediate model of the R-P on one side and the Trilling and Keller-Miksis models on the other. The largest disadvantage of the R-P model is that it does not include radiation damping, which is energy loss caused by radiation of sound. This is accounted for in the Trilling and the Keller-Miksis models, which both include a finite but constant speed of sound in the liquid. However, both the Trilling and Keller-Miksis model has a risk of becoming numerical unstable when the bubble wall velocity becomes comparable to the speed of sound (acoustic Mach numbers, $M = \dot{R}/c$, around unity). This happens for high oscillation amplitudes and causes the models to have an unphysical negative inertia. Instead, Hilgenfeldt et al.[28] have used a modified version of the R-P model that includes the radiation damping term from the Trilling and Keller-Miksis models. This version is implemented in Bubblesim and the model selected for the parameter investigation. It was chosen because of its numerical stability, which is important when doing many simulations spanning a wide range of variable changes. The modified R-P model is[24]

$$\rho R\ddot{R} + \frac{3}{2}\rho\left(\dot{R}\right)^2 - p_L + p_{ov} + p_{ac}(t) - \frac{R}{c}\cdot\dot{p_L} = 0, \quad (1)$$

where ρ is the surrounding liquid density, R is the bubble radius, $\dot{R} = \frac{dR}{dt}$ denotes derivation w.r.t. time t, p_L is the pressure at the bubble surface, p_{ov} is the static background overpressure, p_{ac} is the driving acoustic pressure,

and c is the speed of sound. The first term describes the pressure as function of the bubble wall acceleration, whereas the second term describes the pressure as a function of the bubble wall velocity. $p_\infty = p_{ov} + p_{ac}$ is the background pressure describing the pressure in the liquid far from the bubble surface. p_L includes contributions from the gas, the viscosity, and the effects of the shell encapsulating the bubble. Finally, the last term including $\dot{p_L} = \frac{dp_L}{dt}$ is the one accounting for the radiation damping. Any numerical solver can be used to solve the ODE in (1). Examples are the Runge-Kutta algorithm of order 4 and 5 (`ODE45`) and the multistep ODE solver of variable order from 1 to 5 (`ODE15s`), which are both available in Matlab as a standard. In this study, the solver of variable order has been selected as it should be more reliable and stable for solving situations where the differential equation becomes stiff[24]. This occurs for example when the bubble radius changes slowly during the expansion phase but goes through very fast changes in radius and velocity under compression. The choices on simulation model and numerical solver, as well as other general setup parameters, for the simulations in this study are summarized in Table I.

TABLE I. List of simulation parameters regarding the general setup of Bubblesim.

Parameter	Designation
ODE solver	`ODE15s`
Simulation model	`Modified Rayleigh-Plesset`
Thermal damping	`Isothermal`
Liquid	`Water`

In its standard form, Bubblesim has a flexible graphical user interface, which makes it easy to perform single simulations for minor investigations. In this study, a batch mode has been created for two reasons: It gives a bit more control and, more importantly, it makes it possible to perform multiple simulations automatically, which is essential in a parameter study like this. Furthermore, one modification has been made to Bubblesim. In its original form, it is not possible to change the ambient overpressure parameter denoted p_{ov} in (1). Since this is crucial, when investigating microbubbles' sensitivity to ambient pressure changes, this feature has been enabled by small modifications to the source code.

While the bubble size distribution can be determined with a multisizer, it is somewhat more difficult to specify the parameters related to the surrounding shell of today's UCA microbubbles. One way to do this is to perform a combination of experiments and model fitting as described by de Jong and associates[19,23,24]. This will, however, only give an estimate of proper designations and usually an interval for some of the parameters is given. The procedure has been used by Yu et al.[29] and Hoff[24] to estimate suitable parameters for the commercial contrast agents Levovist (Schering AG, Berlin, Germany) and Sonazoid (GE Healthcare, Oslo, Norway), respectively. These values used in the investigation were fixed for all simulations and are listed in Table II. Before a simulation can be carried out, a driving pulse must be selected. Since the emphasis of this study was to optimize the subharmonic sensitivity to ambient pressure changes as a function of the excitation pulse, a large number of different driving pulses were examined. The driving pulse was generated based on four different characteristics being the center frequency, f_c, the number of pulse cycles, N_c, the maximum acoustic pressure, p_{ac}, and the shape of the pulse. The possible designations used for the investigation are listed in the upper part of Table III. The center frequency was selected based on a preliminary study optimizing the energy of the subharmonic component to the fundamental as shown for Sonazoid in Fig. 1. As can be seen from Table III, 30 different settings for the acoustic pressure is used. This was decided to ensure determination of the growth stage of the subharmonic component with a reasonable precision. Although an acoustic pressure of 950 kPa will probably destroy the microbubbles in real measurements, the high values were selected to cover the entire range of subharmonic growth and saturation. The bottom row of Table III lists the designations of the ambient overpressures which were used in the simulations. As can be seen, the range covers the interval between 0 and 25 kPa in steps of 5 kPa. In this way, the most common human blood pressure values are covered. Combining all the parameters in Table III gives a total of 3600 different simulations for each contrast agent.

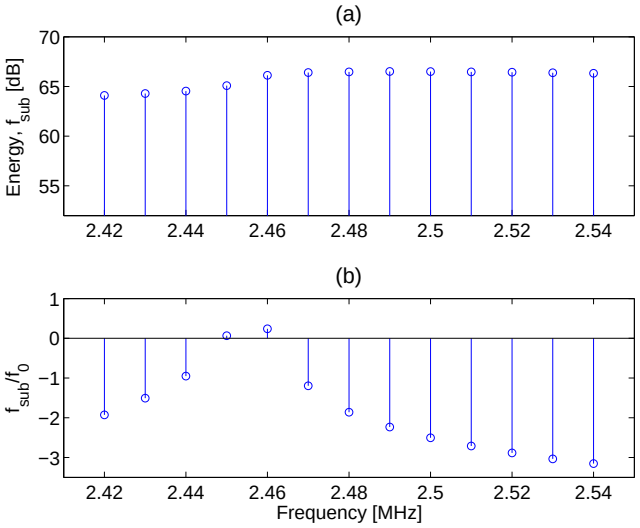

FIG. 1. (a) shows the energy of the subharmonic component as a function of emitted frequency, while (b) shows the relation of the subharmonic to the fundamental component.

When Bubblesim has completed a simulation, the simulated scattered pressure is returned and the Fourier transformation is applied. Next, a search for the fundamental (f_0), the first subharmonic ($\frac{1}{2}f_0$), and the second harmonic ($2f_0$) component is performed and the energy of each component is calculated. The center frequencies of the harmonic bands were selected as multiples of the emitted center frequency, f_c. It should, however, be

TABLE II. List of the parameters from Yu et al.[29] and Hoff[24] used to describe the two different types of bubbles for the simulations in Bubblesim.

Contrast agent	Bubble Radius [μm]	Shell Thickness [nm]	Shear Modulus [MPa]	Shear Viscosity [Pa s]
Levovist	3.0	6.0	80	1.3
Sonazoid	3.2	4.0	52	0.99

TABLE III. List of parameters used in combination with the contrast agents listed in Table II. Combining all settings gives 3600 simulations in total for each agent.

Parameter	Designation										Unit
f_c	2.06	2.46									[MHz]
N_c	1	2	5	10	20	32	48	64	128	256	[cycles]
p_{ac}	100	150	200	250	275	300	325	350	375	400	[kPa]
	425	450	475	500	550	575	600	650	675	700	
	725	750	775	800	825	850	875	900	925	950	
Pulse shape	`'rectangular'`				`'hanning'`						
p_{ov}	0	5	10	15	20	25					[kPa]

noted that initial simulations show that the frequency of the subharmonic component shifts slightly as the acoustic driving pressure is increased. The energy has been chosen over the peak amplitude since this is a more robust measure. The bandwidth to calculate the energy within was selected as the -10 dB bandwidth of the excitation pulse.

III. RESULTS AND DISCUSSION

This section presents the results obtained through the simulation study. First, the fundamental, subharmonic, and second harmonic dependence on acoustic pressure will be presented. This is a natural step for two reasons: First of all, generation of the subharmonic component must be ensured before looking into the ambient pressure dependency. Another reason is to see at which acoustic pressures the growth stage of the subharmonic occurs for the two types of microbubbles. Along with this investigation, the scattered responses and spectra have been examined to ensure useful responses and proper selection of the bandwidth intervals to calculate the energy of the respective frequency components within. Since these results are rather trivial and takes up a lot of space, only a few selected examples are presented in this section. In the last part of this section, the influence of ambient overpressure will be examined.

A. Dependence on Acoustic Pressure

Fig. 2 shows the energy of the subharmonic, fundamental, and second harmonic component of Sonazoid as a function of acoustic pressure when a rectangular driving pulse for a different number of cycles is used. Each curve has been normalized by 88 dB, which corresponds to the maximum energy observed among all simulations for both agents. Examining the subharmonic component, three characteristic stages are clearly observed. In the occurrence stage for acoustic pressures below 300 kPa, the subharmonic is weak compared to the other components. For acoustic pressures in the interval between 300 kPa and 425 kPa, the subharmonic increases rapidly and this part can be characterized as the growth stage. When increasing the acoustic pressure further, the growth eases off and can be compared to the saturation stage observed in measurements. Finally, when the acoustic pressure exceeds 875 kPa the energy decreases again. At these levels, the corresponding spectra look more noisy and should be discarded. The pattern is the same for pulses of other lengths than displayed here, although the subharmonic component cannot be distinguished from the fundamental for driving pulses smaller than 5 cycles. The chaotic behavior at high acoustic pressure levels predicted in the simulations is actually in good correspondence with experimental results of free bubbles achieved by Lauterborn and Cramer[30]. Looking at the fundamental, it increases almost linearly as expected. However, a slight drop is seen in the pressure interval corresponding to the growth stage of the subharmonic.

When the shape of the driving pulse is changed by applying a Hanning window, especially the subharmonic and second harmonic change behavior as can be seen in Fig. 3. Regarding the subharmonic component, the three stages pattern is the same as observed for the rectangular driving pulse, although the interval of the growth period seems to have increased. This makes sense since

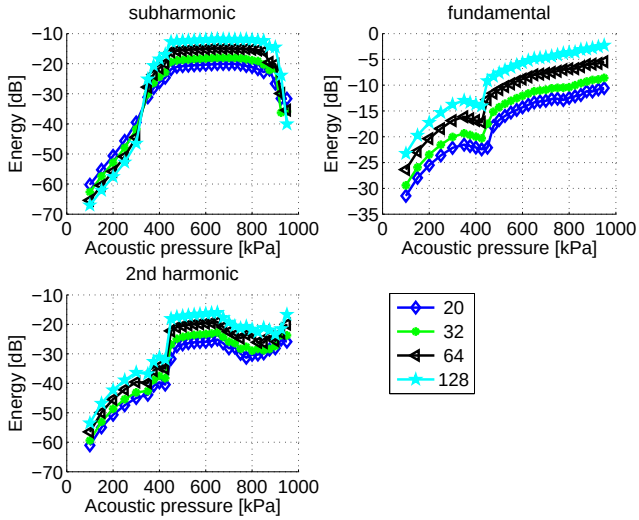

FIG. 2. Energy as a function of acoustic pressure for Sonazoid. The driving pulse is a rectangular shaped sinusoid. Upper left graph shows the subharmonic behavior, upper right shows the first harmonic, and lower left presents the behavior of the second harmonic component. Each curve represent a different number of cycles in the driving pulse as displayed in the legend to the lower right in the figure.

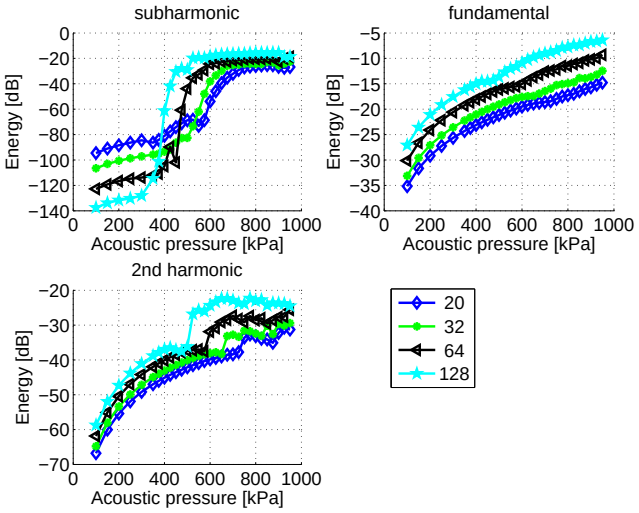

FIG. 3. Energy as a function of acoustic pressure for Sonazoid. The driving pulse is a Hanning shaped sinusoid. Upper left graph shows the subharmonic behavior, upper right shows the first harmonic, and lower left presents the behavior of the second harmonic component. Each curve represent a different number of cycles in the driving pulse as displayed in the legend to the lower right in the figure.

less energy is transmitted using a Hanning shaped driving pulse compared to a rectangular signal of the same acoustic strength. Another interesting observation is that the acoustic pressure interval of the growth stage now is more dependent on the length of the driving pulse. The same pulse length dependent behavior is also seen for the second harmonic component. The fundamental, on the other hand, does not seem to be affected much although the small drop in energy observed for the rectangular driving pulse is hardly visible anymore.

The results for the simulations of Levovist as a function of acoustic pressure using a rectangular driving pulse is shown in Fig. 4 (a). Once again, the three stages behavior of the subharmonic component is observed. However, now the growth stage first occurs in the interval from 600 to 900 kPa. Although the increase in energy is the same, the interval is much higher than experimental results achieved by Shi et al.[10], who observed it to be between 300 and 600 kPa for Levovist using a 64 cycles rectangular driving pulse with a center frequency of 2 MHz. The fundamental and second harmonic more closely resembles the obtained measurement results, except the simulated saturation is not as pronounced in the measurements. The simulations of Levovist using a Hanning shaped excitation pulse indicates it is very hard to generate the subharmonic component for this type of driving pulse, see Fig. 4 (b). In fact, the subharmonic component is hardly visible in any of the spectra, not even a the very high driving pressures. Regarding the fundamental and second harmonic component, they are similar to what was observed using the rectangular driving pulse.

Except, possibly, for the last setup, common for all the simulations is that the subharmonic component has a threshold and is present only above a certain acoustic pressure. This observation was also reported by Prosperetti[31] who examined this experimentally on free bubbles and, as mentioned, by Shi et al.[10]. One difference between the simulations and the measurements is, however, that the simulated threshold seems to be higher than the measured. A reason for this can be the selection of the shell parameters for Levovist as the simulated threshold of Sonazoid is comparable to the measured threshold of Levovist. In contrast to the threshold behavior of the subharmonic, the higher harmonics seems to be present to various degrees for all driving pressures. Finally, one interesting observation regarding the scattered pressure, when using the Hanning shaped driving pulse for excitation of Sonazoid, should be noted. When the driving pressure is increased to a level where the subharmonic is generated, the scattered response suddenly changes characteristics halfway in the pulse as shown in Fig. 5 (a). In the first half, the traditional harmonic distortion is clearly observed but no subharmonics. Halfway in the signal, the characteristic oscillation at twice the driving period is seen and continues for the rest of the scattered response. As can be seen from the corresponding spectrum in Fig. 5 (b), this is what gives rise to the sub- and ultraharmonics.

B. Dependence of Overpressure

In this section, the simulation results achieved when changing the ambient overpressure will be shown. Fig. 6 shows an example of how the scattered spectrum changes,

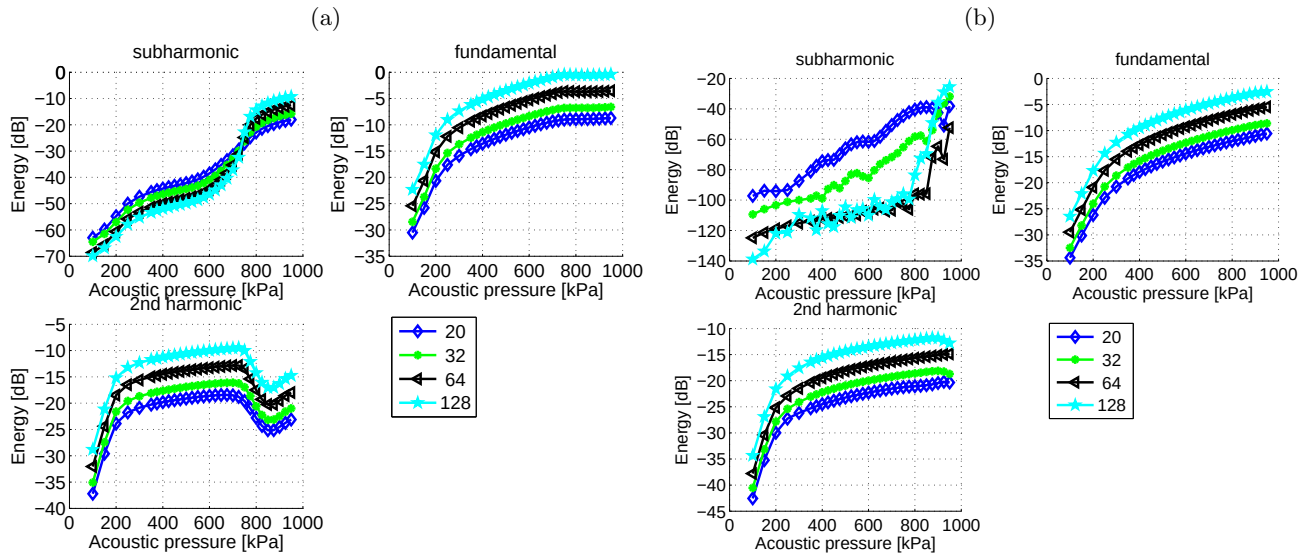

FIG. 4. Energy as a function of acoustic pressure for Levovist. The driving pulse is a rectangular shaped (a) and Hanning shaped (b) sinusoid, respectively. Upper left graph shows the subharmonic behavior, upper right shows the first harmonic, and lower left presents the behavior of the second harmonic component. Each curve represent a different number of cycles in the driving pulse as displayed in the legend to the lower right in the figure.

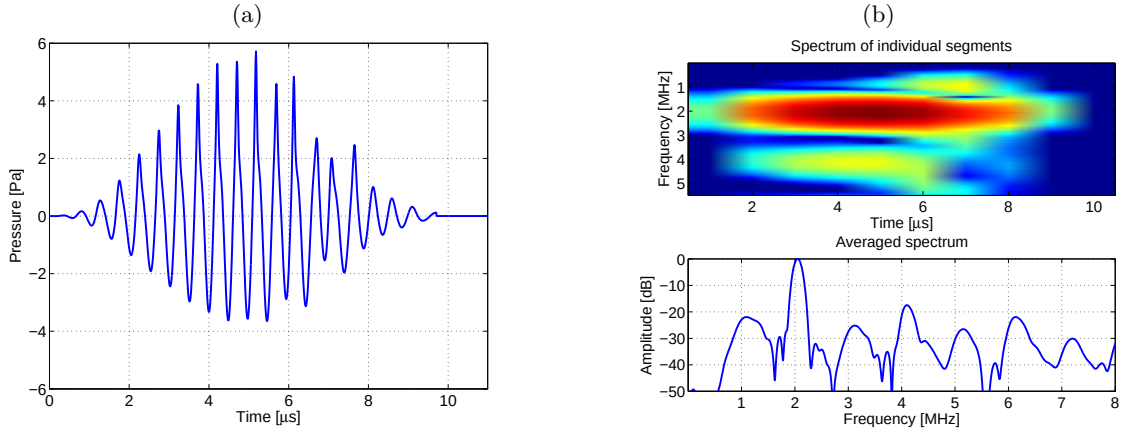

FIG. 5. Example of scattered pressure (a) and it's corresponding spectrum (b) when using a Hanning shaped driving pulse. Sonazoid is used and the excitation is a 20 cycles Hanning shaped signal with a center frequncy of 2 MHz and an acoustic pressure of 525 kPa.

when the ambient pressure is the only parameter that is changed from one simulation to another. The example is for Levovist when driven by a rectangular pulse with 32 cycles and an acoustic pressure of 800 kPa. In Fig. 6 (a), the scattered spectrum is shown when no pressure is seen and Fig. 6 (b) shows the spectrum when an overpressure of 25 kPa is applied. Comparing the two spectra, a clear reduction of the subharmonic component at 1 MHz is observed. Looking at the fundamental at 2 MHz and the second harmonic component at 4 MHz, it is seen that these increases when overpressure is applied. In fact, this is a clear tendency from many of the simulations.

Fig. 7 shows the effect on the subharmonic component when the pulse length is varied. It displays the energy of the subharmonic component when using the same setup as used to create Fig. 6. There is a clear tendency for all pulse lengths that the energy decreases as the overpressure is increased. Furthermore, the total decrease in energy also seems to be dependent on the number of cycles in the driving pulse. However, Fig. 7 also indicates that the decrease is not completely linear in all cases. For easy comparison of the change in energy for the different simulation setups, Fig. 8 shows the energy of the three frequency components as function of ambient overpressure when each simulation has been normalized to their respective maximum. Looking at the results for the fundamental, it is seen that this component is not affected by ambient pressure changes. The second har-

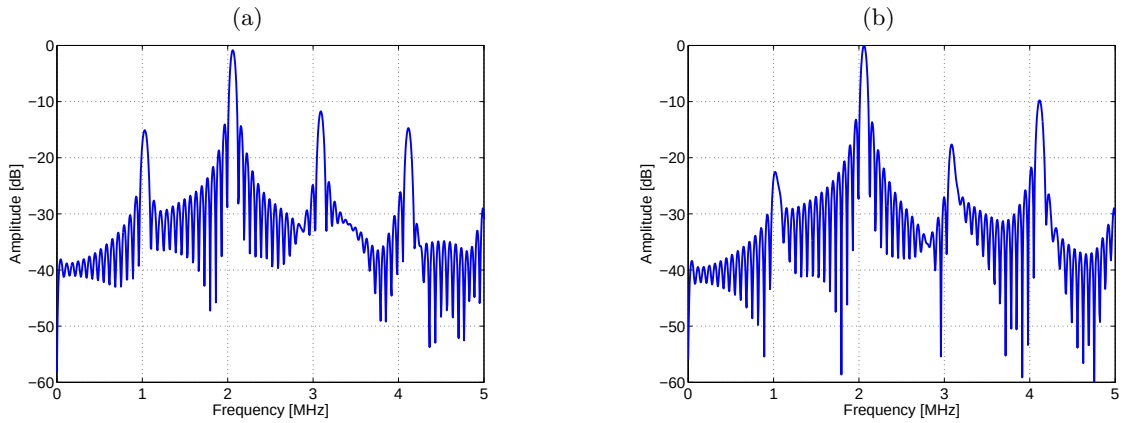

FIG. 6. Example of spectrum of scattered response from excitation of microbubble corresponding to Levovist. The driving pulse is a 32 cycles rectangular shaped signal with a center frequncy of $f_c = 2$ MHz and an acoustic pressure of $P_{ac} = 800$ kPa. (a) is when no overpressure is applied and (b) shows the response when a overpressure of 25 kPa is applied.

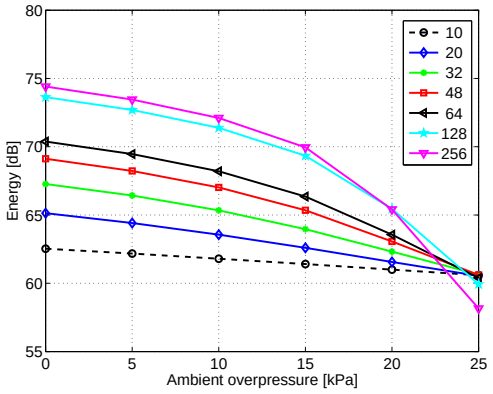

FIG. 7. Energy of the subharmonic component scattered by Levovist when using a rectangular shaped driving pulse with an acoustic pressure of 800 kPa. The energy is displayed as a function of ambient pressure and each curve in the plot represents a different number of cycles in the driving pulse as indicated by the legend.

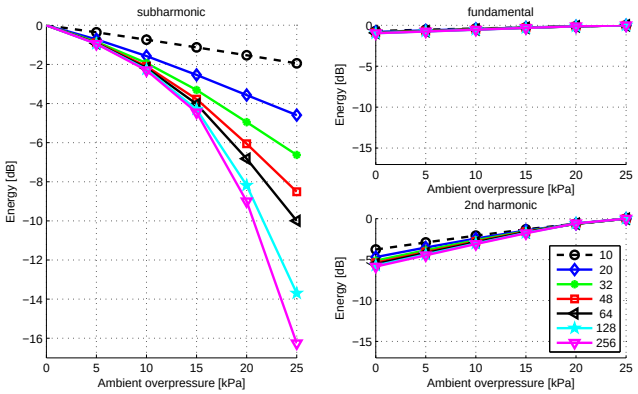

FIG. 8. Decrease in energy of respective frequency components scattered by Levovist when using a rectangular shaped driving pulse with an acoustic pressure of 800 kPa. The energy is displayed as a function of ambient pressure and each curve in the plots represents a different number of cycles in the driving pulse as indicated by the legend.

monic seems to be affected and increases about 5 dB, slightly dependent on the pulse length. This increase is quiet in contradiction to the experiments by Shi et al.[10], who excited Levovist in the growth stage using a 64 cycles rectangular pulse. They found that the second harmonic decreases by 1.8 dB over the same ambient pressure interval. When examining the subharmonic in Fig. 8, a highly pulse length dependent decrease is observed. As the number of pulse cycles is increased, the reduction in energy also increases. However, the decrease becomes less linear as the pulse length increases. For the driving pulse with 64 cycles, a decrease of 9.9 dB is found. This is in very good agreement with the experimental results by Shi et al.[10], who measured a reduction of 9.6 dB.

Fig. 9 shows the ambient pressure sensitivity of the subharmonic component when the ambient pressure is increased from 0 to 25 kPa. The sensitivity corresponds to the absolute reduction divided by 25 and is shown as a function of the acoustic pressure and number of pulse cycles. Fig. 9, thereby, summarizes 252 of the most promising simulations of Levovist. Furthermore, to get a measure of the linearity between the energy of the subharmonic component and the overpressure, a straight line has been fitted using linear regression for each simulation setup, when only the overpressure is changed. Next, the correlation coefficient, r, has been calculated to see how well a linear relationship between subharmonic energy and ambient overpressure can be assumed. The respective correlation coefficients are shown to the right in Fig. 9.

Fig. 9 shows very clearly two characteristics: The optimal driving pressure is 775 kPa, which is in the upper end of the growth stage of the subharmonic component. Furthermore, the sensitivity is increased as the driving

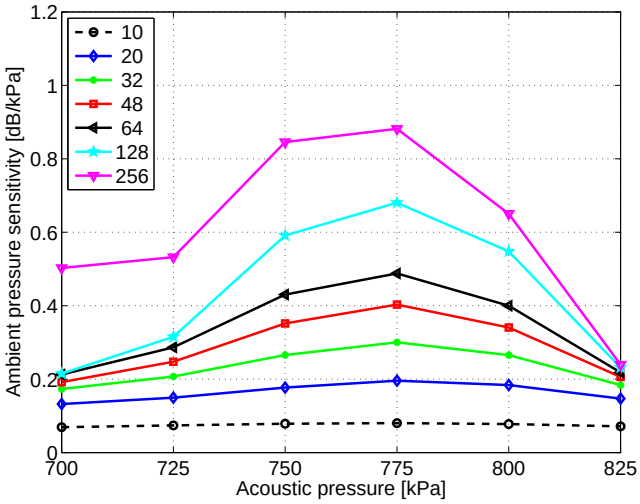

N_c	P_{ac} 700	725	750	775	800	825
10	0.07	0.07	0.08	0.08	0.08	0.07
20	0.13	0.15	0.18	0.20	0.18	0.15
32	0.17	0.21	0.27	0.30	0.27	0.18
48	0.19	0.25	0.35	0.40	0.34	0.21
64	0.21	0.29	0.43	0.49	0.40	0.22
128	0.21	0.32	0.59	0.68	0.55	0.23
256	0.50	0.53	0.85	0.88	0.65	0.24

Pressure sensitivity [dB/kPa]

N_c	P_{ac} 700	725	750	775	800	825
10	1.00	1.00	1.00	1.00	1.00	1.00
20	1.00	1.00	1.00	1.00	1.00	0.99
32	1.00	1.00	0.99	1.00	0.99	0.99
48	1.00	1.00	0.99	1.00	0.98	0.98
64	1.00	0.99	0.99	1.00	0.97	0.98
128	0.99	0.99	0.97	0.99	0.96	0.97
256	1.00	1.00	0.97	0.99	0.93	0.97

Correlation coefficients

FIG. 9. Ambient pressure sensitivity of the subharmonic component for Levovist when the ambient pressure is increased from 0 to 25 kPa. The sensitivity is shown as a function of acoustic pressure and number of cycles in the rectangular driving pressure. To the right, the respective correlation coefficients, when using a linear regression model, are shown.

pulse length is increased. This indicates, unfortunately, that a compromise between axial resolution and pressure sensitivity exists. The correlation coefficients to the right in Fig. 9 indicate a very good linearity. In fact, it can be seen that the two lowest coefficients are actually for the two simulations in Fig. 8 with 256 and 128 cycles, respectively. The rest of the coefficients are all equal to or above $r = 0.97$. The maximum sensitivity for Levovist was achieved using a rectangular pulse of 256 cycles with a driving pressure of 775 kPa. Using this setting, a reduction of the subharmonic was simulated to be 22.0 dB ($r = 0.99$) giving a pressure sensitivity of 0.88 dB/kPa. For a shorter driving pulse with 64 cycles, the best pressure sensitivity was found to be 0.49 dB/kPa ($r = 1.0$).

Examining the results for Sonazoid gives the same indications as for Levovist, although the results are not as symmetric around a certain acoustic pressure. However, once again there is a clear tendency that a specific acoustic pressure in the upper end of the growth stage will optimize the ambient pressure sensitivity. Furthermore, the simulations also indicate the same relation between sensitivity and pulse length. The findings for Sonazoid are summarized in Fig. 10, which is the same as Fig. 9 for Levovist. Using a rectangular driving pulse with 256 cycles, a maximum pressure sensitivity of 1.14 dB/kPa ($r = 0.96$) was found. For a driving pulse with 64 cycles, the best sensitivity was found to be 0.65 dB/kPa with a linear correlation coefficient of $r = 0.99$.

IV. CONCLUSION

A simulation study consisting of 7200 simulations has been carried out to investigate and optimize the subharmonic response sensitivity to ambient pressure changes. Two different types of ultrasound contrast agents, corresponding to Levovist and Sonazoid, were simulated. While the parameters of the microbubbles were kept fixed, the parameters describing the driving pulse and ambient overpressure were changed in each simulation. Simulations show that the subharmonic component is more easily generated using a rectangular shaped driving pulse compared to a Hanning shaped signal. For the case of Levovist, it was not possible to generate the subharmonic using the Hanning shaped excitation even for very high acoustic driving pressures. This dissimilarity in responses makes a study of the differences in shell properties of Levovist and Sonazoid interesting.
Investigations of the subharmonic energy as function of ambient overpressure showed two tendencies very clearly: The amount of reduction in energy of the subharmonic component is dependent on acoustic driving pressure and peaks when the acoustic pressure is in the upper end of the growth stage. Second, the investigations also showed a clear relation between the amount of energy reduction and length of the driving pulse. Simulations of Levovist indicate a linear change in energy of the subharmonic component as a function of ambient overpressure. Changing the overpressure from 0 to 25 kPa indicates a pressure sensitivity of 0.49 and 0.88 dB/kPa for a rectangular driving pulse with 64 and 256 cycles, respectively. For Sonazoid, the sensitivity was found to be 0.65 and 1.14 dB/kPa when using the same excitation pulses as for Levovist.

Acknowledgments

The authors wish to thank Lars Hoff for making Bubblesim public available. This work was supported by grant 26-04-0024 from the Danish Science Foundation, the Technical University of Denmark, and by B-K Medical Aps.

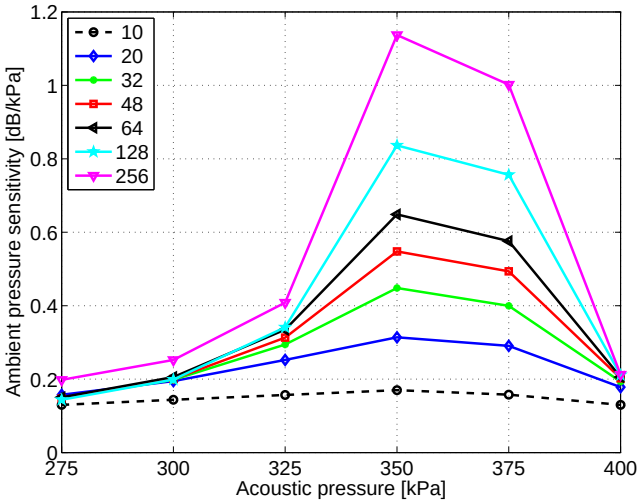

N_c	P_{ac} 275	300	325	350	375	400
10	0.13	0.14	0.16	0.17	0.16	0.13
20	0.16	0.19	0.25	0.31	0.29	0.18
32	0.15	0.20	0.29	0.45	0.40	0.19
48	0.15	0.20	0.31	0.55	0.49	0.20
64	0.15	0.21	0.33	0.65	0.58	0.21
128	0.14	0.20	0.34	0.84	0.76	0.21
256	0.20	0.25	0.41	1.14	1.00	0.21

Pressure sensitivity [dB/kPa]

N_c	P_{ac} 275	300	325	350	375	400
10	1.00	1.00	1.00	1.00	1.00	1.00
20	0.99	1.00	1.00	1.00	0.99	0.99
32	1.00	0.99	0.99	0.99	0.98	0.99
48	1.00	0.99	0.99	0.99	0.97	0.99
64	1.00	0.99	0.98	0.99	0.96	0.98
128	1.00	0.99	0.98	0.97	0.94	0.98
256	1.00	1.00	0.98	0.98	0.90	0.98

Correlation coefficients

FIG. 10. Ambient pressure sensitivity of the subharmonic component for Sonazoid when the ambient pressure is increased from 0 to 25 kPa. It is shown as a function of acoustic pressure and number of cycles in the rectangular driving pressure.

[1] D. H. Evans, W. N. McDicken, R. Skidmore, and J. P. Woodcock. *Doppler Ultrasound, Physics, Instrumentation, and Clinical Applications*. John Wiley & Sons, New York, 1989.

[2] A. C. Burton. *Physiology and Biophysics of the Circulation*. Year Book Medical Publishers, Chicago, 2nd edition, 1972.

[3] A. L. Strauss, F. J. Roth, and H. Rieger. Noninvasive assessment of pressure gradients across iliac artery stenoses: duplex and catheter correlative study. *J. Ultrasound Med.*, 12:17–22, 1993.

[4] W. M. Fairbank and M. O. Scully. A new noninvasive technique for cardiac pressure measurements: resonant scattering of ultrasound from bubbles. *IEEE Trans. Biomed. Eng.*, 24:107–110, 1977.

[5] B. Hok. A new approach to noninvasive manometry: Interaction between ultrasound and bubbles. *Med. Biol. Eng. Comp.*, 19:35–39, 1981.

[6] P. M. Shankar, J. Y. Chapelon, and V. L. Newhouse. Fluid pressure measurement using bubbles insonified by two frequencies. *Ultrasonics*, 24:333–336, November 1986.

[7] V. L. Newhouse and P. M. Shankar. Bubble size measurements using the nonlinear mixing of two frequencies. *J. Acoust. Soc. Am.*, 75(5):1473–1477, 1984.

[8] A. Bouakaz, P. J. Frinking, N. de Jong, and N. Bom. Noninvasive measurement of the hydrostatic pressure in a fluid-filled cavity based on the dissappearance time of micrometer-sized free gas bubbles. *Ultrasound Med. Biol.*, 25(9):1407–1415, 1999.

[9] A. Bouakaz, P. J. Frinking, and N. de Jong. Noninvasive pressure measurement using microbubble contrast agent and wavelet transforms. *Proc. IEEE Ultrason. Symp.*, pages 1907–1910, 2000.

[10] W. T. Shi, F. Forsberg, J. S. Raichlen, and L. Needleman. Pressure dependence of subharmonic signals from contrast microbubbles. *Ultrasound Med. Biol.*, 25:275–283, 1999.

[11] L. M. Leodore, F. Forsberg, and W. T. Shi. In vitro pressure estimation obtained from subharmonic contrast microbubble signals. *Proc. IEEE Ultrason. Symp.*, 2007.

[12] F. Forsberg, J-B Liu, W. T. Shi, J. Furuse, M. Shimizu, and B. B. Goldberg. In vivo pressure estimation using subharmonic contrast microbubble signals: Proof of concept. *IEEE Trans. Ultrason., Ferroelec., Freq. Contr.*, 52:581–583, 2005.

[13] D. Adam, M. Sapunar, and E. Burla. On the relationship between encapsulated ultrasound contrast agent and pressure. *Ultrasound Med. Biol.*, 31:673–686, 2005.

[14] K. S. Andersen and J. A. Jensen. In vitro measurement of ambient pressure changes using a realistic clinical setup. In *Proc. IEEE Ultrason. Symp.*, 2008.

[15] K. S. Andersen and J. A. Jensen. Non-invasive estimation of blood pressure using ultrasound contrast agents. In *Int. Congr. Ultrason.*, 2009.

[16] Lord Rayleigh. On the pressure developed in a liquid during the collapse of a spherical cavity. *Philos. Mag.*, 34:94–98, 1917.

[17] M. Minnaert. On musical air-bubbles and the sound of running water. *Philos. Mag.*, 16:235–248, 1933.

[18] M. S. Plesset. The dynamics of cavitation bubbles. *J. Appl. Mech.*, 16:277–282, 1949.

[19] N. de Jong and L. Hoff. Ultrasound scattering properties of albunex microspheres. *Ultrasonics*, 31:175–181, 1993.

[20] C. C. Church. The effects of an elastic solid surface layer on the pulsations of gas bubbles. *J. Acoust. Soc. Am.*, 97:1510–1521, 1995.

[21] K. E. Morgan, J. S. Allen, P. A. Dayton, J. Chomas, A. Klibanov, and K. Ferrara. Experimental and theoretical evaluation of microbubble behavior: effect of transmitted phase and bubble size. *IEEE Trans. Ultrason., Ferroelec., Freq. Contr.*, 47:1494–1509, 2000.

[22] H. J. Vos, F Guidi, E. Boni, and P. Tortoli. Method for microbubble characterization using primary radiation force. *IEEE Trans. Ultrason., Ferroelec., Freq. Contr.*, 54(7):1333–1345, 2007.

[23] N. de Jong, L. Hoff, and N. Bom. Absorption and scatter of encapsulated gas filled microspheres: theoretical considerations and some measurements. *Ultrasonics*, 30:95–103, 1992.

[24] L. Hoff. *Acoustic Characterization of Contrast Agents for Medical Ultrasound Imaging*. Kluwer Academic Publishers, 2001.

[25] K. S. Andersen and J. A. Jensen. Simulation of microbubble response to ambient pressure changes. *Med. Imag. V Symp.*, 6920:692016, 2008.

[26] L. Trilling. The collapse and rebound of a gas bubble. *J. Applied Phys.*, 23:14–17, 1952.
[27] J. B. Keller and M. Miksis. Bubble oscillations of large amplitude. *J. Acoust. Soc. Am.*, 68:628–633, 1980.
[28] S. Hilgenfeldt and D. Lohse. The acoustics of diagnostic microbubbles: dissipative effects and heat deposition. *Ultrasonics*, 38:99–104, 2000.
[29] J-F Yu, D. Zhang, X-F Gong, Y-J Gong, Z-M Zhu, and X-M Liu. Frequency dependences of sound attenuation and phase velocity in suspensions containing encapsulated microbubbles. *Chin. Phys. Lett.*, 22(4):892–895, 2005.
[30] W. Lauterborn and E. Cramer. Subharmonic route to chaos observed in acoustics. *Phys. Rev. Letters*, 47:1445–1448, 1981.
[31] A. Prosperetti. Application of the subharmonic threshold to the measurement of the damping of oscillating gas bubbles. *J. Acoust. Soc. Am.*, 61:11–16, 1977.

D.3 K. S. Andersen and J. A. Jensen, *In vitro* measurement of ambient pressure changes using a realistic clinical setup, *2008 IEEE International Ultrasonics Symposium - Proceedings*

This paper was published in the journal *Proceedings - IEEE Ultrasonics Symposium*, Page no. 1096-1099, November 2008. Conference title: *2008 IEEE Ultrasonics Symposium, IUS*.

In vitro measurement of ambient pressure changes using a realistic clinical setup

Klaus Scheldrup Andersen and Jørgen Arendt Jensen
Center for Fast Ultrasound Imaging, Department of Electrical Engineering,
Bldg. 349, Technical University of Denmark, 2800 Kgs. Lyngby, Denmark

***Abstract*—Many attempts to find a non-invasive procedure to measure the local blood pressure have been made. In the last decade independent experiments have indicated that the amplitude of the subharmonic response from contrast agents is sensitive to the ambient pressure. This paper presents a new experimental setup for measuring the acoustic response of a contrast agent when subjected to ambient over pressure. The setup is very flexible offering completely arbitrary excitation and data acquisition, fast and accurate ambient pressure control, and precise timing. More importantly, it resembles a realistic clinical setup using a single array transducer for transmit and receive. In this experiment, the acoustic response of SonoVue (Bracco, Milano, Italy) was measured twice at six different ambient hydrostatic pressures in the interval 0 to 25 kPa with an accuracy within 0.5 kPa. The acquired RF data was filtered and beamformed before further processing. To compensate for variations in bubble response and to make the estimates more robust, the relation between the energy of the subharmonic and the fundamental component was chosen as a measure over the subharmonic peak amplitude. The results of the first measurement sequence show an ambient pressure sensitivity of 0.42 dB/kPa having a linear correlation coefficient of 0.94. In the second sequence, a sensitivity of 0.41 dB/kPa with a correlation coefficient of 0.89 was found.**

I. Introduction

Finding a noninvasive and reliable approach to measure the human blood pressure locally in the body would provide doctors with a new tool to diagnose diseases related to the blood pressure. A noninvasive approach, which is based on flow estimation and a modification of the Bernoulli equation, already exists [1]. This gives an estimate of the pressure gradient, but was concluded not to provide reliable or reproducible results by Strauss et al. [2] and Reddy et al. [3]. Another existing procedure is to insert a pressure sensor directly into the vessel by means of a catheter. However, the presence of a pressure sensor inside the vessel will change the flow and, thereby, the blood pressure. Moreover, as this is an invasive approach, it is inconvenient to the patient and accompanied with a risk of infection.

Because of the high compressibility of gas, microbubbles containing air or gas can be used as local pressure sensors [4], [5], [6]. The idea of using an ultrasound contrast agent (UCA) to measure the cardiac pressure noninvasively was first proposed by Fairbank and Scully [4] in 1977. They claimed that the acoustic properties of the microbubbles change when the size of the bubbles change. To measure these size dependent oscillations, they suggested to measure the shift in resonance frequency but the results were, however, inconclusive. Other suggestions to measure the resonance shift at that time were made by Tickner [7] in 1982, Ishihara [8] in 1988, and Schlief and Poland [9] in 1993. Another approach was presented by Newhouse and Shankar [10], [11] in 1986. They showed theoretically and experimentally that accurate bubble size measurements are possible using a double frequency technique for determination of the sum and difference frequencies. The rapid dissolution time of free air bubbles prevented, however, any practical implementation at that time.

Since the introduction of the more stable second generation UCAs, new attempts to take advantage of the ambient pressure dependent acoustic properties have been initiated. In 1999, Bouakaz et al. [12], [13] presented an approach for measuring the disappearance time of free bubbles, which were generated at the region of interest by rupturing the contrast agent microbubbles using a low-frequency high acoustic amplitude pulse. Despite successful *in vitro* experiments and suggestions for further sensitivity improvements, no *in vivo* results or further investigations using this approach have been presented yet. Around the same time, Shi et al. [6] observed from experiments, using two single element transducers, that the subharmonic component of Levovist is highly sensitive to ambient pressure changes compared to the fundamental and the second harmonic component. They reported a 9.9 dB linear decrease of the peak amplitude of the subharmonic component when increasing the ambient pressure from 0 to 24.8 kPa (1 kPa = 7.5 mmHg). Recently, the same group have presented similar results for Sonazoid, which was found to have an average decrease of 13.3 dB [14]. Furthermore, in 2005 they presented *in vivo* results for proof of concept of the capabilities of the subharmonic response [15]. However, as the measurements were performed directly on the abdominal cavity and the aorta by incision of two dogs, this can hardly be characterized as noninvasive. Also in 2005, Adam et al. [16] did a thorough and interesting study to understand the mechanisms of acoustic scattering and attenuation of Optison when subjected to ambient over pressure. One of the conclusions confirmed that the subharmonic of the transmitted frequency can be used to detect ambient pressure variations. Andersen and Jensen [17] has recently performed a parameter study to optimize the subharmonic sensitivity to ambient over pressure and found two very clear tendencies. First, the linear reduction of the subharmonic component, or the pressure sensitivity, is dependent on the acoustic driving pressure and peaks when in the upper end of the growth stage, which occurs when the

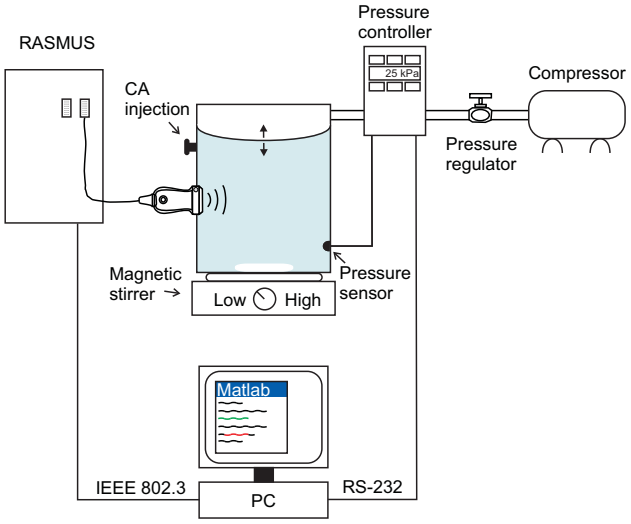

Fig. 1. Block diagram of the measurement setup. The left part shows the ultrasound acquisition part. The right part illustrates the pressure management system.

acoustic driving pressure causes the subharmonic to increase rapidly from background noise level to clearly visible in the spectrum. Second, the investigation also showed a clear relation between ambient pressure sensitivity and the length of the driving pulse.

As a setup using two transducers is not optimal in a clinical setting [16], this paper presents an experimental setup for measuring the fundamental and subharmonic response of a contrast agent when subjected to ambient over pressure, which more realistic resembles a clinical setting. The setup has been used to measure the pressure sensitivity of SonoVue (Bracco, Milano, Italy) using a standard ultrasound acquisition procedure and signal processing steps, which can easily be implemented in any commercial ultrasound scanner.

II. Method

A. Experimental setup

A block diagram of the measurement setup is shown in Fig. 1. The measurement is controlled from a single standard PC running Matlab (The MathWorks Inc., Natick, MA) under Linux. The ultrasound acquisition is carried out using the experimental ultrasound scanner RASMUS [18], which is controlled from the PC through an ethernet connection. It is a real-time ultrasound system providing full control of the transducer both in transmit and receive. It is capable of storing 16 GBytes of raw ultrasound data with a sampling frequency of 40 MHz and a precision of 12 bits for offline processing, which is essential in an experiment like this. For the acquisition, a single 64 element phased array transducer (B-K Medical, Herlev, Denmark) is connected to the RASMUS system. It has a center frequency of 3 MHz and a -6 dB bandwidth of 60 percent. The transducer is sealed to the measuring chamber giving no barrier between the contrast agent and the transducer. The measuring chamber is airtight and consists of two parts separated by a rubber membrane. The bottom part has a volume of 605 ccm and can be filled with either water or saline. The walls are coated with acoustic damping material to reduce ultrasound reflections from prior emissions. It also has inlets for the transducer, fast injection of contrast agent, and a sensor to monitor the pressure within the chamber. A magnetic stirrer IKA RCT (IKA-Werke GmbH & Co. KG, Staufen, Germany) is used to keep the bubbles in motion. The purpose of the lid, which has a dead volume of 12.5 ccm, is to change the pressure inside the chamber without mixing the inflated air with the bubbles. The pressure is managed by a custom designed dual valve pressure controller PCD4-10PSIG (Alicat Scientific, Tucson, AZ). It has an external pressure sensor and is fully programmable in real time through a RS-232 serial interface connected to a PC. The compressed air is generated by a silent oil-less compressor OF301-4M (Jun-Air International A/S, Nørresundby, Denmark) providing a feed pressure of 4 bar. This is reduced to a constant feed pressure of 2 bar using a separate precision regulator from ATD Tools (Wentzville, MO).

TABLE I
Various setup parameters for the experiment. First part describes the excitation pulse. The second part is related to the emission sequence. The final part denotes the ambient pressure set points.

Parameter	Designation	Unit
f_0	4.0	[MHz]
N_c	32	[cycles]
P_{ac}	485	[kPa]
Shape	10 % cosine tapered	
N_{emis}	50	[emissions]
f_{prf}	50	[Hz]
p_{ov}	0 5 10 15 20 25	[kPa]

B. Experimental procedure

The setup parameters for the measurement are listed in Table I. The acoustic bubble response was measured at six different ambient pressures between 0 and 25 kPa (1 kPa = 7.5 mmHg) corresponding to the common physiological blood pressure range in the human body. The measurement was initiated 90 seconds after injection of 0.5 ml of SonoVue (Bracco, Milano, Italy) into 0.6 l of saline. 50 pulses was emitted with a pulse repetition frequency of 50 Hz at each ambient pressure. The ambient pressure was increased in steps of 5 kPa every 2 second until a peak ambient pressure of 25 kPa and was then decreased in steps of 5 kPa. The ambient pressure was allowed 1 second to adjust in between acquisition at each pressure setting. The entire measurement lasted 21 seconds and provided two sets of scattered ultrasound data at each ambient pressure, except at 25 kPa. The excitation pulse was a steered beam with an acoustic pressure of 485 kPa and a focus at a depth of 30 mm from the transducer surface. It consisted of a 32 cycles cosine tapered pulse with a center frequency of 4 MHz. The acquired data was first filtered allowing the subharmonic, $f_{sub} = 2$ MHz, and the

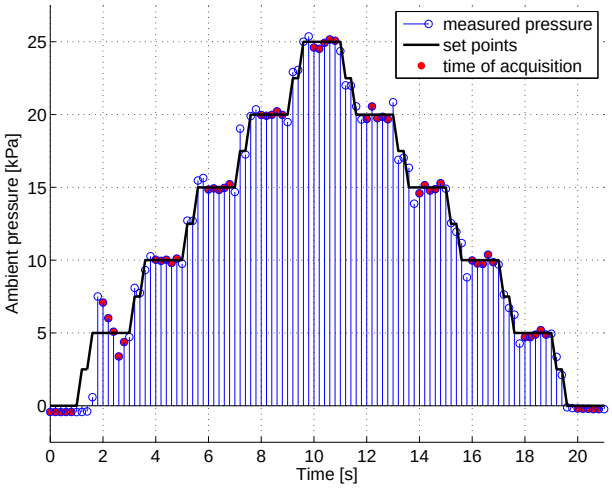

Fig. 2. Ambient pressure measured during the experiment. The stems show the pressure measured inside the chamber. The solid thick line indicates the pressure set points transmitted to the pressure controller. Finally, the dots inside the circles denote the time of ultrasound data acquisition.

fundamental, $f_0 = 4$ MHz, components to pass. Next, each acquisition line was beamformed and 20 data segments of 80 samples each were extracted, using a 50 percent overlap according to Welch [19]. The periodogram was found using Bartlett's method [20] and applying a Hanning window to each segment before calculating the Fourier spectrum. Next, the energy of the subharmonic and fundamental component was calculated using a bandwidth of 0.5 MHz centered around the respective peak amplitude. To reduce factors like UCA concentration and time dependency, the relation between the energy of the subharmonic and the fundamental is found before averaging over 10 consecutive emissions. As 50 lines are acquired, this yields 5 estimates at each ambient pressure set point.

III. Results

A summary of the ambient pressure control during the measurement is shown in Fig. 2. It displays the instantaneous pressure, measured by the sensor inside the chamber, along with the desired pressure transmitted from the PC. The time intervals for acquiring the ultrasound data is furthermore indicated by the filled circles. The relatively large overshoot when applying an ambient over pressure for the first time is not fully understood. However, the most likely explanation is that the rubber membrane got stuck to the inlet for compressed air. To compensate, the pressure controller increases the feed pressure and, eventually, pushing the membrane downward rather powerfully. To fix this, the space between the membrane and the inlet of the feed pressure can be increased as this is only 2 mm in the current setup. A larger dead volume (with limitations) would probably also reduce the general ripple when changing the set point and, thereby, refine the precision and speed of the ambient pressure regulation. Disregarding the first set point at 5 kPa, the measured ambient pressure is

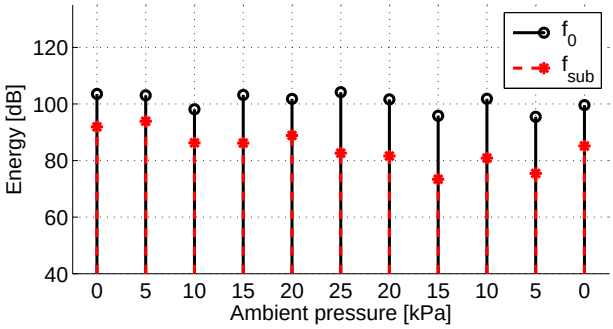

Fig. 3. Energy of the fundamental and subharmonic component estimated at the 11 different ambient pressures. Each value is the mean of five estimates which has been found based on 200 separate spectra each.

within 0.5 kPa of the desired set points. The maximum relative deviation in respect to the desired set point is 5.8 %, which is observed during the second measurement at 5 kPa.

Fig. 3 shows the calculated energy of the fundamental and subharmonic component as a function of ambient pressure and in order of time for the respective measurements. The energy of the fundamental component is more or less stable until about $p_{ov} = 25$ kPa, where it seems to start decreasing. The subharmonic component seems to drop from the beginning of the experiment to the end. According to Shi and colleagues [6], [14], this was expected for the first six measurement points. But the fact that the energy continues to drop for at least the next two measurement points ($p_{ov} = [20\ 15]$ kPa) could indicate that the bubbles are being dissolved. Looking at the results for pressure setting one and six constituting the first measurement series, the energy of the fundamental component changes 0.6 dB. In the same interval, the energy of the subharmonic component is reduced by 9.2 dB. Both these observations correspond well to the results presented in [6] and [14]. However, the fluctuating nature and the overall decrease in energy seen in Fig. 3 necessitates a more robust measure. Therefore, the relation between the energy of the subharmonic and the fundamental component is used in this experiment. The result is shown in top of Fig. 4, which also includes the standard deviation of the five estimates at each ambient pressure setting. According to Welch's method, the standard deviation scales with the number of segments used in the periodogram [19]. As 20 segments in each of 10 emissions are used for the estimate, the minimum standard deviation expected is $\sigma^2 \approx \frac{1}{200} P_x^2(f)$. Looking at the standard deviation in Fig. 4, it is rather high compared to this. Part of the reason can be because of the low pulse repetition frequency. However, to understand the deviation fully and to improve the accuracy, a more thorough investigation regarding the choice on number of segments and emissions, as well as the f_{prf}, should be carried out. Despite the high standard deviation, a clear trend can still be observed from the two measurement series in the plot in top of Fig. 4. As the ambient pressure is increased, the relationship seems to drop. To investigate this further, each measurement series has been normalized

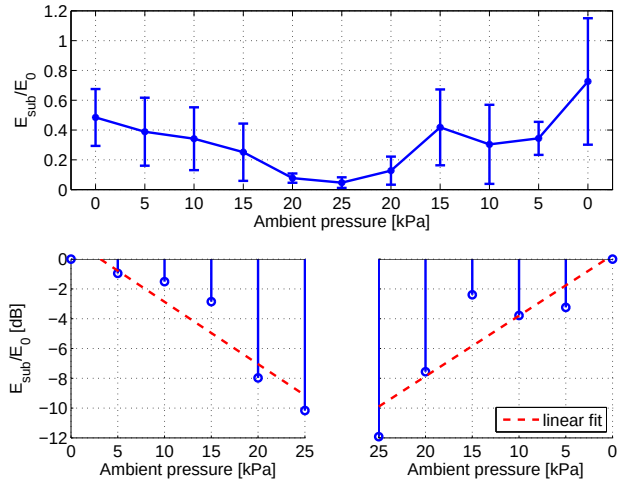

Fig. 4. The plot on top shows the relation between the energy of the subharmonic and the fundamental component estimated at each of the 11 ambient pressures. The error bars show the standard deviation which has be calculated based on five estimates. Below, the relation has been normalized and the logarithm applied for each of the two measurement series.

according to its peak value at 0 Pa before applying the logarithm. The results are shown in the two bottom plots in Fig. 4. The dashed lines indicate a first order polynomial fit, which minimizes the error in a least-squares sense. For the first measurement series displayed to the bottom left in Fig. 4, the linear fit indicates an ambient pressure sensitivity of 0.42 dB/kPa with a linear correlation coefficient of 0.94. In the second measurement series, the pressure sensitivity is 0.41 dB/kPa having a correlation coefficient of 0.89.

IV. Conclusion

An experimental measurement setup for investigating the ambient pressure sensitivity of an UCA has been designed. It consits of a single phased array transducer and equipment for automatic ambient pressure regulation and acquisition of raw ultrasound data. The setup has been used to measure the acoustic response of SonoVue when subjected to six different ambient hydrostatic pressures. The pressure management system proved capable of regulating the pressure inside the chamber within 1 second with a maximum relative deviation of 5.8 %. During the experiment, 21 seconds of data was acquired. As the amplitude as well as the energy of the subharmonic component was found to be useless as a measure by itself, the relationship of the energy between the subharmonic and the fundamental component was used. This yielded an ambient pressure sensitivity of 0.42 and 0.41 dB/kPa for the two measurement series carried out. The linear correlation coefficient was 0.94 and 0.89, respectively.

Acknowledgment

This work was supported by grant 26-04-0024 from the Danish Science Foundation, the Technical University of Denmark, and by B-K Medical Aps.

References

[1] A. C. Burton, *Physiology and Biophysics of the Circulation*, 2nd ed. Chicago: Year Book Medical Publishers, 1972.

[2] A. L. Strauss, F. J. Roth, and H. Rieger, "Noninvasive assessment of pressure gradients across iliac artery stenoses: duplex and catheter correlative study," *J. Ultrasound Med.*, vol. 12, pp. 17–22, 1993.

[3] A. K. Reddy, G. E. Taffet, and S. Madala, "Noninvasive blood pressure measurement in mice using pulsed doppler ultrasound," *Ultrasound Med. Biol.*, vol. 29, pp. 379–385, 2003.

[4] W. M. Fairbank and M. O. Scully, "A new noninvasive technique for cardiac pressure measurements: resonant scattering of ultrasound from bubbles," *IEEE Trans. Biomed. Eng.*, vol. 24, pp. 107–110, 1977.

[5] B. Hok, "A new approach to noninvasive manometry: Interaction between ultrasound and bubbles," *Med. Biol. Eng. Comp.*, vol. 19, pp. 35–39, 1981.

[6] W. T. Shi, F. Forsberg, J. S. Raichlen, and L. Needleman, "Pressure dependence of subharmonic signals from contrast microbubbles," *Ultrasound Med. Biol.*, vol. 25, pp. 275–283, 1999.

[7] E. G. Tickner, "Precision microbubbles for right side intracardiac pressure and flow measurements," *Meltzer RS, Roelandt JTCR, eds. Contrast echocardiography*, vol. 15, pp. 313–324, 1982.

[8] K. Ishihara, A. Kitabatake, J. Tanouchi, K. Fujii, M. Uematsu, Y. Yoshida, T. Kamada, T. Tamura, K. Chihara, and K. Shirae, "New approach to noninvasive manometry based on pressure dependent resonant shift of elastic microcapsules in ultrasonic frequency characteristics," *Jpn. J. Appl. Phys.*, vol. 27, pp. 125–127, 1988.

[9] R. Schlief and H. Poland, "Ultrasonic manometry process in a fluid by means of microbubbles, US patent number 5,195,520," March 1993.

[10] V. L. Newhouse and P. M. Shankar, "Bubble size measurements using the nonlinear mixing of two frequencies," *J. Acoust. Soc. Am.*, vol. 75, no. 5, pp. 1473–1477, 1984.

[11] P. M. Shankar, J. Y. Chapelon, and V. L. Newhouse, "Fluid pressure measurement using bubbles insonified by two frequencies," *Ultrasonics*, vol. 24, pp. 333–336, November 1986.

[12] A. Bouakaz, P. J. Frinking, N. de Jong, and N. Bom, "Noninvasive measurement of the hydrostatic pressure in a fluid-filled cavity based on the dissappearance time of micrometer-sized free gas bubbles," *Ultrasound Med. Biol.*, vol. 25, no. 9, pp. 1407–1415, 1999.

[13] A. Bouakaz, P. J. Frinking, and N. de Jong, "Noninvasive pressure measurement using microbubble contrast agent and wavelet transforms," *Proc. IEEE Ultrason. Symp.*, pp. 1907–1910, 2000.

[14] L. M. Leodore, F. Forsberg, and W. T. Shi, "*In vitro* pressure estimation obtained from subharmonic contrast microbubble signals," *Proc. IEEE Ultrason. Symp.*, 2007.

[15] F. Forsberg, J.-B. Liu, W. T. Shi, J. Furuse, M. Shimizu, and B. B. Goldberg, "In vivo pressure estimation using subharmonic contrast microbubble signals: Proof of concept," *IEEE Trans. Ultrason., Ferroelec., Freq. Contr.*, vol. 52, pp. 581–583, 2005.

[16] D. Adam, M. Sapunar, and E. Burla, "On the relationship between encapsulated ultrasound contrast agent and pressure," *Ultrasound Med. Biol.*, vol. 31, pp. 673–686, 2005.

[17] K. S. Andersen and J. A. Jensen, "Simulation of microbubble response to ambient pressure changes," *Med. Imag. V Symp.*, vol. 6920, p. 692016, 2008.

[18] J. A. Jensen, O. Holm, L. J. Jensen, H. Bendsen, H. M. Pedersen, K. Salomonsen, J. Hansen, and S. Nikolov, "Experimental ultrasound system for real-time synthetic imaging," in *Proc. IEEE Ultrason. Symp.*, vol. 2, 1999, pp. 1595–1599.

[19] P. D. Welch, "The use of fast Fourier transform for the estimation of power spectra: A method based on time averaging over short, modified periodograms," *IEEE Trans. Au. Electroacous.*, vol. AU-15, pp. 70–73, 1967.

[20] M. S. Bartlett, "Smoothing periodograms from time series with continuous spectra," *Nature (London)*, vol. 161, pp. 686–687, May 1948.

D.4 K. S. Andersen and J. A. Jensen, Non-invasive estimation of blood pressure using ultrasound contrast agents, *Proceedings of the International Congress on Ultrasonics 2009*, awarded the *R.W.B. Stephens Prize*

This paper was produced in connection with an invited talk at the *International Congress on Ultrasonics*, January 15, 2009. The first part closely follows [79] shown in Appendix D.3. The second part includes the same results as well as results for another measurement using a different excitation pressure. Along with the presentation, the paper was selected to receive an *Honorable Mention* for the *R.W.B. Stephens Prize*.

> "This prize is given in recognition of your excellent work in ultrasonics and your fine presentation of your results. This prize is sponsored by Elsevier and the journal *Ultrasonics* and in remembrance of Professor R.W.B. Stephens who was a pioneer in the field of ultrasonics, a great teacher and equally importantly, a wonderful human being."

Paper #???? Presented at the International Congress on Ultrasonics, Chile, January 12 - 16, 2009, Session S11: Tissue characterization

Non-invasive estimation of blood pressure using ultrasound contrast agents

Klaus Scheldrup Andersen, Jørgen Arendt Jensen

Technical University of Denmark, Center for Fast Ultrasound Imaging, Departments of Electrical Engineering, Ørsteds Plads, Build. 349, DK-2800 Kgs. Lyngby, Denmark, ksa@elektro.dtu.dk

Abstract: Local blood pressure measurements provide important information on the state of health of organs in the body and can be used to diagnose diseases in the heart, lungs, and kidneys. This paper presents an experimental setup for investigating the ambient pressure sensitivity of a contrast agent using diagnostic ultrasound. The setup resembles a realistic clinical setup utilizing a single array transducer for transmit and receive. The ambient pressure sensitivity of SonoVue (Bracco, Milano, Italy) was measured twice using two different acoustic driving pressures, which were selected based on a preliminary experiment. To compensate for variations in bubble response and to make the estimates more robust, the relation between the energy of the subharmonic and the fundamental component was chosen as a measure over the subharmonic peak amplitude. The preliminary study revealed the growth stage of the subharmonic component to occur at acoustic driving pressures between 300 and 500 kPa. Based on this, the pressure sensitivity was investigated using a driving pressure of 485 and 500 kPa. At 485 kPa, a linear pressure sensitivity of 0.42 dB/kPa was found having a linear correlation coefficient of 0.94. The second measurement series at 485 kPa showed a sensitivity of 0.41 dB/kPa with a correlation coefficient of 0.89. Based on the measurements at 500 kPa, this acoustic driving pressure was concluded to be too high causing the bubbles to be destroyed. The pressure sensitivity for these two measurement series were 0.42 and 0.25 dB/kPa with linear correlation coefficients of 0.98 and 0.93, respectively.

Key words: Blood pressure, contrast agent, pressure estimation.

A. Introduction

Knowledge of the blood pressure locally in the body can help doctors to diagnose diseases in vessels and other organs that are related to the blood pressure. Today, two different approaches are already used in the hospital. One procedure is to use an A-cannula which is also used to measure the gases in the blood at the same time. This is most often used in intensive care units. Another procedure is to insert a catheter with a pressure sensor and guide it to the area of interest through the vessels. Both approaches are invasive and especially the presence of a thin plastic tube inside the body must be considered inconvenient to the patient and also connected to a certain risk. Besides, as the sensors are located inside the vessel of interest, both approaches introduce changes to the blood flow and thereby the blood pressure. Furthermore, it is not possible to monitor all areas inside the body using neither of these approaches. A noninvasive approach, which already exists, gives an estimate of the pressure gradient based on flow estimation and a modification of the Bernoulli equation [1]. It was, however, concluded not to provide reliable or reproducible results by Strauss et al. [2] and Reddy et al. [3].

Due to the high compressibility of gas, microbubbles containing air or gas can be used as local pressure sensors [4], [5], [6]. Fairbank and Scully [4] was the first to suggest the idea of using an ultrasound contrast agent (UCA) to measure the cardiac pressure noninvasively in 1977. They claimed that the acoustic properties of the microbubbles change when the size of the bubbles change. To measure these changes, they suggested measuring the shift in resonance frequency. However, they found the results to be inconclusive. Other suggestions to measure the resonance shift at that time were made by Tickner [7] in 1982, Ishihara et al. [8] in 1988, and Schlief and Poland [9] in 1993. Another approach was presented by Newhouse and Shankar [10], [11] in 1986. They showed theoretically and experimentally that accurate bubble size measurements are possible using a double frequency technique for determination of the sum and difference frequencies. The rapid dissolution time of free air bubbles, however, prevented any practical implementation at that time.

Since the introduction of the more stable second generation UCAs, new attempts to take advantage of the ambient pressure dependent acoustic properties have been initiated. In 1999, Bouakaz et al. [12], [13] presented an approach for measuring the disappearance time of free bubbles, which were generated at the region of interest by rupturing the contrast agent microbubbles using a low-frequency high acoustic amplitude pulse. Despite successful *in vitro* experiments and suggestions for further sensitivity improvements, no *in vivo* results or further investigations using this approach have been presented yet. Around the same time, Shi et al. [6] observed from experiments, using two single element transducers, that the subharmonic component of Levovist is highly sensitive to ambient pressure changes compared to the fundamental and the second harmonic component. They reported a 9.9 dB linear decrease of the peak amplitude of the subharmonic component when increasing the ambient pressure from 0 to 24.8 kPa (1

kPa = 7.5 mmHg). Recently, the same group has presented similar results for Sonazoid, which was found to have an average decrease of 13.3 dB [14]. Furthermore, in 2005 they presented *in vivo* results for proof of concept of the capabilities of the subharmonic response [15]. However, as the measurements were performed directly on the abdominal cavity and the aorta by incision of two dogs, this can hardly be characterized as noninvasive. Also in 2005, Adam et al. [16] did a thorough and interesting study to understand the mechanisms of acoustic scattering and attenuation of Optison (at the time Mallinckrodt Medical GmbH, Hennef, Germany) when subjected to ambient over pressure. One of the conclusions confirmed that the subharmonic of the transmitted frequency can be used to detect ambient pressure variations. Andersen and Jensen [17] have recently performed a parameter study to optimize the subharmonic sensitivity to ambient over pressure and found two very clear tendencies. First, the linear reduction of the subharmonic component, or the pressure sensitivity, is dependent on the acoustic driving pressure and peaks when in the upper end of the growth stage, which occurs when the acoustic driving pressure causes the subharmonic to increase rapidly from background noise level to clearly visible in the spectrum. Second, the investigation also showed a clear relation between ambient pressure sensitivity and the length of the driving pulse.

This paper presents an approach to experimentally investigate the fundamental and subharmonic response of a contrast agent as a function of the ambient pressure, which continuously is changed. Basically, the experimental setup consists of an airtight chamber and a single phased array transducer. Compared to a setup utilizing two transducers, which is not optimal in the clinic [16], this resembles a clinical setup more realistically. The setup was first used to investigate the current batch of SonoVue (Bracco, Milano, Italy) in respect to the acoustic pressure of the emitted ultrasound pulse. Next, the pressure sensitivity was measured using a standard ultrasound acquisition procedure and signal processing steps, which can easily be implemented in any commercial ultrasound scanner. Some part of this work has been presented at the 2008 IEEE International Ultrasonics Symposium [18].

B. Method

B.1. Experimental setup

Fig.1 shows a block diagram of the experimental setup used in the measurements. The measurement is controlled from a single standard PC equipped with connections for ethernet and serial communication running Matlab (The MathWorks Inc., Natick, MA) under Linux. The ultrasound acquisition is carried out using the experimental ultrasound scanner RASMUS [19], which is controlled from the PC through an ethernet connection. It is a real-time ultrasound system and provides full control of the transducer in both transmit and in receive. It is capable of storing 16 GBytes of raw ultrasound data with a sampling frequency of 40 MHz and a precision of 12 bits for offline processing, which is essential in an experiment like this. For the acquisition, a single 64 element phased array transducer (B-K Medical, Herlev, Denmark) is connected to the RASMUS system. It has a center frequency of 3 MHz and a –6 dB bandwidth of 60 percent. The transducer is sealed to the measuring chamber giving no barrier between the contrast agent and the transducer. The measuring chamber is airtight and consists of two parts separated by a rubber membrane. The bottom part has a volume of 605 ccm and can be filled with either water or saline. The walls are coated with acoustic damping material to reduce ultrasound reflections from prior emissions. It also has inlets for the transducer, fast injection of contrast agent, and a sensor to monitor the pressure within the chamber. To keep the bubbles in motion, a magnetic stirrer IKA RCT (IKA-Werke GmbH & Co. KG, Staufen, Germany) is used. The purpose of the lid, which has a dead volume of 75.9 ccm, is to change the pressure inside the chamber without mixing the inflated air with the bubbles injected into the liquid. The pressure is managed by a custom designed dual valve pressure controller PCD4-10PSIG (Alicat Scientific, Tucson, AZ). It has an external pressure sensor and is fully programmable in real time through a RS-232 serial interface connected to a PC. The compressed air is generated by a silent oil-less compressor OF301-4M (Jun-Air International A/S, Nørresundby, Denmark) providing a feed pressure of 4 bar. This is reduced to a constant feed pressure of 2 bar using a separate precision regulator from ATD Tools (Wentzville, MO).

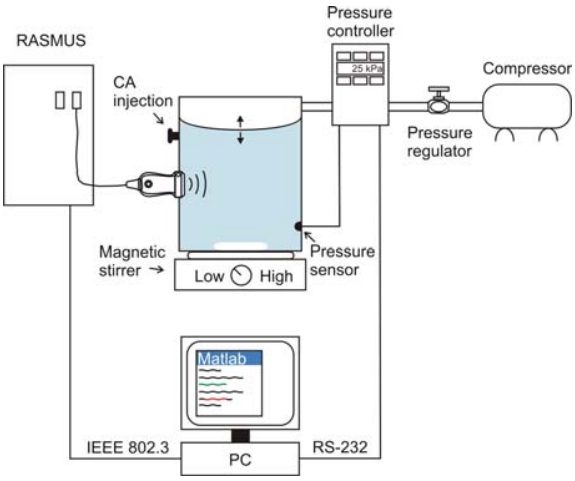

Fig.1. Block diagram of the measurement setup. The left part shows the ultrasound acquisition part. The right part illustrates the pressure management system.

B.2. Experimental procedure

B.2.1. Acoustic driving pressure

Two types of measurements were carried out. The response of SonoVue (Bracco, Milano, Italy) was initially investigated as a function of 14 different acoustic driving pressures denoted P_{ac}. At each acoustic pressure setting, N_{emis} = 50 cosine tapered pulses consisting of N_c = 32 cycles with a center frequency of f_0 = 4 MHz were emitted using a pulse repetition frequency of f_{prf} = 50 Hz. After the data acquisition, the energy of the subharmonic and the fundamental component was calculated using a

bandwidth of 0.5 MHz centered around f_{sub} = 2 and f_0 = 4 MHz, respectively. For this experiment, 0.5 ml of Sonovue was injected into 0.6 l of saline. The setup parameters for the measurement are listed in Table 1.

Table 1. Setup parameters for the experiment investigating the dependence on the acoustic driving pressure.

Parameter	Designation	Unit
f_0	4.0	[MHz]
N_c	32	[cycles]
Shape	10 % cosine tapered	
P_{ac}	100 200 300 325 350	[kPa]
	375 400 450 485 500	
	550 600 700 900	
N_{emis}	50	[emissions]
f_{prf}	50	[Hz]
Contrast agent	SonoVue, batch 8A008D	

B.2.2. Ambient pressure sensitivity

To investigate the ambient pressure sensitivity, the acoustic bubble response was measured at six different ambient pressures between 0 and 25 kPa. This corresponds to the common physiological blood pressure range in the human body. The measurement was initiated within 3 minutes after injection of 0.5 ml of SonoVue into 0.6 l of saline. At each ambient pressure, 50 lines were acquired using a pulse repetition frequency of 50 Hz. Every 2 seconds, the ambient pressure was increased in steps of 5 kPa until the peak ambient pressure of 25 kPa was reached. It was then decreased in steps of 5 kPa. The ambient pressure was allowed 1 second to adjust in between acquisition at each pressure setting. The entire measurement, thereby, lasted 21 seconds and provided two series of scattered ultrasound data at each ambient pressure, except at 25 kPa – one set when increasing the ambient pressure and another set when decreasing the ambient pressure. The emitted ultrasound pulse was a steered beam identical to the one used to investigate the acoustic driving pressure dependent behavior. Two similar experiments were carried out using an acoustic driving pressure of 485 and 500 kPa, respectively. These acoustic pressure settings were selected based on the initial experiment, which indicated this to be in the upper end of the subharmonic growth stage. The acquired data was first filtered, allowing only the subharmonic and the fundamental components to pass. Next, each acquisition line was beamformed and 25 data segments of 80 samples each were extracted, using a 50 percent overlap according to Welch [20], to estimate the power density spectrum. The periodogram was found using Bartlett's method [21] and applying a Hanning window to each segment before calculating the Fourier spectrum. Next, the energy of the subharmonic and fundamental component was calculated using a bandwidth of 0.5 MHz centered around the respective peak amplitude. To reduce factors like UCA concentration and time dependency, the relation between the energy of the subharmonic and the fundamental components is found before averaging over 10 consecutive emissions. As 50 lines are acquired, this yields 5 estimates at each ambient pressure set point. The measurement parameters that deviate from the first experiment listed in Table 1 are presented in Table 2.

Table 2. Setup parameters for the experiment investigating the ambient pressure sensitivity. Only parameters which deviate from Table 1 are listed.

Parameter	Designation	Unit
P_{ac}	485 500	[kPa]
P_{ov}	0 5 10 15 20 25	[kPa]

C. Results

C.1. Acoustic driving pressure

Fig.2 shows the energy of the fundamental and subharmonic component calculated for each of the 14 different acoustic driving pressures. Looking at the fundamental component, an almost linear increase in energy is observed as the acoustic driving pressure is increased. The energy of the subharmonic component behaves, however, differently. For acoustic pressures below 300 kPa, almost no change in the amount of energy is seen and the subharmonic component is not (or almost not) visible in the spectra. For acoustic pressures between 300 and 500 kPa a rapid increase in energy is suddenly observed. This part is often referred to as the growth stage and implies that the subharmonic component gets more and more pronounced in the spectra. For acoustic pressure levels above 500 kPa, the increase in energy decays and this part is known as the saturation stage. In this stage, a general increase in energy for all frequencies has also been reported, indicating that the bubbles are being disrupted [22], [23].

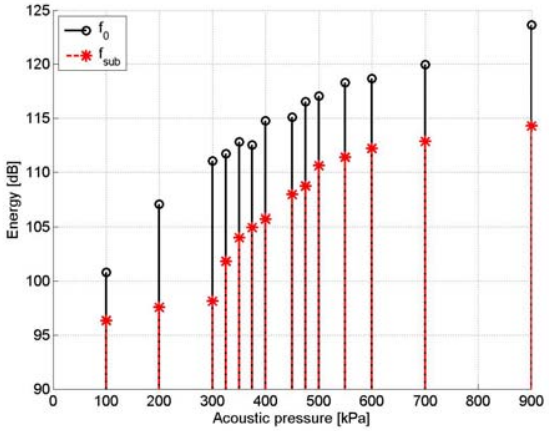

Fig.2. Energy of the fundamental and subharmonic component as function of the acoustic driving pressure.

C.2. Ambient pressure sensitivity

Based on the results in Section C.1, two different acoustic driving pressures have been selected to investigate the ambient pressure sensitivity. Before showing these results, an example of the ambient

pressure management is first given. Next, the pressure sensitivity using an acoustic driving pressure of 485 kPa is presented in Section C.2.2 followed by the results using an acoustic pressure of 500 kPa in section C.2.2.

C.2.1. Ambient pressure management

As the pressure logs, which summarizes the ambient pressure control during the measurement, are very similar, only the one for P_{ac} = 500 kPa is presented here. Fig.3 shows the instantaneous pressure, measured by the sensor inside the chamber and the desired pressure transmitted from the PC. The time intervals for acquiring the ultrasound data is furthermore indicated by the filled circles. As can be seen in Fig.3, the pressure measured inside the chamber is following the desired set points closely, except for a single high overshoot when increasing the ambient pressure to 5 kPa at the very beginning. When focusing on the ambient pressure measured at the time of ultrasound acquisition, only two time intervals has a deviation of 1 kPa or more. This is observed once at each of the two pressure settings at 5 kPa. Excluding these, the maximum deviation from the desired ambient pressure is 0.7 kPa. This occurs at the second setting at 15 kPa and yields at the same time the maximum relative deviation which is 5.3 %.

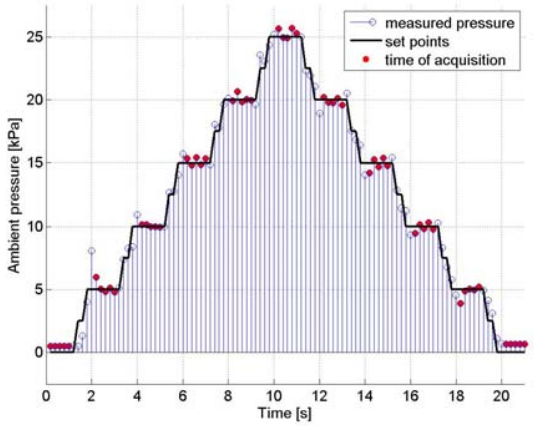

Fig.3. Example of the ambient pressure measured inside the chamber during an experiment. This is for the measurement with P_{ac} = 500 kPa. The solid thick line indicates the pressure set points transmitted to the pressure controller. Finally, the dots inside the circles denote the time of ultrasound data acquisition.

C.2.2. Acoustic driving pressure of 485 kPa

Fig.4 shows the calculated energy of the fundamental and the subharmonic component as a function of ambient pressure and in order of time for the respective measurements. The energy of the fundamental component is more or less stable until about P_{ov} = 25 kPa, where it seems to start decreasing. The subharmonic component seems to drop from the beginning of the experiment to the end. According to Shi and colleagues [6], [14], this was expected for the first six measurement points. But the fact that the energy continues to drop for at least the next two measurement points, P_{ov} = [20 15] kPa, could indicate that the bubbles are being dissolved.

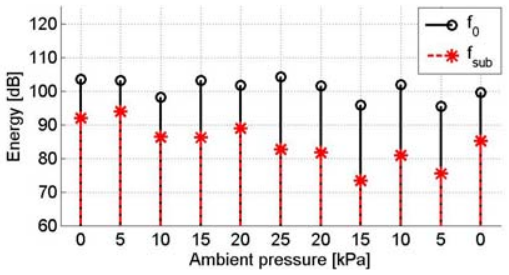

Fig.4. Energy of the fundamental and subharmonic component estimated at the 11 different ambient pressures when using an acoustic pressure of 485 kPa. Each value is the mean of five estimates, which has been found based on 200 separate spectra each.

When looking at the results for pressure setting one (0 Pa) and six (25 kPa), constituting the first measurement series, the energy of the fundamental component changes by 0.6 dB. In the same interval, the energy of the subharmonic component is reduced by 9.2 dB. Both these observations correspond well to the results presented in [6] and [14]. However, the fluctuating nature and the overall decrease in energy seen in Fig.4 necessitate a more robust measure. Therefore, the relation between the energy of the subharmonic and the fundamental component is used in this experiment. The result is shown in top of Fig.5, which also includes the standard deviation of the five estimates at each ambient pressure setting.

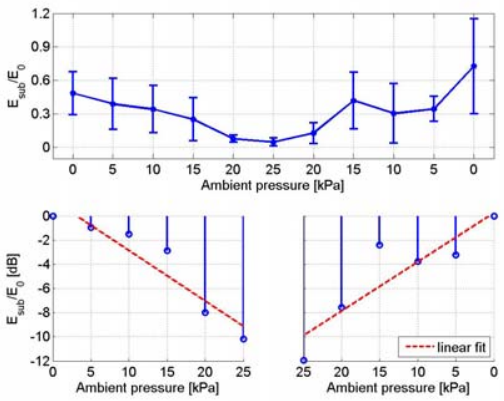

Fig.5. The top plot shows the relation between the energy of the subharmonic and the fundamental component estimated at each of the 11 ambient pressures. The error bars show the standard deviation, which has been calculated based on five estimates. Below, the relation has been normalized and the logarithm applied for each of the two measurement series.

According to Welch's method, the standard deviation scales with the number of segments used in the periodogram [20]. As 20 segments in each of 10 emissions are used for the estimate, the minimum standard deviation expected is $\sigma^2 \approx P_x^2/200$, where P_x is the power spectrum. Looking at the standard deviation in Fig.5, it is rather high compared to this. Part of the reason can be because of the low pulse repetition frequency, which was selected not to harm the bubbles too much and to prevent acquisition of reverberations. However, to understand the deviation fully and to improve the

accuracy, a more thorough investigation regarding the choice on number of segments and emissions, as well as the f_{prf}, should be carried out. Despite the high standard deviation, a clear trend can still be observed from the two measurement series in the plot in top of Fig.5. As the ambient pressure is increased, the relationship seems to drop. To investigate this further, each measurement series has been normalized according to its peak value at 0 Pa before applying the logarithm. The results are shown in the two bottom plots in Fig.5. The dashed lines indicate a first order polynomial fit, which minimizes the error in a least-squares sense. For the first measurement series displayed to the bottom left in Fig.5, the linear fit indicates an ambient pressure sensitivity of 0.42 dB/kPa with a linear correlation coefficient of 0.94. In the second measurement series, the pressure sensitivity is 0.41 dB/kPa having a correlation coefficient of 0.89.

C.2.3. Acoustic driving pressure of 500 kPa

The energy of the fundamental and the subharmonic component is shown in Fig.6 as a function of the ambient pressure when using an acoustic driving pressure of 500 kPa. Comparing this to Fig.4, a somewhat different behavior is observed. First of all, the energy of the fundamental component is seen to drop significantly as the ambient pressure is increased or over time, or a combination of this. This continues until the ambient pressure is decreased to above 20 kPa, where a linear increase is suddenly observed. However, comparing the energy of the fundamental component at pressure setting one (0 Pa) and 11 (0 Pa), is has decreased by 10.4 dB. This indicates that a lot of bubbles have been destroyed most likely due to the high acoustic pressure, but possible also because of the ambient pressure effects. The subharmonic component behaves almost the same as the fundamental, except it does not increase further as the ambient pressure is decreased from 10 to 0 kPa in the second measurement series. One explanation for this could be that the size of the bubbles left at this point has reduced and in that way makes it more difficult to generate a subharmonic component at 2 MHz.

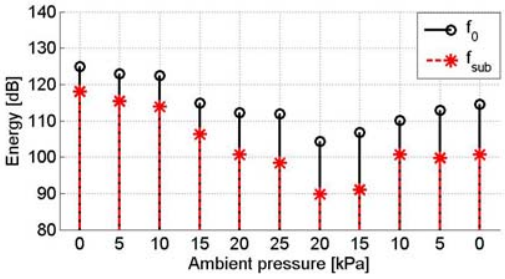

Fig.6. Energy of the fundamental and subharmonic component estimated at 11 different ambient pressures when using an acoustic driving pressure of 500 kPa.

Despite the clear indication of bubble destruction observed in Fig.6, the relation between the energy of the subharmonic and the fundamental component has still been investigated and is shown in top of Fig.7. Looking at the first measurement series when decreasing the ambient pressure, an almost completely linear reduction is seen. In fact, the correlation coefficient calculated for the first order polynomial fit is 0.98. The linear fit also indicates an ambient pressure sensitivity of 0.42 dB/kPa, which is the same as for P_{ac} = 485 kPa. This is not as expected according to the simulation study by Andersen and Jensen [17], which predicted an increase in sensitivity as the acoustic driving pressure is increased. This deviation, thereby, confirms the suggestion that the acoustic driving pressure was selected too high, which then destroys the bubbles. This theory is corroborated further when drawing the attention to the second measurement series in the lower right corner of Fig.7. In this case, the linear fit reveals that the ambient pressure sensitivity has been reduced to 0.25 dB/kPa (R = 0.93). To investigate the conclusions in [17] it is, therefore, suggested to use a lower acoustic driving pressure in future experiments.

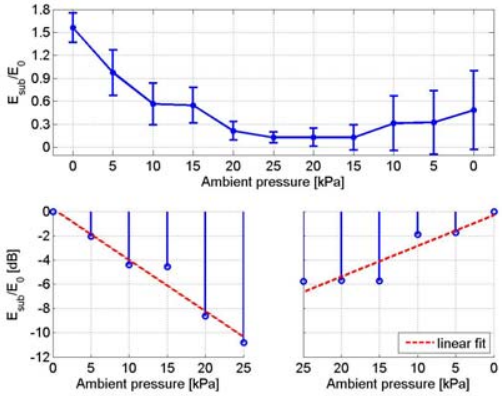

Fig.7. The plot on top shows the relation between the energy of the subharmonic and the fundamental component when using an acoustic driving pressure of 500 kPa. Below, the corresponding reduction plots for each measurement set are shown.

D. Conclusion

A realistic clinical setup has been used to examine the pressure sensitivity of an ultrasound contrast agent. The setup consists of an airtight chamber with connections for a single array transducer and inlets for automatic regulation of the ambient pressure and fast injection of contrast agent. The acquisition of raw ultrasound data and management of the ambient pressure is controlled from a single standard PC. The setup was first used to measure the acoustic response of SonoVue as a function of acoustic driving pressure. The growth period of the subharmonic component was found to be in the interval between 300 and 500 kPa. A driving pressure of 485 and 500 kPa, respectively, where next used to investigate the ambient pressure sensitivity. The driving pressure at 500 kPa where found to cause too much bubble destruction to be useful in a practical situation. At 485 kPa, the ambient pressure sensitivity was found to be 0.42 and 0.41 for two consecutive measurement series. The linear correlation coefficients for these measurements were 0.94 and 0.89, respectively.

E. Aknowledgements

This work was supported by grant 26-04-0024 from the Danish Science Foundation, the Technical University

of Denmark, and by B-K Medical Aps. The authors furthermore want to thank Copenhagen University Hospital for providing the contrast agent.

F. Literature

[1] A. C. Burton, Physiology and Biophysics of the Circulation, 2nd ed. Chicago: Year Book Medical Publishers, 1972.

[2] A. L. Strauss, F. J. Roth, and H. Rieger, “Noninvasive assessment of pressure gradients across iliac artery stenoses: duplex and catheter correlative study,” J. Ultrasound Med., vol. 12, pp. 17–22, 1993.

[3] A. K. Reddy, G. E. Taffet, and S. Madala, “Noninvasive blood pressure measurement in mice using pulsed doppler ultrasound,” Ultrasound Med. Biol., vol. 29, pp. 379–385, 2003.

[4] W. M. Fairbank and M. O. Scully, “A new noninvasive technique for cardiac pressure measurements: resonant scattering of ultrasound from bubbles,” IEEE Trans. Biomed. Eng., vol. 24, pp. 107–110, 1977.

[5] B. Hok, “A new approach to noninvasive manometry: Interaction between ultrasound and bubbles,” Med. Biol. Eng. Comp., vol. 19, pp. 35–39, 1981.

[6] W. T. Shi, F. Forsberg, J. S. Raichlen, and L. Needleman, “Pressure dependence of subharmonic signals from contrast microbubbles,” Ultrasound Med. Biol., vol. 25, pp. 275–283, 1999.

[7] E. G. Tickner, “Precision microbubbles for right side intracardiac pressure and flow measurements,” Meltzer RS, Roelandt JTCR, eds. Contrast echocardiography, vol. 15, pp. 313–324, 1982.

[8] K. Ishihara, A. Kitabatake, J. Tanouchi, K. Fujii, M. Uematsu, Y. Yoshida, T. Kamada, T. Tamura, K. Chihara, and K. Shirae, “New approach to noninvasive manometry based on pressure dependent resonant shift of elastic microcapsules in ultrasonic frequency characteristics,” Jpn. J. Appl. Phys., vol. 27, pp. 125–127, 1988.

[9] R. Schlief and H. Poland, “Ultrasonic manometry process in a fluid by means of microbubbles, US patent number 5,195,520,” March 1993.

[10] V. L. Newhouse and P. M. Shankar, “Bubble size measurements using the nonlinear mixing of two frequencies,” J. Acoust. Soc. Am., vol. 75, no. 5, pp. 1473–1477, 1984.

[11] P. M. Shankar, J. Y. Chapelon, and V. L. Newhouse, “Fluid pressure measurement using bubbles insonified by two frequencies,” Ultrasonics, vol. 24, pp. 333–336, November 1986.

[12] A. Bouakaz, P. J. Frinking, N. de Jong, and N. Bom, “Noninvasive measurement of the hydrostatic pressure in a fluid-filled cavity based on the dissappearance time of micrometer-sized free gas bubbles,” Ultrasound Med. Biol., vol. 25, no. 9, pp. 1407–1415, 1999.

[13] A. Bouakaz, P. J. Frinking, and N. de Jong, “Noninvasive pressure measurement using microbubble contrast agent and wavelet transforms,” Proc. IEEE Ultrason. Symp., pp. 1907–1910, 2000.

[14] L. M. Leodore, F. Forsberg, and W. T. Shi, “*In vitro* pressure estimation obtained from subharmonic contrast microbubble signals,” *Proc. IEEE Ultrason. Symp.*, 2007.

[15] F. Forsberg, J.-B. Liu, W. T. Shi, J. Furuse, M. Shimizu, and B. B. Goldberg, “In vivo pressure estimation using subharmonic contrast microbubble signals: Proof of concept,” IEEE Trans. Ultrason., Ferroelec.,Freq. Contr., vol. 52, pp. 581–583, 2005.

[16] D. Adam, M. Sapunar, and E. Burla, “On the relationship between encapsulated ultrasound contrast agent and pressure,” Ultrasound Med. Biol., vol. 31, pp. 673–686, 2005.

[17] K. S. Andersen and J. A. Jensen, “Simulation of microbubble response to ambient pressure changes,” Med. Imag. V Symp., vol. 6920, p. 692016, 2008.

[18] K. S. Andersen and J. A. Jensen, “In vitro measurement of ambient pressure changes using a realistic clinical setup”, Proc. IEEE Ultrason. Symp. 2008, to be published.

[19] J. A. Jensen, O. Holm, L. J. Jensen, H. Bendsen, H. M. Pedersen, K. Salomonsen, J. Hansen, and S. Nikolov, “Experimental ultrasound system for real-time synthetic imaging”, Proc. IEEE Ultrason. Symp., vol. 2, 1999, pp. 1595–1599.

[20] P. D. Welch, “The use of fast Fourier transform for the estimation of power spectra: A method based on time averaging over short, modified periodograms,” IEEE Trans. Au. Electroacous., vol. AU-15, pp. 70–73, 1967.

[21] M. S. Bartlett, “Smoothing periodograms from time series with continuous spectra,” Nature (London), vol. 161, pp. 686–687, May 1948.

[22] P. A. Dayton, K. Morgan, A. L. Klibanov, G. Brandenburger, K. W. Ferrara, “Simultaneous optical and acoustical observation of contrast agents”, Proc. IEEE Ultrason. Symp., 1997, pp. 1583-1591.

[23] W. T. Shi, F. Forsberg, H. Oung, “Spectral broadening in conventional and harmonic doppler measurements with gaseous contrast agents”, Proc. IEEE Ultrason. Symp., 1997, pp. 1575-1578.